Schriftenreihe Umweltingenieurwesen

Agrar- und Umweltwissenschaftliche Fakultät

Band 104

Dissertation

Martin Rinas

Sediment Transport in Pressure Pipes

PROFESSUR **Wasserwirtschaft**

Universität Rostock Traditio et Innovatio

ISBN 978-3-86009-523-2
DOI: https://doi.org/10.18453/rosdok_id00002962

Schriftenreihe Bd. 104 Umweltingenieurwesen ▪ Wasserwirtschaft

Schriftenreihe Umweltingenieurwesen

Band 104

Dissertation

Martin Rinas

Sediment Transport in Pressure Pipes

Professur

Wasserwirtschaft

Agrar- und Umweltwissenschaftliche Fakultät

Universität Rostock Traditio et Innovatio

Dissertation

HERAUSGEBER

Prof. Dr.-Ing. habil. Jens Tränckner
Universität Rostock
Agrar- und Umweltwissenschaftliche Fakultät
Professur Wasserwirtschaft
18051 Rostock

CIP-KURZTITELAUFNAHME

Dissertation Martin Rinas
Universität Rostock
Agrar- und Umweltwissenschaftliche Fakultät
Rostock, 2021

BEZUGSMÖGLICHKEITEN

Universität Rostock
Universitätsbibliothek, Schriftentausch,
18051 Rostock
Tel.: 0381/498-8637, Fax: 0381/498-8632
E-Mail: maria.schumacher@ub.uni-rostock.de

Universität Rostock
Agrar- und Umweltwissenschaftliche Fakultät
Professur Wasserwirtschaft
Satower Straße 48, 18059 Rostock
Tel.: 0381/498-3461, Fax: 0381/498-3462

ISBN 978-3-86009-523-2
DOI: https://doi.org/10.18453/rosdok_id00002962

Universität Rostock
Professur Wasserwirtschaft

Foreword

Pumps are commonly used in wastewater technology, both for sewage transport and in many technological applications. In sewage transport, pumps are by far the biggest energy user but also decisive for the functioning of the complete system. Currently, most pumping station are operated in simple switch on/switch off mode. Since pumps are designed for maximum flow, the operation point is in those cases mostly far above the actually required demand. Since the friction losses in force mains increase with the square of flow velocity, the key of a minimized energy demand is flow control applying frequency control units. However, reduced flow velocity goes along with reduced sediment transport capacity. So, the implementation of energy efficient flow control in sewage transport in rarely found in practice due to suspected sediment risks.

The objective of this work is the enlightenment and mathematical description of the governing sediment transport processes in wastewater pressure pipelines and the derivation of recommendations for a flow control which provides both, energy efficiency and operation reliability.

This work is an important contribution for an improved understanding of sediment transport processes of domestic sewage which has significantly different composition than combined sewage. In a well structured approach combining lab and full-scale experiments with process modelling, Martin Rinas could show a completely different settling and resuspension behavior of the mainly organic suspended matter in domestic sewage at separate systems. Based on his experimental results in lab and full scale, he successfully developed and calibrated a numeric process model which can be used to investigate the effect of pump operation on sediment transport. Summarised, due to the almost absence of mineral particles and to the low required shear stress for resuspension, domestic sewage pipes could be operated with much lower flow velocities compared to existing guidelines.

Though his findings and model reliability are validated in long-term full-scale operation, the implementation in practice remains a long way to go. It requires both, open-minded operators and a more differentiated formulation of design and operational standards for wastewater pumping stations. In turn, the work can be a valuable contribution to reduce the energy demand in sewage transport and this way to mitigate the anthropogenic climate change.

Large parts of the work were developed in project, funded by the Deutsche Bundesstiftung Umwelt DBU. We thank for the successful cooperation with partners in science and practice, above all the chair of numeric mathematics at Rostock University, the WILO group and the regional wastewater operators Eurawasser GmbH and Nordwasser GmbH.

Prof. Dr.-Ing. habil. Jens Tränckner

Universität Rostock

Traditio et Innovatio

Aus der Professur für Wasserwirtschaft

der Agrar- und Umweltwissenschaftlichen Fakultät

Sediment Transport in Pressure Pipes

Kumulative Dissertation

zur Erlangung des akademischen Grades
Doktor der Agrarwissenschaften Doktor der Ingenieurwissenschaften (Dr.-Ing.)

an der Agrar- und Umweltwissenschaftlichen Fakultät
der Universität Rostock

vorgelegt von M.Sc. Martin Rinas,
Rostock

Rostock, 21.06.2020

Gutachter: Prof. Dr.-Ing. Jens Tränckner, Universität Rostock, Agrar- und Umweltwissenschaftliche Fakultät, Professur für Wasserwirtschaft

Gutachter: Prof. Dr. Peter Krebs, Technische Universität Dresden, Institut für Siedlungs- und Industriewasserwirtschaft, Professur für Siedlungswasserwirtschaft

Gutachter: Prof. Dr. Klaus Neymeyr, Universität Rostock, Mathematisch-Naturwissenschaftliche Fakultät, Institut für Mathematik

Jahr der Einreichung: 2020

Jahr der Verteidigung: 2021

List of Publications

This cumulative dissertation consists of the following four scientific articles:

Chapter 3:

M. Rinas, J. Tränckner and T. Koegst. Sedimentation of Raw Sewage: Investigations For a Pumping Station in Northern Germany under Energy-Efficient Pump Control. *Water*. 2019, vol. 11, no. 1, pp. 40. Available from DOI: 10.3390/w11010040.

Author contributions: Conceptualization, M.Rinas, J.Tränckner and T.Koegst; Data curation, M.Rinas; Formal analysis, M.Rinas; Funding acquisition, J.Tränckner; Investigation, M.Rinas; Methodology, M.Rinas; Project administration, J.Tränckner; Software, M.Rinas; Supervision, J.Tränckner; Validation, M.Rinas; Visualization, M.Rinas; Writing—original draft, M.Rinas; Writing—review and editing, J.Tränckner and T.Koegst.

Chapter 4:

M. Rinas, J. Tränckner and T. Koegst. Erosion characteristics of Raw Sewage: Investigations For a Pumping Station in Northern Germany Under Energy-efficient Pump Control. *Water Science and Technology*. 2018. ISSN 02731223. With permission from the copyright holders, IWA Publishing. Available from DOI: 10.2166/wst.2018.474.

Author contributions: Conceptualization, M.Rinas, J.Tränckner and T.Koegst; Data curation, M.Rinas; Formal analysis, M.Rinas; Funding acquisition, J.Tränckner; Investigation, M.Rinas; Methodology, M.Rinas; Project administration, J.Tränckner; Software, M.Rinas; Supervision, J.Tränckner; Validation, M.Rinas; Visualization, M.Rinas; Writing—original draft, M.Rinas; Writing—review and editing, J.Tränckner and T.Koegst.

Chapter 5:

M. Rinas, J. Tränckner and T. Koegst. Sediment Transport in Sewage Pressure Pipes, Part I: Continuous Determination of Settling and Erosion Characteristics by In-Situ TSS Monitoring Inside a Pressure Pipe in Northern Germany. *Water*. 2019, vol. 11, no. 10, pp. 2125. Available from DOI: 10.3390/w11102125.

Author contributions: Conceptualization, M.Rinas, J.Tränckner and T.Koegst; Data curation, M.Rinas; Formal analysis, M.Rinas; Funding acquisition, J.Tränckner; Investigation, M.Rinas; Methodology, M.Rinas; Project administration, J.Tränckner; Software, M.Rinas; Supervision, J.Tränckner; Validation, M.Rinas; Visualization, M.Rinas; Writing—original draft, M.Rinas; Writing—review and editing, J.Tränckner and T.Koegst.

Chapter 6:

M. Rinas, A. Fricke, J. Tränckner, K. Frischmuth and T. Koegst. Sediment Transport in Sewage Pressure Pipes, Part II: 1 D Numerical Simulation. *Water*. 2020, vol. 12, no. 1, pp. 282. Available from DOI: 10.3390/w12010282.

Author contributions: Conceptualization, M.Rinas, J.Tränckner and K.Frischmuth; Data curation, M.Rinas; Formal analysis, M.Rinas, A.Fricke and K.Frischmuth; Funding acquisition, J.Tränckner; Investigation, M.Rinas; Methodology, M.Rinas, K.Frischmuth and J.Tränckner; Project administration, J.Tränckner; Software, A.Fricke, K.Frischmuth and M.Rinas; Supervision, J.Tränckner; Validation, M.Rinas and A.Fricke; Visualization, M.Rinas; Writing—original draft, M.Rinas; Writing—review and editing, J.Tränckner, T.Koegst, A.Fricke and K.Frischmuth.

In this work, the above-mentioned contributions are presented in standardized typeface, uniform citation format and harmonized abbreviations. Furthermore, the chapter, equation, figure and table designations are numbered consecutively. For better readability, the citations to the above articles that are part of this cumulative dissertation have been replaced by chapter references.

The content of the original contributions has not been changed.

Contents

List of Figures

List of Tables

List of Abbreviations and Symbols

ADE	-	advection-dispersion equation
CSO	-	combined sewer overflow
FDM	-	finite difference method
PS	-	pumping station
PVC	-	polyvinyl chloride
TSS	$\frac{mg}{L}$	total suspended solids
WWTP	-	wastewater treatment plant
VFD	-	variable-frequency drive
A	m^2	pipe cross section
A_{pipe}	m^2	pipe cross section
A_s	m^2	pipe cross section occupied by sediments in Chapter 3
A_s	m^2	surface area of erosion in Chapter 5
A_T	m^2	free cross section of pipe
a	$\frac{mg}{L}$	fitting coefficient in Chapter 3
a	$\frac{kg}{m\,s}$	erosion rate in Chapter 5
$a(w,v)$	$\frac{kg}{m\,s}$	eroded mass per pipe length and time in Chapter 6
$a(\tau)$	$\frac{kg}{m\,s}$	eroded mass per length and time in Chapter 4
$a(\tau,w)$	$\frac{kg}{m\,s}$	eroded mass per length and time in Chapter 4 and Chapter 5
a_0	m	fitting coefficient
a_1	$\frac{h}{m^2}$	fitting coefficient
a_2	$\frac{h}{m^2}$	fitting coefficient
b	-	fitting coefficient
$C(t)$	$\frac{mg}{L}$	settling rate
C_0	$\frac{mg}{L}$	first TSS concentration in each single settling event
C_{rest}	$\frac{mg}{L}$	final solids concentration at the end of each single settling event
c	-	fitting coefficient
D_{xx}	$\frac{m^2}{s}$	dispersion coefficient
D_T	m	hydraulic diameter
d	-	fitting coefficient in Chapter 3
d	mm	pipe diameter in Chapter 3, Chapter 5 and Chapter 6

d	s	erosion parameter in Chapter 4, Chapter 5 and Chapter 6
d_m	mm	grain size fraction
e_a	$\frac{kg}{m\,s}$	measured erosion rate
ex_{max}	-	maximum light attenuation
ex_{min}	-	minimum light attenuation
F	Hz	frequency of variable-frequency drive
$F(v_s)$	$\%$	settling velocity distribution
g	$\frac{m}{s^2}$	acceleration due to gravity
H	m	total head loss
$H_A(Q)$	m	pipe or system curve function
H_c	mm	height of settling column
h_{geo}	m	hydraulic head
h_r	m	friction loss
h_s	m	deposit's height
l	m	pipe length
l_{pipe}	m	pipe length
Δl	m	length of pipe segment/grid size for simulation
$M(t)$	$\frac{mg}{L}$	cumulative growth of settled mass
m_s	$\%$	cumulative settled mass inside pipe
n_{t_s}	-	number of logged data points in switch-off sequence
P	$\frac{mm}{d}$	daily precipitation in Chapter 3
P	$\frac{kg}{m^3\,s}$	production of a substance to be transported in Chapter 6
P_s	m	deposit's perimeter
P_T	m	wetted perimeter
p	-	fitting coefficient
Q	$\frac{m^3}{h}$	flow rate/discharge
Q_{inflow}	$\frac{L}{s}$	inflow rate to the PS
Q_{pipe}	$\frac{m^3}{h}$	flow rate/discharge
R^2	-	coefficient of determination
$RMSE$	-	root-mean-square error
r	$\frac{kg}{m^3 s}$	reaction of a substance
S	$\frac{kg}{m^3\,s}$	sinking or degradation of a substance to be transported
$S(t)$	$\frac{mg}{L}$	cumulative growth of pre-settled mass
s_f	-	settling factor
$s(u)$	$\frac{kg}{m^3\,s}$	particle loss inside the fluid in Chapter 6
TSS_{cal}	$\frac{mg}{L}$	total suspended solids calibrated sensor data

TSS_{dry}	$\frac{mg}{L}$	total suspended solids under dry weather inflow
TSS_{ref}	$\frac{mg}{L}$	total suspended solids reference
TSS_{sens}	$\frac{mg}{L}$	total suspended solids sensor data
TSS_{wet}	$\frac{mg}{L}$	total suspended solids under wet weather/storm water inflow
t	s	settling duration in Chapter 3 and Chapter 5
t	s	time coordinate in Chapter 6
t_s	s	cumulative settling duration
Δt	s	time increament for simulation step
u	$\frac{kg}{m^3}$	particle concentration inside the fluid section
u_{inflow}	$\frac{mg}{L}$	TSS inflow concentration to the PS
u_{model}	$\frac{mg}{L}$	modelled TSS concentration inside the pressure pipe
$u_{reference}$	$\frac{mg}{L}$	reference TSS concentration from TSS sensor
V	L	volume of erosion cylinder
V_c	L	volume of settling column
v	$\frac{m}{s}$	flow velocity
v_{50}	$\%$	settling velocity of 50 % of particles
v_s	$\frac{mm}{s}$	settling velocity
$v_{s,pipe}$	$\frac{mm}{s}$	settling velocity threshold of pipe
w	m	deposit's width in Chapter 3
w	$\frac{kg}{m}$	current particle mass on pipe bottom in Chapter 5 and Chapter 6
w_{pipe}	kg	current particle mass on pipe bottom in Chapter 4
x	m	space coordinate
α	s^{-1}	exponential decay rate or settling parameter
λ	-	friction factor
ζ	-	discharge coefficient
ρ	$\frac{kg}{m^3}$	fluid density
ρ_S	$\frac{kg}{m^3}$	density of applied sand
σ	-	standard deviation
τ	$\frac{N}{m^2}$	bed shear stress inside pipe
τ_{100}	$\frac{N}{m^2}$	total resuspended bed shear stress
τ_{pipe}	$\frac{N}{m^2}$	bed shear stress inside pipe
τ_c	$\frac{N}{m^2}$	critical bed shear stress for eroding sand particles
τ_{crit}	$\frac{N}{m^2}$	critical bed shear stress
$\tau_{c,shields}$	$\frac{N}{m^2}$	Shields critical bed shear stress

1 Acknowledgments

The following manuscript is the final chapter of my scientific work at the University of Rostock.

Thank's to everyone at the university for supporting me during this time: Prof. Dr. K. Frischmuth, Dr. C. Stapel, Dr. A. Fricke, Dr. T. Koegst, M.Sc. B. Richter, M.Eng. M. Wachsmuth, M.Sc. M.Sc. W. Klehr, M. Sc. M. Kramer, B. Sc. A. Melzer and S. Lorenz. I always look back to this time with a smile.

Furthermore, I would like to thank the Eurawasser Nord GmbH and the Nordwasser GmbH for their cooperation during the project period and beyond.

Prof. Dr. Jens Tränckner and Dr. Thilo Koegst made this work possible in the first place. I would like to thank you especially for your honest interaction, criticism, praise and motivation.

My thanks for the proofreading goes to Philipp Rinas and Verena Schwindeler.

Thanks also to my parents Ingrid and Harald Rinas for all their support. And finally a very special word of thanks goes to Verena Schwindeler and Adam Rinas.

2 Introduction

2.1 Background

Although it is generally known that global warming is of anthropogenic origin, global greenhouse gas emissions are rising due to further increases in the primary energy demand [1, 2]. The energy production is primarily based on fossil fuels. If climatic changes are to be limited as far as possible, alternative energy sources must be used more for energy production. Furthermore, primary energy production itself and its consumption must be continuously made more efficient.

The general objective is to limit the rise in temperature. Under the Paris Climate Convention of 2016, it was decided to limit the temperature increase to below 2° C (relative to pre-industrial levels). Furthermore, significant efforts must be made to limit the temperature increase to a maximum of 1.5° C [3]. The agreement is part of the “United Nations Framework Convention on Climate Change” and will come effective in 2020, replacing the Kyoto Protocol. According to the ”IPCC Special Report” of 2018, the 1.5° C target can only be met with great effort in all relevant system areas [4].

Hence, it also includes transitions in urban infrastructure and concluding the water management sector [4]. A large proportion of energy consumption is attributable to the water management sector [4–6]. Besides ground- and surface water abstraction, treatment and distribution of clean drinking water, sewage collection and treatment are the main energy consuming processes in water management. According to [7], wastewater facilities are the main consumers on municipal level. 20 % of the local energy demand is related to wastewater treatment plants (WWTPs) and pumping stations (PS) [7]. While savings potentials of up to 25 % are estimated in the field of WWTPs, it is also assumed that there is great potential for savings in the area of the sewage collection [6]. In the following we will deal with the savings potential of PS.

This above-mentioned assumption is based on the fact that wastewater PS are used to a large extent for wastewater collection. Mostly for the simple reason that drainage is otherwise not possible due to geodetic height differences. Hence, sewage PS are fundamentally essential and can therefore hardly be deconstructed. The only way to save energy in sewage collection is therefore to increase the energy efficiency of a PS.

If the savings potential is to be quantified, only estimates can be given. It depends on the respective shares of the individual system components (e.g., size of the catchment area, number and size of the pumping stations, type of collection system, wastewater

treatment and disposal). Local conditions such as treatment technology, topography and electricity mix, have a considerable influence on the results, see also [8, 9].

The following example illustrates the energy saving potential for the operation of wastewater PS in an urban region in northern Germany with a large city and its periphery. The water company in Rostock (Nordwasser GmbH, Warnow-Wasser- und Abwasserverband) is responsible for the supply of drinking water and the disposal of wastewater for $\approx 268\,000$ people in a disposal area of $\approx 869\,km^2$. This includes 11 waterworks, 15 sewage treatment plants and a total of 347 sewage PS. Based on the annual report of the water company, $\approx 64\,\%$ of the total power consumption for water management is attributable to the wastewater sector [10]. Of this, $\approx 70\,\%$ is consumed by WWTPs and $\approx 30\,\%$ by PS.

In 2018, 3 862 965 kWh electricity was consumed in sum by all PS. At an electricity price of about 0.15 €/kWh, this corresponds to a financial expenditure of $\approx 580\,000$ € and to a CO_2 emission of $\approx 1831\,t$ (assuming a CO_2 emission factor of 474 g/kWh [11]). The average specific energy consumption of all PS was $\approx 0.12\,kWh/m^3$ (total electricity consumption devided by total amount of wastewater pumped). This value is comparatively low (see [8]), although in [10] only the pure energy consumption of the PS was calculated against the total volume of wastewater pumped. Nevertheless, energy saving potentials still exist and should be used for economic, ecologic and technical reasons.

Assuming the previously mentioned energy saving potential of 25 % for all PS, this would result in a saving of 965 741 kWh and thus 144 861 € every year. In return, the reinvestment of these savings could be used to modernize other technical facilities and thus enhance the efficiency further on. The savings would also have an impact on emission levels. The CO_2 savings would then amount to $\approx 458\,t$. These energy savings not only reduce the greenhouse gas burden on the atmosphere, but also contribute positively to the companies energy management. Energy management in turn can lead to tax concessions, e.g. reduced renewable energy levies. The results are further cost savings that can be reinvested for optimization. Summarized, in addition to the general effort to protect the climate, there are numerous economic reasons for companies to increase energy efficiency continuously.

In order to investigate the potential for energy savings at wastewater PS, the research project "Untersuchung der Möglichkeiten eines energieeffizienten Betriebsmanagements von Abwasserfördersystemen" ("Investigation of the possibilities of energy-efficient operational management of wastewater pumping systems") was initiated in 2012 [12]. The cooperation included the University of Rostock (Insititute for urban water management and hydromechanics and Institute for mathematics), the WILO SE and the Abwasserzweckverband Darß (local sewer systems operator). To increase energy savings, an energy-efficient pump strategy based on speed control was developed, tested and optimized in a real sewer system [12–14].

Ultimately, energy savings of 25 % (annual mean value) could be achieved by using the speed control on the tested PS [13].

The pilot results showed a large savings potential for wastewater operators. However, it was also concluded that there are risks for the operation. The energy savings are only achieved in favour of changed operating conditions. This concerns primarily the flow velocities in the pressure pipe. A reduction of the flow velocity can lead to various risks for operating safety. In fact, a sewer systems operator will never accept operational risks in favour of energy savings. Therefore, a follow-up project has been initiated to investigate the operational risks arising from the energy-efficient control.

From 2014 to 2016, the research project “Optimale Strategien zur Überwachung und Vermeidung von Sedimentation beim Einsatz drehzahlgeregelter Abwasserpumpen” (“Optimal strategies for monitoring and prevention of sedimentation in the use of speed-controlled sewage pumps”) mainly focuses on the operational risks during an energy-efficient pumping operation at an exemplary PS in Rostock-Schmarl (northern Germany) [15]. The main objective was to investigate the effects on the sediment transport behaviour within a pressure pipe. Finally, it has been demonstrated that an energy-efficient pumping operation does not exclude a safe sediment transport inside a pressure pipe.

The energy-efficient pump control developed in the two projects is the focus of the dissertation of Dr. rer. nat. Alexander Fricke, defended in 2015 [13].

The investigation of the sediment transport behaviour in context of this energy-efficient pump control is the central focus of this cumulative dissertation. It is the result of my scientific work within the follow-up project.

2.2 State of the art

Pressure drainage systems are used for lifting wastewater from settlement structures in almost all urban areas. For drainage against the natural slope, the difference in height and the sum of friction losses (called total hydraulic head) must be overcome by the pump power of a PS. The design of pressure drainage systems is based on this total hydraulic head, as well as the expected peak inflow rate. The inflow rate is not generally known and can be determined for existing systems from measurements or consumption data. For new areas to be planned, this is determined on the basis of technical codes, e.g. [16].

The pumping capacity of the pump system is designed for this inflow quantity. Thus, the disposal in case of dimensioning is given. However, the current inflow rate is predominantly below the maximum flow rate, as peak inflows occur only once a day for a short period of time. As a result, the PS usually delivers at unnecessarily high flow rates. Figure 1 illustrates this problem for a PS in Rostock. The dimensioning pump capacity is

equal to the actual pump demand only for a very short period. For the rest of the day, there is a more or less strong surplus of pumping capacity. The case in point shows that the full power two-point control mode leads to an enormous capacity reserve, which is not needed in dry weather conditions.

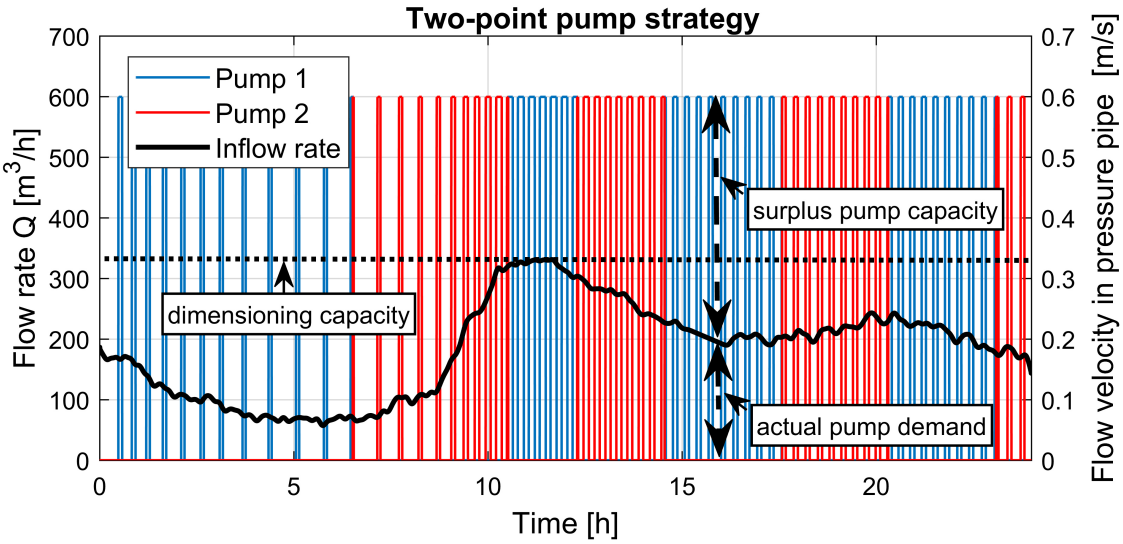

Figure 1. Pump capacity dimensioning and diurnal inflow rate to a PS in Rostock

The pump control in Figure 1 shows the usually control mode of a wastewater PS, a two-point control strategy. The water level in the pump sump rises through the sewage inflow. The level measurement gives a signal for control as soon as the switch-on level is reached. The pump then delivers with the rated power. When the switch-off level is reached, the control unit switches the pump off. In addition, there are controls for parallel operation and forced runs.

According to Darcy-Weisbach, the friction losses increases with the square of the flow velocity. The simple two-point control results in high friction losses due to the predominantly unnecessarily high conveying capacity. The consequences are high-energy consumption, increased wear of mechanical components due to an increased number of switching operations and increased sedimentation due to extended pump pauses. It therefore makes sense to adjust the capacity during periods of low inflow (see also [17]). The flow rate can be adjusted by controlling the speed of the drive motor by means of a variable-frequency drive (VFD). VFD are state of the art and are used in many wastewater PS, especially larger ones, to increase efficiency.

Based on a frequency control, an energy-efficient pumping strategy was developed in [13, 14] and implemented in several PS. The determined, energetically optimal frequency is specific to the PS and represents the new duty point as long as the simultaneously measured inflow rate does not exceed it. Otherwise, the flow rate is directly adapted to the inflow rate. As a result, energy savings between 11 % and 47 % for different PS could

be achieved [15]. Further information on the control system are provided by [12–14].

Irrespective of the type of control, a frequency change leads to changed operating conditions. Reduced flow velocity must be accepted in order to achieve energy savings. However, this can have a negative effect on the transport of solids and consequently increases the risk of sedimentation and the formation of deposits inside the pressure pipe. If thresholds of transport (flow velocity and bed shear stress) are undercut, solids settling to pipes bottom and may not be eroded again, which leads in its worst case to pipe blockages.

Recommendations by technical codes, usually minimum flow velocity in pipes, are intended to prevent deposits formation. In [18] the recommended values for minimum flow velocities ranges from 0.5 m/s up to 1 m/s depending on the daily operating time of the PS and the sewage composition. Further details are not given. Recommendations for pipe diameters from 100 mm up to 200 mm with 0.7 m/s up to 0.9 m/s minimum flow velocity respectively, are given by [19]. [20] recommends minimum flow velocities for pipe diameters from 100 mm up to 400 mm with 0.7 m/s up to 1.2 m/s respectively, at least once per day. For self-cleaning conditions, flow velocities from 0.6 m/s up to 1.2 m/s at least once per day are recommended by [21].

In January 2020, a new technical code, “DWA-A 113: Hydraulische Dimensionierung und Leistungsnachweis von Abwasserdrucksystemen” (“Hydraulic dimensioning and performance verification of wastewater pressure systems”) [22], was published dealing especially with dimensioning of pressure pipe systems. For the first time, concrete recommendations for transport threshold (minimum flow velocities) depending on the pressure pipe diameter are given. Figure 2 shows the recommended minimum flow velocity inside the pressure pipe for various pipe diameters, adapted from [22]. These values must be guaranteed at least once per day according to [22] to prevent deposits formation. Furthermore, these minimum flow velocities do not include the transportation of sand.

To get an overview, the technically maximum possible flow velocities of the five main PS in Rostock are visualized as points in Figure 2. The circular points represent the maximum flow velocity in single pump operation for each PS. All angular points mark the maximum flow velocity in parallel or triple pump operation. It can be clearly seen that even in parallel or triple operation, the recommended values cannot be achieved. This means that either the pumps are too small or the pipe is too large, or the recommended minimum flow velocities are strongly safety oriented. However, the origin of the threshold values given in [22] is not specified.

Concluding, there is a need for further investigations on transport thresholds inside sewage pressure pipes, because of a lack of reliable data and problems of technical implementation of recommendations.

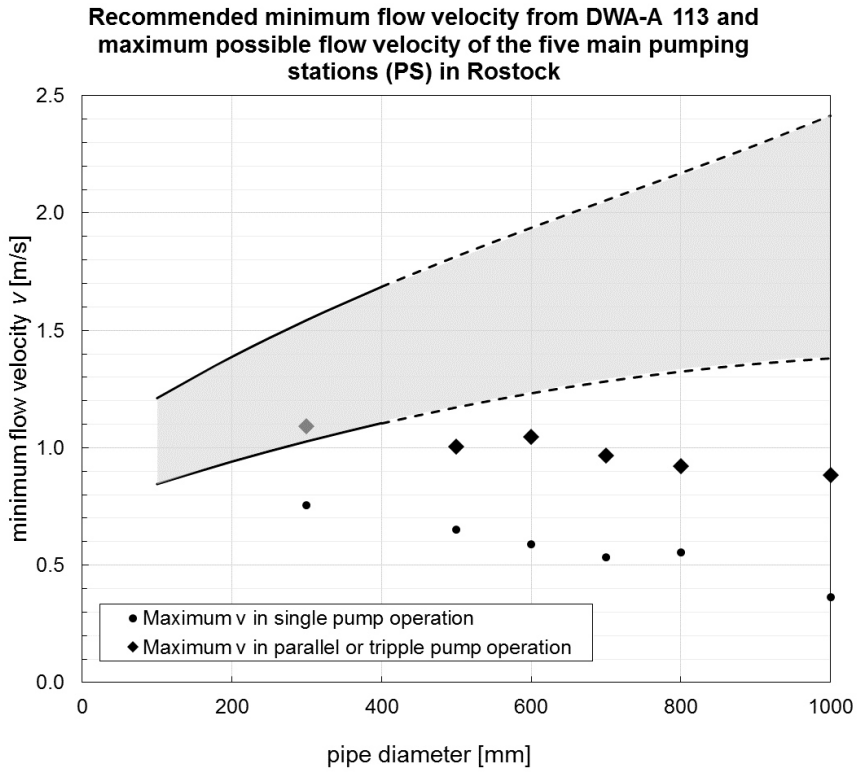

Figure 2. Recommended minimum flow velocity from DWA-A 113 [22] and maximum possible flow velocity of the five main PS in Rostock.

Operators of sewer systems are anxious to avoid deposits in the sewer system. The guarantee of operational safety is the focus. Nevertheless, they are also dependent on an increase in efficiency due to rising operating costs (energy, acquisition, investment and personnel costs). Moreover, not only commercial aspects play a role. The reduction of greenhouse gas emissions is a major component of energy-intensive water management. As already explained in Section 2.1, reasons for increasing energy efficiency are numerous.

2.3 Thematic classification

The present cumulative dissertation deals with the effects of energy-efficient pumping operation on the solid transport in sewage pressure pipes.

In order to classify the present work thematically, the individual contributions must be categorized in the literature context, as described in this paragraph. Thematically, this cumulative dissertation can be divided into two main topics: (i) the investigation and determination of the transport behaviour of particulate matter in raw sewage within a pressure pipe (Chapters 3 to 5). (ii) the simulation of the transport of solids in the pressure pipe to define the effects of energy-efficient pump operation on solids transport

(Chapter 6), based on the preceding determination of transport parameters.

The literature review in all four contributions showing the clear trend of today's scientific work. The investigation of the particle transport phenomena (e.g., sedimentation and erosion) focuses on gravity sewers, mainly carried out in combined systems (see literature review in Chapters 3 to 5). There are hardly any studies on pure waste water systems, especially regarding pressure drainage, dealing with sediment transport. Common methodologies split into ex situ tests (primary laboratory experiments) and in situ measurements (primary online measurements via sensors).

The present thesis contributes to the investigation of the transport phenomena sedimentation and erosion for pressurized sewers by means of ex- as well as in situ methods. The aim of all four publications is to investigate and describe the sediment transport in sewage pressure pipes under reduced flow conditions. Therefore, each of the four articles focuses on a specific subfield.

The investigation of the raw sewage sedimentation behaviour is the priority of Chapter 3. By means of a laboratory settling construction (ex situ), numerous settling experiments were conducted with raw sewage samples from the inflow stream to a PS in Rostock-Schmarl (operated in energy-efficient control, see Section 2.1). Hence, the results are comparable to similar investigations on gravity sewers. The determined settling parameter α is further used for the sediment transport simulation, see Figure 3. The laboratory tests were conducted in 2015 and 2016 within the follow-up project. The research results were published in 2019 as open access publication in *Water*, see [23].

The focus of Chapter 4 is the definition of the erosion behaviour of the raw sewage samples from the inflow stream to PS Rostock-Schmarl. The erosion properties of the wastewater were investigated by a laboratory erosion apparatus (ex situ) in 2015 and 2016. The results are as well comparable to similar investigations on gravity sewers found in the literature, although there is no standardised design or investigation methodology. The determined erosion parameters d and τ_{crit} are further used for the sediment transport simulation, see Figure 3. The research was published in *Water Science & Technology* in 2018, see [24].

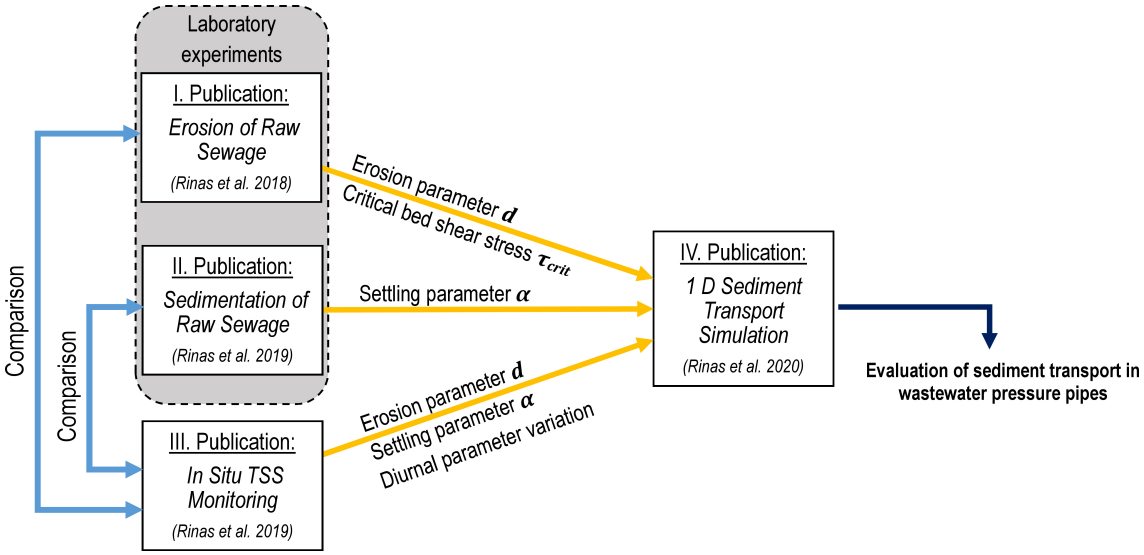

Figure 3. Overview and context of the publications. Laboratory sedimentation and erosion experiments providing the calibration parameters α, d and τ_{crit}. The in situ online measurements also provide the calibration parameters α and d as well as their hydrographs. In the final publication, the information is then combined into a sediment transport model. This allows the sediment transport in pressure pipes to be evaluated.

In Chapter 5, the sedimentation and erosion properties of the wastewater are determined by online turbidity measurements directly inside the pressure pipe (in situ) during the energy-efficient pump control. Two turbidity sensors were installed from 2015 to 2016 in PS Rostock-Schmarl and in the WWTP Rostock. This case-specific investigation is compared with the laboratory results from Chapters 3 to 4. According to the author's knowledge, direct sensor measurements regarding total suspended solids (TSS) inside wastewater pressure pipes are not part of todays scientific literature. Hence, due to the lack of alternatives, external literature data could not be compared. The determined settling and erosion parameters α and d as well as their diurnal variation are further used for the sediment transport simulation, see Figure 3. The study was published in 2019 as open access publication in *Water*, see [25].

To gain a better understanding of sediment transport in the pressure pipe (especially under energy efficient transport conditions), a sediment transport model was developed in 2015 and 2016 together with the institute of numerical mathematics at University of Rostock. The formerly presented studies providing the calibration parameters (α, d and τ_{crit}, see Figure 3) for the simulation of the transport mechanisms sedimentation and erosion. Based on various methodologies, numerous scientific work dealing with the simulation of the particle transport in gravity sewers (see literature review in Chapter 6). This 1 D numerical simulation is based on a mathematical transport approach, the advection-dispersion equation (ADE). The sediment transport model was extended in 2019 by a pump control simulation that allows the simulation of various pump control modes and strategies. This allows a large number of scenarios to be created and simulated. The study was published in 2020 as an open access publication in *Water*, see [26].

This article represents the last part of the investigations on the solid transport inside pressure pipes.

Chapters 3 to 6 present all four publications in a thematically meaningful order. There are no reconciliations between the individual chapters. Section 3.5, 4.5 and 5.5 are added additionaly within this work. The are dealing with recommendations and notes on laboratory and sensor tests. In Chapters 7 to 8 a summarizing discussion and conclusion follows. Finally, perspectives on possible future developments in the field are given in Chapter 9.

2.4 Key points

The transport of solids in sewers often represents an uncertain factor. The sediment transport is therefore viewed very critically. Recommendations and rules for a safe transportation seems to be mostly one-sided and safety-oriented. Results from combined sewage that is highly susceptible to sedimentation and difficult to erode are used as references due to the lack of alternatives. However, as already mentioned in [27], the results cannot simply be transferred to other drainage systems.

This arises from the fact that each drainage system differs in the drainage method (combined- or separation system), the connection structure and wastewater composition (domestic, commercial and industrial sewage) and, last but not least, the catchment area structure (building density, degree of sealing, etc.). Hence, values of transport are case-specific. The transport behaviour of raw sewage from separate sewers is different to combined sewage or storm runoff. A wastewater case-specific consideration should be the basis for the evaluation of the transport of solids in the respective wastewater system. Especially since new drainage systems are necessarily constructed as separating sewers, the following question arises: why should recommendations from the investigations of combined sewers be implemented in separating sewers?

Energy saving intentions leading to reduced flow conditions in sewage pressure pipes. Therefore, precise knowledge of the transport behaviour of the wastewater is of particular importance here, as maintenance and repair measures on pressure pipes are difficult and can cause considerable costs that overweigh possible savings. Is an energy-efficient pump control able to work successfully at all, taking into account the local wastewater composition?

It follows that the clarification of the individual transport characteristic is the basic prerequisite for the application of an energy-efficient pump control. The transportation of solid matters in raw sewage can be expressed by simple transport parameters. It is sufficient to define transport parameters for the effects sedimentation and erosion.

Both can be determined by means of ex situ laboratory experiments. Alternatively, turbidity sensors, even directly mounted inside a pressure pipe, can also be used for the characterization of the transport behaviour. Furthermore, the ex- and in situ measurements are also able to describe the modification of the transport characteristic, e.g. by storm water inflow.

Additionally, a detailed insight into the transport behaviour within the sewer can be gained by creating a sediment transport model based on the transport parameters resulting from the above described measurements. This allows the evaluation for various pump strategies based on a combined pump-, sediment transport simulation for pressure pipes.

In this way, it can be demonstrated that it is possible to reconcile reliable wastewater pumping with an energy-efficient control strategy. Ultimately, a case-specific investigation can provide suitable recommendations for an optimal pump control regarding energy saving and transport of solids.

3 Sedimentation of Raw Sewage: Investigations For a Pumping Station in Northern Germany under Energy-Efficient Pump Control

3.1 Introduction

Sewage transport in urban drainage systems involves in many cases the use of PS. Pumps are usually designed to handle maximum design inflow, which rarely occurs under normal operating conditions. Typically, a PS is operated in a simple switch-on/switch-off mode. While the pump sump is filled with sewage the pump switches on at a defined level before overflow occurs and switches off before it runs dry (two-point control). For most inflow conditions, pump flow exceeds by far the actual demand, resulting in unnecessary friction losses and consequently in a high energy consumption.

The key of a minimized energy demand is the reduction of friction losses, resulting from low flow velocities and engendered lower shear stress in connected pressure pipes. To increase efficiency and minimize energy demand, sewage PS can be equipped with frequency control. Combined with an intelligent, rule-based control strategy, significant energy savings can be achieved [14]. Identified side effects are the reduction of operation and maintenance costs and an expected increased durability of pumping aggregates, armatures and electric engines due to smoother operation conditions.

A benefit of a typical two-point control lies in its high design flow, as recommended flow velocities to avoid sedimentation risks are ensured in switch-on mode (e.g., in Germany a flow velocity of 0.6 to 1.2 m/s inside a pressure pipe system at least once per day, [21]). The challenge in energy optimization of PS is therefore to consider recommended flow velocities to avoid sedimentation risks and minimize energy demand in parallel. Hence, there is a trade-off between minimization of energy consumption and safe sewage transport avoiding blockage.

For good reasons operators of PS evaluate the safe sewage transportation higher than possible energy savings. By feeling, most operators assume that switch-on/switch-off mode is less risky with regard to sediment formation. But this estimation suffers from: (i) unknown knowledge of the actual settling behaviour of local sewer and

(ii) missing information about the occurrence of settling processes inside the pumping system. Hence, detailed information of both parts helps to control those systems in an efficient and reliable way. Applied correctly, the presented information in this article helps to increase the efficiency of the sewerage systems regarding energy optimization and sediment transport at once.

Sediments in sewers have for decades been the subject of many investigations, mainly focusing on combined systems. Many experimental procedures to determine settling behaviour of sewage are proposed, with different pros and cons. Starting with investigations on combined sewer overflow events [28], several experiments and methods have been developed to understand and describe sedimentation processes in sewer systems [29–34]. The original driver has often been the assessment of particle bound pollution transport in combined sewer systems [33], or storm water systems [34, 35]. The underlying principle of those activities is to determine particle mass fractions of different settling velocity classes by laboratory experiments (ex situ), mainly performed in settling columns (also used for river sediments [36]). In situ devices are trying to define the settling velocities for individual or specific types of particles, e.g., by image analysis of synthetic spheres [37], by optical backscatter sensors for sediment flocs [38], or fine-grained sediments of estuaries [39].

Theoretical work is trying to describe the settling process by models (e.g., the effect of lift forces on the settling behaviour by [40]) or equations for the settling velocity of particles and sediments [41–43]. Often, experimental data of settling experiments are processed by fitting a sigmoidal logistic function $M(t)$ [44–46]. After fitting three parameters b, c and d within the $M(t)$ function, settling velocity curves $F(v_s)$ enable a continuous description of accumulated mass fraction as function of the respective settling velocity.

The foremost objective of this article is to minimize energy demand in operation of a PS without risking unintended sediment formation in connected pressure pipes. How flow control influences this system is a priori hardly predictable, since lower flow velocities increase sedimentation risk while shorter pump pauses reduce it. This work contributes to this subject by addressing the following aspects:

- investigation of the settling behaviour of typical raw sewage at the inflow side of an urban influenced PS
- evaluation of the modification of the settling behaviour by wet weather inflow (road runoff)
- calculation of the sediment formation inside the connected pressure pipe in (i) two-point control and (ii) energy-efficient control
- verification by determining the deposits height inside the pressure pipe by a daily observation of the pipe curve.

3.2 Materials and Methods

3.2.1 Pumping Station, Control Modes and Monitoring

Pumping Station

The studied PS Rostock–Schmarl is located in the city of Rostock in northern Germany. The PS is mainly influenced by untreated domestic sewage ($\approx$ 40 000 inhabitants) combined with industrial/commercial wastewater (hotels, shipyards, local municipal utility, cruise ships). Although main roads runoff is also connected to the PS, it is part of the separate sewerage system in Rostock (roof runoff is discharged into a storm water system). Under dry weather conditions, pure sewage is transported, with its specific particle characteristics (low density, no ideal sphere form of particles, flocculate-matter and synthetic material as a mixture, particle interferences, sewage composition changes permanently). The connected separate sewerage system sums up to 80 km. The PS is equipped with a rake on the inflow side (space bar opening of 20 mm) to retain large obstacles. The sewage is transported in two parallel pipelines (cast iron, diameter = 600 mm, length = 4100 m) by four pumps, each with a power of 55 kW, to the central WWTP in Rostock.

Two-Point Control

The usual operation mode of PS Rostock–Schmarl is a typical two-point control strategy in which pumps switch on and off at defined water levels inside the sump. The PS is equipped with a VFD to balance the feed to the WWTP. By this, mains frequency is reduced from 50 Hz to 43 Hz. Accordingly, power input, engine speed, flow and friction losses are reduced, so next to the balanced feed, energy savings can already be achieved by the two-point control. The key aspects of this control strategy are shown in Table 1.

Table 1. Key aspects of pump control modes for PS Rostock–Schmarl

Control strategy	On-level (m)	Off-level (m)	Operation at frequency (Hz)	Soft start duration (s)	Duty point Q (L/s)	Duty point H (m)	Control rules
Two-point control	0.8	0.4	43–45	60	130	17.8	Transport rules
Rule-based control	0.8	0.4	41 (energy optimum)	60	110	17.45	Energy- & transport rules

Rule-Based Control

To achieve further energy savings, a rule-based control strategy was added to the PS for one year. Pumps were controlled by a PC, while the control rules were formulated in Matlab. The rule-based control is explained in detail in [14]. The general idea is to pump only the incoming flow until the energetic minimum (expressed as kWh per m^3) is reached. Lower flows (i.e., frequencies and impeller speeds) would lead an increased energy demand because of a decreasing degree of efficiency.

In case of lower inflows, the PS operates with the energy optimal flow and shuts off when the sump runs empty. In the case of PS Rostock–Schmarl the energy optimum is reached at 41 Hz. In a condensed formulation, the following control rules apply:

```
if water level > shut off level
        begin operation mode = ON
                if inflow > optimal flow
                        operate at inflow
                else
                        operate at optimal flow
                end
else
        operation mode = OFF
```

Further restrictions have to be considered for a safe sewage transport (transport-rules): minimum flow rate to open check valves, on-off-level restrictions of sump, empty sump regular, min/max engine speed and minimum flow rate to avoid sedimentation formation, flush pipes regular. Key aspects of the control strategy are shown in Table 1.

Monitoring

To verify the influence of the control modes on energy consumption and sediment formation inside the pressure pipe, 10 parameters were logged over two years (one year in each control mode). On the feeding side of the PS: sump level (m) and inflow (L/s). Regarding the pumping aggregate: power input (kW), frequency (Hz), engine speed (1/min), torque (Nm), voltage (V). On the outflow side of the PS: pressure (bar), flow (L/s), TSS (mg/L). Power input, frequency, engine speed, pressure and flow were used in this work for the investigation of sediment formation inside the pressure pipe.

3.2.2 Sampling and Experimental Procedure

Sampling

Altogether, 21 dry- and wet-weather samples were collected from the inflow channel of PS Rostock–Schmarl, during the rule-based control mode period. By this, raw sewage, under dry weather conditions, as well as, combined sewage with road runoff, was collected. Immediately after the samples were taken from the middle of the feed channel (1200 mm diameter) with a ladle, the initial particle concentration (analysis according to [47] by filtration and weight loss) was determined and the settling experiment started. Table 2 shows two selected samples including sampling time, sampling volume, initial total suspended solids TSS_{ref} and related precipitation data.

The selected dry weather example is representative for a maximum daily inflow under dry weather conditions, while the wet weather example represents a nominal inflow, influenced by a rain event with a long duration and changing intensity. The rain events were measured by a weather station of the German Weather Service (DWD) located inside the catchment area.

Table 2. Characteristics of selected dry- and wet-weather examples

Sample	Sampling time	Sampling volume (L)	TSS_{ref} (mg/L)	Remarks
dry	10:00 a.m.	30	390.2	Dry weather inflow
wet	01:00 p.m.	30	544.8	Wet weather inflow: Precipitation height = 10.1 mm/d

Experimental Design and Procedure

The experimental setup and post-processing of data should provide a reasonable compromise between applicability in operational practice, reproducibility and expressiveness concerning the sedimentation characteristics of a distinct raw sewage sample. After a thorough literature review, two methods were combined to determine the settling behaviour of the collected samples. The experimental setup follows the VICPOL protocol [33]. The process itself is simple and the experimental conditions are comparable to real world conditions in stagnant pressure tubes. For the subsequent data processing, the related VICAS protocol [48] was applied to describe the distribution of settling velocities in the sample as continuous mathematical function.

Figure 4 shows a schematic view (similar to [33]) and a photo of the construction. The VICPOL protocol determines n mass fractions with their specific settling velocity v_s (mm/s), by dividing the sewage sample into n sub-samples with n settling times. The choice of the best suitable settling times varies with sewage characteristics. After several pre-tests, a time range between 15 s and 24 h settling was found to cover the expectable range of settling velocities (Table 3), tending to smaller intervals at the beginning, according to the high settling dynamics of wet weather samples. The experiment itself is processed within three main steps:

1. Filling tank and columns: Storage tank is filled with the sewage sample from the PS (30 L). Seven settling columns (each volume V_c = 2.415 L, height H_c = 380 mm) are filled subsequently via separate tubes by gravity from tank till overflow. Settling starts immediately.

2. Settling: Parallel settling in all seven columns until the specific settling duration t reached.

3. Sampling and TSS analysis: After the specific settling duration t , a sample (volume = 0.345 L) is extracted from the bottom of the respective column i and analysed for TSS. The samples were extracted using a central vacuum pump, connected to a 10 mm glass tube, ending 10 mm above columns bottom.

Table 3. Settings for settling tests

Settling column	i	1	2	3	4	5	6	7
Settling duration t	(s)	15	45	180	420	1800	14 400	86 400
Settling velocity $v_s = \frac{H_c}{t}$	(mm/s)	25.3	8.4	2.1	0.9	0.2	0.026	0.004

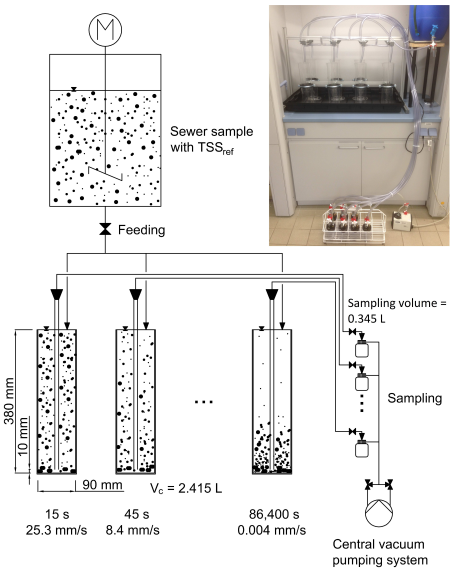

Figure 4. Designed and constructed experimental setup for settling measurement of raw sewage at University of Rostock.

The execution of settling experiments generate TSS and additional chemical parameters from the original sample and from the seven settling columns. The sampling volume (0.345 L) multiplied by seven (columns) equals to a total column volume of 2.415 L. The total reference particle mass of each column i, (TSS_{ref} multiplied by V_c) must correspond to the sum of the ΔTSS_i ($TSS_i - TSS_{i-1}$) of each column i multiplied by sampling volume (100 % settling assumed), see Equation (1). This relationship is helpful to define the required maximal settling time and for error evaluation.

$$\sum_{i=1}^{n} \Delta TSS_i\left(\tfrac{mg}{L}\right)\cdot 2.415(L) \leq TSS_{ref}\left(\tfrac{mg}{L}\right)\cdot 2.415(L) = \textit{total particle mass}(mg) \quad (1)$$

If the relationship from Equation (1) is true, the TSS data is numerically adjusted to a sigmoid function $M(t)$ (Equation (2), [46]), according to method 2 of the VICAS protocol [48]. The fitted $M(t)$ function, a description of the cumulative growth of the settled mass, leads to the $S(t)$ function in Equation (3), the cumulative growth minus the pre-settled mass. Finally, the $S(t)$ function is transferred into the settling velocity curve $F(v_s)$, Equation (4), describing the cumulative settling velocity distribution.

$$M(t) = S(t) + t\frac{dM(t)}{dt} = \frac{b}{1 + \left(\frac{c}{t}\right)^d} \quad (2)$$

$$S(t) = M(t) - t\frac{dM(t)}{dt} = \frac{b\Big(1 + (1-d)\big(\frac{c}{t}\big)^d\Big)}{\Big(1 + \big(\frac{c}{t}\big)^d\Big)^2} \tag{3}$$

$$F(v_s) = 100\Big(1 - \frac{S(t)}{\textit{total Mass}}\Big) \tag{4}$$

3.2.3 Calculation of Sediment Formation and Deposits Height in the Pressure Pipe

Sediment Formation

The sediment formation in the pressure pipe, called m_s (mass settled), is defined as the cumulative settled mass within each switch-off sequence. The settled mass is based on: (i) the settling behaviour of the raw sewage expressed by experimentally derived $F(v_s)$ function and (ii) the cumulative settling duration t_s during each switch-off sequence. For a comparison of the control modes, the mean cumulative settling duration $\overline{t_s}$ (s) is calculated for all switched-off sequences over the studied period (Equation (5)), where n_{t_s} is the number of logged data points in each switch-off sequence). A diurnal course of the settling duration inside the pipe is the result.

$$\overline{t_s} = \frac{1}{n_{t_s}} \sum_{i=1}^{n_{t_s}} t_{s,i} \tag{5}$$

All mass fractions with a settling velocity v_s (mm/s) larger than required to pass the pipe diameter within the mean cumulative settling duration $\overline{t_s}$ (termed $v_{s,pipe}$, settling velocity threshold of the pipe), are defined to form sediments. The related mean settled mass $\overline{m_S}$ (%) is calculated using Equation (6).

$$\overline{m_s}(\overline{t_s}) = 100 - F\big(v_{s,pipe}(\overline{t_s})\big) \tag{6}$$

With $v_{s,pipe}$, the settling velocity threshold of the pipe calculated by Equation (7).

$$v_{s,pipe}(\overline{t_s}) = \frac{\textit{pipe diameter}}{\overline{t_s}} \tag{7}$$

As a result, the mean sediment mass at switch-off mode is derived for each control mode as a mean diurnal course.

Deposits Height

The above described approach simplifies real world conditions and needs to be validated by data of actual sediment formation. However, an integrative deposit height in the pressure pipe cannot be measured directly. Though, an increase of deposits leads to a reduced cross section which in turn increases friction losses. This relation is used to inversely estimate deposit heights from the pipe curve (pressure height $= f(flow)$).

For this, the cross section of the pipe is split into two segments: (i) the free cross section where water is transported A_T (m²) and (ii) the cross section occupied by sediments A_s (m²). Applying the geometric relationships of a circle, the area A_T, wetted perimeter P_T (m) (Figure 5) and hydraulic diameter D_T (m) of free cross section are calculated with Equation (8) to Equation (10).

$$A_T = \textit{Pipe cross section} - A_s = \frac{\pi d^2}{4} - \frac{d}{4}\left(d \cdot arccos\left(1 - \frac{2h_s}{d}\right) - 2\sqrt{h_s(d-h_s)} \cdot \left(1 - \frac{2h_s}{d}\right)\right) \quad (8)$$

$$P_T = \pi \cdot d - P_s + w = \pi \cdot d - d \cdot arccos\left(1 - \frac{2h_s}{d}\right) + 2\sqrt{h_s(d-h_s)} \quad (9)$$

$$D_T = \frac{4 \cdot A_T}{P_T} \quad (10)$$

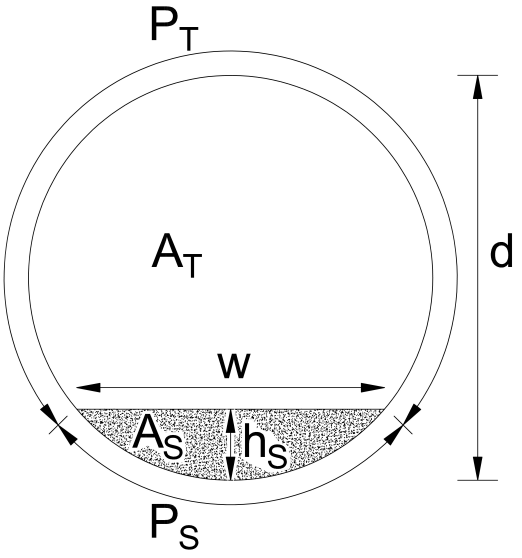

Figure 5. Definition of a pressure pipes geometric parameters for the calculation of the deposits height, A_T = free cross section for transport (m²), A_s = deposits cross section (m²), P_T = wetted perimeter (m), P_s = deposits perimeter (m), w = deposits width (m), h_s = deposits height (m), d = pipe diameter (m).

The pipe curve was daily acquired by varying the control frequency of the pump to achieve in minimum three ($m = 3$) data sets of flow Q (m³/h) and related pressure H (m). The data sets were adjusted to a second order polynomic function $H_A(Q)$ describing the current pipe curve by Equation (11) to Equation (12), with fitting parameters a_0, a_1 and a_2.

$$H_A(Q) = a_0 + a_1 \cdot Q + a_2 \cdot Q^2 \quad (11)$$

$$\min_{a_0 a_1 a_2} \sum_{i=1}^{m} \left(H_i - H_A(Q_i)\right)^2 \quad (12)$$

In a second step, the deposit height h_s (m) is estimated solving Equation (13).

$$\min_{h_s} \sum_{i=1}^{m} \left(h_{geo} + h_{r,i} - H_A(Q_i)\right)^2 \tag{13}$$

With hydraulic head h_{geo} (m) and h_r (m), the calculated friction loss according to Darcy–Weisbach, by Equation (14).

$$h_r = \left(\lambda \cdot \frac{l}{D_T} + \sum_i \zeta_i\right) \cdot \frac{v^2}{2g} = \left(\lambda \cdot \frac{l}{D_T} + \sum_i \zeta_i\right) \cdot \frac{Q^2}{2g3600^2 A_T^2} \tag{14}$$

where λ (-) is the friction factor (calculated after the Colebrook-White equation), ζ the discharge coefficient (-), pipe length l (m), hydraulic diameter D_T (m), g the acceleration due to gravity (m/s^2) and v the flow velocity (m/s). v can be replaced by the flow rate Q (m^3/h) and the free cross section for transport A_T (m^2).

3.3 Results and Discussion

3.3.1 Monitoring the Control Modes

The results of the continuous monitoring of PS Rostock–Schmarl is shown in Figure 6. A stacked bar graph illustrates the settling and pump duration per day (h), which always sum up to 24 h. The mean daily frequency (Hz) is given as hydrograph, while daily precipitation P is visualised in inverse direction as bars (mm/d). The sampling dates for the lab scale experiments are indicated. The varying settling and pump duration is a consequence of the control mode and the inflow condition. Pumps, controlled in rule-based mode, are working for longer sequences at the energy optimal frequency of 41 Hz, leading to longer switch-on sequences. Accordingly, the sum of the daily settling duration decreases significantly (average daily settling duration 11.9 h). Pumps, controlled in two-point mode, working for shorter sequences in the predefined frequency (43 Hz). The sum of the daily settling duration increases (average daily settling duration 15 h).

Next to the control mode, the pump duration is influenced by the sewage inflow as well. A rainfall event increases the inflow rate (main roads runoff), which leads in both control modes to longer pump sequences. If the inflow is too high, a second pump is switched on automatically (parallel pumping). This, in turn, decreases the pump duration due to higher flow rates. The effect of longer pump sequences is more pronounced in rule-based mode, because of the formulated rule: if inflow $>$ optimal flow, then operate at inflow. This delays parallel operation. In two-point control mode, pumps operate at a constant level until the critical limit is reached. The effect of longer pump sequences is greatly reduced.

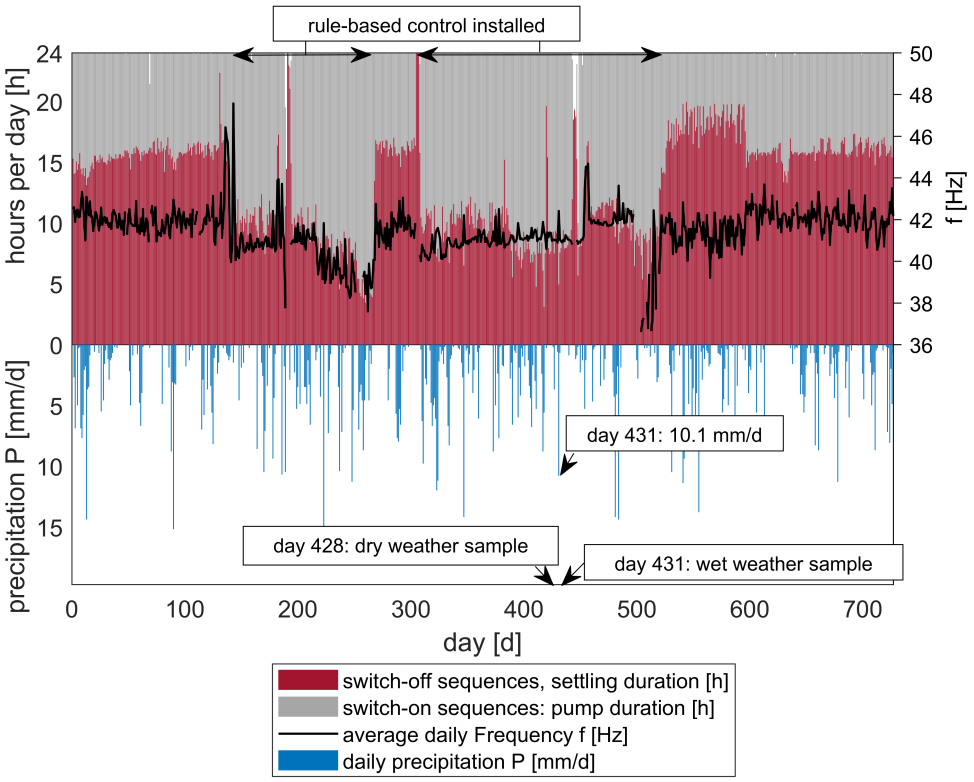

Figure 6. Results after two years monitoring PS Rostock–Schmarl: daily settling and pump duration as stacked bar graph, frequency hydrograph and precipitation including marks for sampling dates.

All these effects create the up-and-down course of the settling and pump duration in Figure 6. The average daily frequency hydrograph follows this course. A high frequency in two-point control leads into a maximized settling duration (e.g., 16 h settling with 44 Hz frequency on day 631). The same high frequency in rule-based control, leads to a greatly reduced settling duration (only 8.3 h on day 484).

The effects of a reduced settling potential are: (i) the control rules and (ii) a reduction of the frequency (reduced flow rate). It can therefore be expected, that the significantly reduced settling durations in rule-based control, will lead to less dangerous sediment formation. This becomes evident, regarding the diurnal course of the sedimentation process in combination with the settling properties of the raw sewage.

3.3.2 Settling Properties of Dry and Wet Weather Samples

Sediment formation inside the pipe is, next to the duration of the settling sequences, linked to the settling properties of the transported raw sewage. A fast settling mixture causes sediment problems, even within short settling sequences. With the characterization of the sedimentation behaviour based on the explained experimental procedure, a first estimation of the sediment formation in the pipe can be made. The settling behaviour of the transported raw sewage for PS Rostock–Schmarl is expressed as settling velocity curves $F(v_s)$.

The resulting $F(v_s)$ for dry and wet weather sample (from Table 2), are shown in Figure 7 (line plot). The boxplots indicate the determined settling characteristics of the sewage inflow of PS Rostock–Schmarl due to numerous experiments.

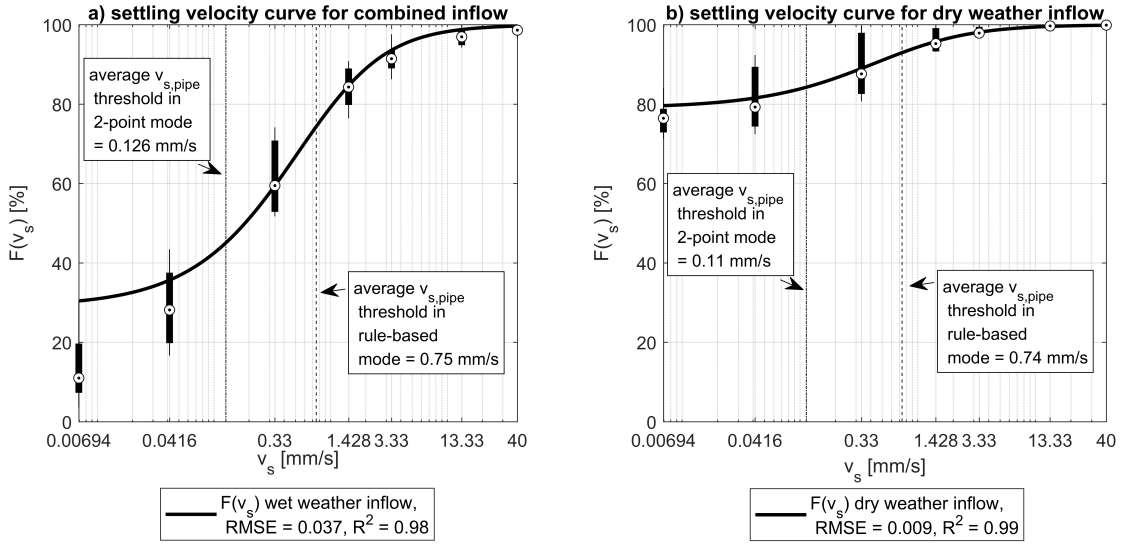

Figure 7. Results for settling measurement of sewage samples from PS Rostock–Schmarl, exemplary settling velocity curves $F(v_s)$ for a wet (**a**) and dry (**b**) weather sample including fit results, boxplots with results for all collected samples and average settling velocity thresholds of two-point- and rule-based pump control.

The experimental procedure and subsequent calculation methods are well applicable for both inflow conditions. The $M(t)$ function (Equation (2)), as basis for the $F(v_s)$ curves, is characterized by fitting results with a minimum R^2 of 0.98 and a maximum root-mean-square error ($RMSE$) of 0.037. This enables well founded statements about the settling characteristics of the raw sewage inflow. An in depth investigation of the experimental procedure, provided by [48], has already shown the applicability to dry- and wet-weather sewage samples as well as the reproducibility of the experimental procedure.

The sewage settling characteristics showing significant differences due to the inflow condition. Settling velocity curves measured for storm water conditions (”wet curves”) tend to faster settling. This behaviour is well known in the literature [33, 48, 49]. A strict decline was observed from the fourth (1.43 mm/s $\widehat{=}$ 420 s settling) up to the last measurement (0.00694 mm/s $\widehat{=}$ 24 h settling). In contrast, curves measured for dry weather inflow condition (”dry curves”), tending to gradual decline, with a flattened end at 24 h settling. This variation in the settling behaviour can be lead back to two main reasons: (i) particles washed off (road runoff) and entering the sewer network and (ii) high flow rates (after rain events) inside the feeding channels, spilling particles from wash-off and previously deposited sediments to the PS. In fact, the proportion of each particle (velocity) class changes by a runoff event.

[33] also mentioned the erosion of deposits due to higher mobilization in combined flows as a reason for a faster settling of wet weather samples (see also [49]).

Table 4 shows the average proportional change in each v_s-class, from dry to wet curves. Especially the proportion of particles with v_s from 0.007 mm/s up to 1.43 mm/s increases (in sum 54.5 %). It shows, that primarily medium-speed particles were washed off and entered the sewer network. The proportion of particles with $v_s \geq$ 1.43 mm/s (fast settling particles) increases only marginally (in sum 10.94 %). The proportion of the slowest particle class decreases drastically ($-$65.43 %), according to the increase of the medium speed fraction. The key message is here: the particle spectrum did not change from dry- to wet-weather inflow (same v_s-classes observed), but rather the proportion of particles, especially in the medium speed fraction.

Table 4. Results for settling measurement of sewage samples from PS Rostock–Schmarl, average change in class proportion from dry to wet samples

v_s range (mm/s)	$F(v_s)_{wet} - F(v_s)_{dry}$ (%)
$v_s \geq$ 40	+1.19
13.3$\leq v_s <$ 40	+1.55
3.3$\leq v_s <$ 13.3	+3.72
1.43$\leq v_s <$ 3.3	+4.49
0.33$\leq v_s <$ 1.43	+17.19
0.04$\leq v_s <$ 0.33	+22.98
0.007$\leq v_s <$ 0.04	+14.33
$v_s <$ 0.007	-65.43

Comparing the $F(v_s)$ curves to the literature [33, 48, 49], the particulate matter of the collected samples at PS Rostock–Schmarl settles significant slower, regardless to the inflow condition (dry, wet). This might be to design of the PS upstream sewerage system, as a separating sewer but with a main road runoff connected. Typical sewerage systems investigated in the literature are namely combined sewers or storm water systems [33, 34, 48, 49].

To get a first insight into the settling process inside the pressure pipe, the average settling velocity thresholds of the pipe ($\overline{v_{s,pipe}}$), one for each control mode and inflow condition, are shown in Figure 7 (vertical line plots). These were calculated from the overall average settling duration in the switch-off sequences over two years monitoring, in rule-based mode to 813 s (0.74 mm/s respectively) for dry weather inflow and 796 s (0.75 mm/s respectively) under combined inflow, while in two-point mode to 5454 s (0.11 mm/s respectively) for dry weather inflow and 4762 s (0.126 mm/s respectively) under combined inflow. Particle classes with $v_s \geq \overline{v_{s,pipe}}$, settle completely. With all four $\overline{v_{s,pipe}}$ values lying in the range of the medium speed particle classes, the changed particle composition due to the combined inflow affects the settling processes in both control modes,

but significantly reduced in rule-based mode. In rule-based control, higher $\overline{v_{s,pipe}}$ is the result of the formulated control rules (with pump flow = inflow, 17.13 h parallel mode in the studied period). Especially for a combined inflow, with pipe flow = inflow, the formulated control rules leading into shorter parallel pumping sequences (in sum 17.13 h in one year). In two-point control, pumps switch earlier into parallel mode (with pump flow $\gg$ inflow, in sum 141.7 h in one year), resulting in a lower $\overline{v_{s,pipe}}$ and a high sediment formation potential. Accordingly, a significant reduction in deposits formation has to be expected for combined inflow, while a slightly change for dry weather inflow is assumed.

3.3.3 Sediment Formation

An in-depth insight into the pumping process allows well-founded statements about the sediment formation. Detailed pumping data is analysed with Equation (5). The results are shown in Figure 8 within six single plots, where the left three plots show the results for the rule-based mode and the right three plots the two-point control results. The first row shows the average diurnal course of the settling duration. By the use of Equation (7), this course is transformed into a diurnal course of the settling velocity threshold $v_{s,pipe}$ (second row). Particle classes with $v_s > v_{s,pipe}$ settle completely. Knowing the settling properties of the transported raw sewage ($F(v_s)$) leads to the sediment formation profile, using Equation (6), see Figure 8, third row.

Both settling duration profiles (dry and wet) in the two-point control (upper right plot) show the invert course of a typical sewage inflow for an urban PS. This course is still in existence in rule-based mode (upper left plot), but because of the formulated control rules significantly smoothed. It results in reduced settling sequences, primarily during phases of low inflow (09:00 p.m. to 09:00 a.m. and in the afternoon). Pump pauses of 2.5 h during the night were reduced to $\approx$ 40 min by the rule-based control. Besides, it leads to a more balanced feed of the WWTP, by a significant reduction of peak loads.

The v_s threshold profiles are changing accordingly. Consistently, higher values resulting, with $v_{s,pipe} \geq$ 0.5 mm/s in the night phases (while $<$ 0.1 mm/s in two-point control). From $\approx$ 09:00 a.m. to 11:00 p.m. $v_{s,pipe}$ does not fall below 0.74 mm/s, with peaks up to 2.25 mm/s in the afternoon. Under combined inflow, nearly the same $v_{s,pipe}$ profile occurs, with peaks of 3.5 mm/s in the afternoon. High $v_{s,pipe}$ values in two-point mode were only reached during phases of high inflow, especially under combined inflow with peaks up to 1.75 mm/s. However, higher $v_{s,pipe}$ values under combined inflow (for both control modes) are counteracted by the faster settling characteristics during rain events. The respective sediment formation profiles clearly shows this situation. The sediment formation is dominated by the settling characteristics of the sewage.

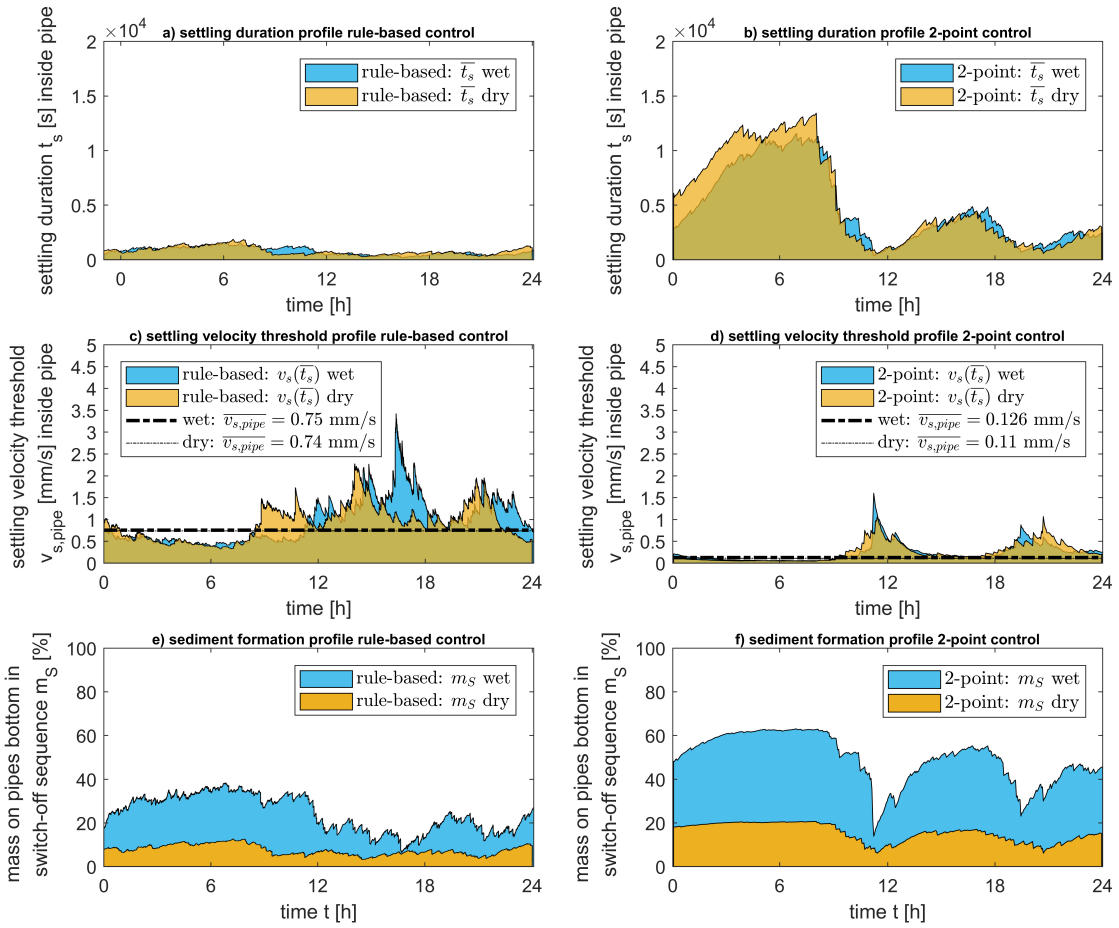

Figure 8. Results for sediment formation calculation after two years monitoring, average diurnal courses of the settling duration (**a** and **b**), settling velocity threshold (**c** and **d**) and settled mass (ms) on pipes bottom (**e** and **f**), for rule-based- (**a**, **c** and **e**) and two-point control (**b**,**d** and **f**).

Figure 8, third row shows the effectiveness of the control rules, especially under combined inflow. The peaks of the sediment formation could be reduced from m_s = 63 % (two-point control) to m_s = 39.4 % (rule-based control). Assuming the TSS content from Table 2 for combined inflow, the deposits amount, inside the whole pipe, decreases here from ≈ 398 kg ($A_{pipe} \cdot l_{pipe} \cdot TSS_{wet} \cdot 0.63$) to ≈ 240 kg ($\ldots \cdot TSS_{wet} \cdot 0.394$) by 158 kg. In contrast, the peak deposits decrease for dry weather inflow from ≈ 93 kg ($\ldots \cdot TSS_{dry} \cdot 0.2$) to ≈ 70 kg ($\ldots \cdot TSS_{dry} \cdot 0.156$) by only 23 kg. The difference in the control modes becomes clearer with the mean mass on pipes bottom: under rule-based control the mean mass calculates to 7.5 % (dry weather inflow) and 24.2 % (wet weather inflow), while under two-point control 15.4 % of the initial TSS content reaching the pipes bottom under dry weather inflow and 49.3 % under combined inflow. On average, the sediment formation is halved by the rule-based control. The timing of the peaks are marginally affected by the control modes (06:51 a.m. and 06:57 a.m. for combined inflow and 07:51 a.m. and 08:04 a.m. for dry weather inflow). So, the sediment formation (and the risk of blockages) is at its maximum in the morning, just before the feed to the PS rises again.

Conversely, the sediment formation is at its minimum at a high dry weather feed (e.g., 08:50 p.m. and 09:00 p.m.). The constellation of a slow settling sewage and short pump pauses leads to weak deposits. Only 16.4 kg reaching the bottom of the pipe in rule-based (…$TSS_{dry} \cdot 0.036$) mode and 27.6 kg in two-point control (… $\cdot TSS_{dry} \cdot 0.06$).

Summarized, the expected reduction of the sediment formation, from two-point to rule-based control, could be verified by linking the experimental settling characteristics to the high-resolution pumping data. It allows detailed statements about the diurnal sediment formation, which helps to improve the energy savings, as well as the more balanced feed to the WWTP, over 24 h.

3.3.4 Verification by Calculated Deposits Height

To ensure a trouble-free sediment transport beyond 24 h, the pipe curve was determined in a daily interval, using Equation (12). Subsequent, the calculation of the deposits height h_s, by Equation (13), shows the sediment layer thickness over the studied period of two years, see Figure 9.

The mean deposits height in rule-based mode was calculated to 0.137 m, while for two-point control to 0.174 m. Split into dry and combined inflow, the mean deposits height results in: rule-based dry h_s = 0.1375 m, combined h_s = 0.1372 m, two-point dry h_s = 0.1762 m, combined h_s = 0.1721 m. In rule-based mode, h_s is significantly reduced, due to longer pump intervals.

However, in both control modes the average deposits height under dry weather flow is higher compared to combined inflow. As seen in Figure 9, the rain events affecting h_s. Sediments washed-off from main roads or eroded inside an upstream sewer spilled to the PS, changing the settling characteristics and increasing the deposits height long lasting. Apparently, the sediments height increases especially the day after a rain event.

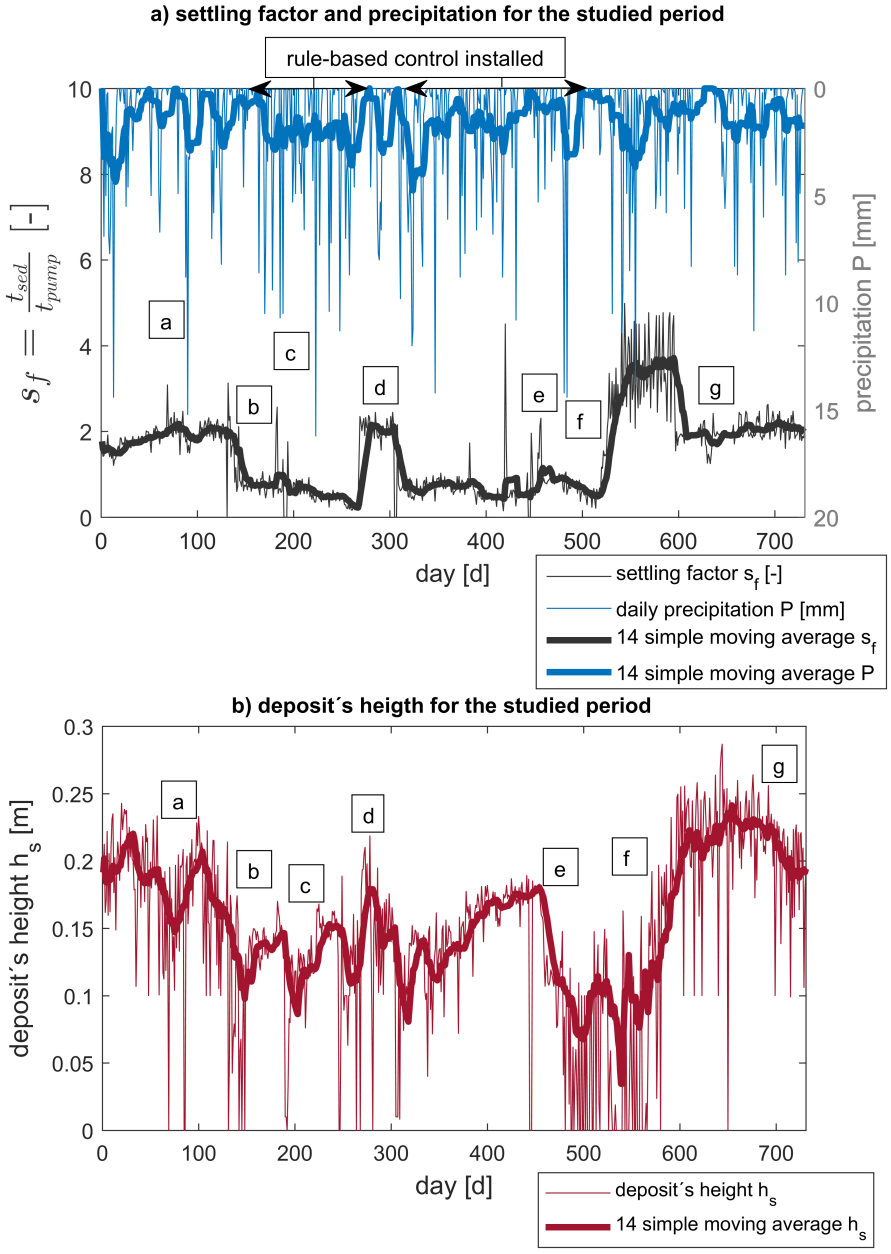

Figure 9. Results for calculation of the deposits height after two years monitoring, settling factor s_f (-) as ratio between the daily settling and pump duration and precipitation P (mm/d) (**a**) and deposits height h_s (m) including simple moving average over 14 d (**b**). a) significant increase of h_s after intense rain (15.2 mm/d), b) h_s reduced by parallel pumping (high s_f), c) increased h_s after intense rain (16.2 mm/d) in rule-based mode, d) increased h_s after re-installing two-point control in parallel with intense rain (33 mm/5d), e) decrease of h_s by parallel pumping after long rule-based period with smooth h_s increase, f) fast increase of h_s after re-installing two-point control, g) h_s normalized under two-point control mode to initial values.

Figure 10 shows the change of the deposits height by specific rain events for both control modes. The deposits height increases with rain events (at day 0), but especially after intense ones with reaching its peak one day after the rain event (day one). Within the two-point control, the deposits change at day 0 is at + 5 cm, while one day after this change is at + 5.5 to 6 cm (0.5 cm to 1 cm further increase to day 0).

On the following days, h_s decreases slowly (- 3 cm to day one). However, h_s is still higher compared to the day before the rain event (+ 3 cm). h_s at day 0 is reduced to + 2 cm, while one day after a rain event h_s increase again by 1 cm (+ 3 cm in total). On day two h_s decreases by 2 cm, but is still 1 cm higher to the initial value. So, the h_s increase is halved by the control rules (if inflow $>$ optimal flow, then operate at inflow) and the main effect itself is limited to day one after rain events.

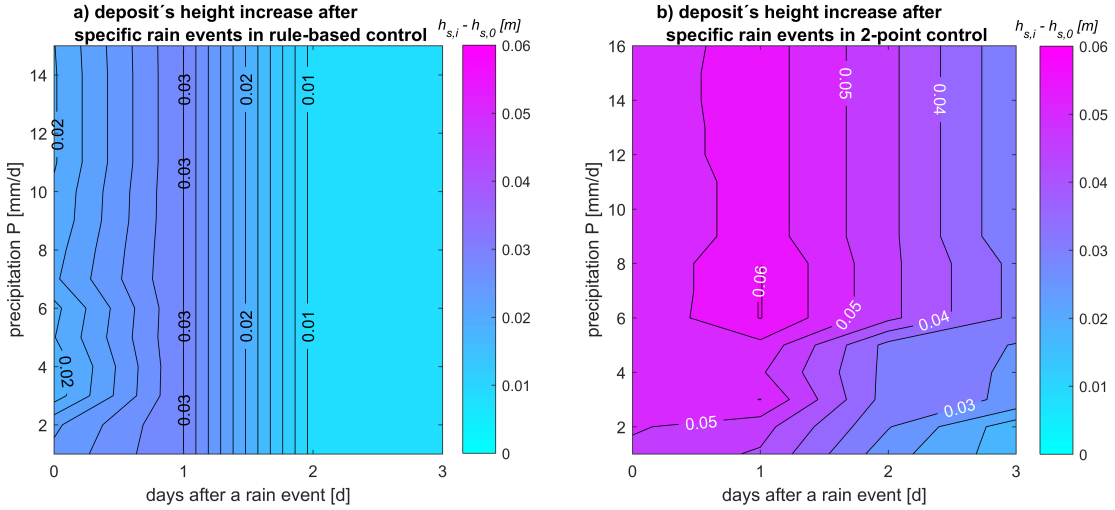

Figure 10. Results for the calculation of the delayed increase of the deposits height h_s inside the pressure pipe after specific rain events for rule-based (**a**) and two-point control (**b**).

As the rain events affecting h_s in both control modes up to several days, there are two fundamental findings: (i) washed-off particles entering the upstream sewer were not entirely spilled to the PS within the storm flow. Deposited particles in the upstream links are then spilled progressively to the PS, which creates the further increase at day one after the rain event. This effect is significantly reduced in rule-based mode. (ii) Slowly decrease of h_s starts after peak h_s increase reached at day one after a rain event, independently to the intensity of the event. Due to a stronger h_s increase in two-point control, this decrease phase lasts longer compared to rule-based mode. This long lasting change of h_s leads to a higher power consumption, due to a reduced cross section.

Next to the evidence of a significantly reduced settling potential, the gained information can be used to solve typical problems in the operation of wastewater facilities. As an example: To overcome increased sedimentation risk, operators often flush pipes randomly. A more targeted pipe flushing is more effective and efficient. Based on the discussed findings, pipe flushing is optimal on day two after a rain event (with no regard to the intensity). However, even after long periods without pipe flushing (see point e in Figure 9), priory deposited particles due to several rain events can easily be removed by parallel pumping.

The calculation of the deposits height clearly shows, that a long term energy saving pumping operation does not lead into an increased sedimentation risk, compared to a conventional pumping operation. In turn, it even reduces the sediment formation significantly, next to the energy savings. This statement can be verified by the results of Chapter 4, where the erodibility of settled raw sewage sediments itself was investigated. The results show that under the energy-efficient control, a resuspension of particles can be guaranteed.

A comparison to the literature regarding the monitoring of sediment heights is hardly available, thus the investigations mainly concentrating on open channel flow, e.g., [50, 51]. Furthermore the used techniques, such as imaging techniques or ultrasonic sensors [50] or sonar devices [51], differ greatly to the presented approach.

3.4 Conclusion

The paper presents settling experiments of municipal raw sewage, their interpretation and their application for the investigation of the sediment formation for an energy-efficient controlled pumping system. The presented results were verified by an indirect determination of the deposits height inside the pressure pipe. Based on the above discussed findings, the following conclusions can be drawn:

- the adapted experimental setup (VICAS/VICPOL-protocol) is robust and provides reproducible results
- settling behaviour from dry to combined inflow changes significantly in medium speed classes
- pump pauses decrease/pump sequences increase from conventional two-point control to rule-based control
- rule-based mode allows higher threshold values of settling velocity, especially for combined inflow, followed by a significant reduction of the sediment formation
- pipe curve observation leads to reliable findings about the deposits height
- daily variations in deposits height were registered, but no significant increase in sedimentation risk.

Summarized, no disadvantages arise over a long period by installing the energy-efficient operation mode. On the contrary, the energy saving pumping operation even lead to a reduced sediment formation potential under the investigated conditions.

Advances in sewage transport, such as energy optimization, are often driven urban water models. Those numerical simulations need accurate calibration data. Providing precise data enables concise models and as a result more sustainable solutions to be designed.

The presented experimental procedure and its subsequent calculation methods allow a precise determination of sedimentation data for raw sewage. It helps to characterize raw sewage more precisely and understand sedimentation processes in energy-optimized urban drainage systems. The published data is exemplary for a separate sewerage system (with storm runoff from main roads) in an urban region.

3.5 Advices for reproduction of the settling experiment

Throughout the process of design of the experimental set up, execution of experiments and data analysis, various experiences were made. These concern namely the sampling times and the sampling volume. It is very important to cover a wide spread of sampling times in order analyse all settling fractions. With the experimental setup, a good coverage for all samples was achieved with sampling times between 15 s and 24 h applying an exponentially increasing distance (e.g. 15, 45, 180, 420, 1800, 14 400, 86 400). The sampling volume is always a trade-off between a desired distinct fraction and reproducible results. A sampling volume of roughly 1/7th of the column volume (345 mL out of 2415 mL, depending on the number of settling columns) was found as best compromise. Additionally the following advices apply:

- Filling:
  - to produce reliable data it is essential that all columns are filled with the same wastewater sample with equal initial particle concentration and distribution. These demands a homogeneous particle concentration in the storage tank = efficient mixing)
- Sampling:
  - sample size must be large enough to observe an increase of TSS with settling duration
  - a large sample size tends to “smear” the fractions and will result in long filtration times. Sample separation is not advised, for reasons of accuracy
  - within a vacuum sampling system, time for build-up of suction head must be equal for all columns
- General:
  - successful sampling of all settled particles is by no means guaranteed. An important plausibility check is the comparison of total mass from the original sample and the cumulated mass from the experiment.

4 Erosion Characteristics of Raw Sewage: Investigations For a Pumping Station in Northern Germany Under Energy Efficient Pump Control

4.1 Introduction

The operation of wastewater facilities depends almost entirely on pumping processes, powered by electricity. Especially in flat and sparsely populated areas, wastewater-pumping stations for pressurized sewage transport take a large share of operation cost. Application of appropriate pump control offers a high-energy savings potential for those facilities. Usually, PS are, operated in a two-point control mode where pumps switch on and off at defined water levels. In shut on mode, the pump works with maximum design flow, which is in most cases higher than required. The related high flow velocity leads to high friction losses and unnecessarily high consumption of electricity.

The use of an electronic speed control solves this drawback of a two-point control. Within a case study at University of Rostock, an urban-influenced PS has been equipped with frequency pump controllers operated by an energy saving pumping strategy. The intention was to operate sewage pumps under an attempt to reduce consumption of energy as far as possible and to ensure safe system operation. The applied rule-based pump control aims at a reduction of friction losses by adapting flow to inflow conditions [14].

The recommended flow velocities for safe operation may often be underrun (0.6 to 1.2 m/s for self-cleaning effects at least once per day, according to [21]). Therefore, operators are confronted with finding a balance between attempted energy reduction and the safe operation of wastewater pressure pipes. In its worst case, blockage of a pipe entails costly repair works.

Safe operation depends on transport conditions inside the pipe, whereby flow velocity and bed shear stress are significantly responsible. Within the switch-off sequence (zero flow rate), particles settle inside the pipe. A previous homogeneous particle distribution over pipe cross-section changes to an increasing concentration from top to bottom.

If bed shear stress in switch-on sequence is below a critical limit (low flow rate), deposited particles only resuspend partially. In nominal condition, at design flow rate, bed shear stress is usually above the critical limit. However, for speed-controlled systems, this limit must be known to avoid harmful sedimentation.

The objective of this article is to define effects of energy saving pumping operation (low flow rate) on solids erosion behaviour within a pressure pipe system. The effect of a reduced flow rate on the safe transport of wastewater is not identified. To assess the transport conditions during the energy saving operation, this article pursues the following procedure:

- investigation of erosion behaviour of a typical, pure sewage dominated wastewater at the inflow side of a PS with a laboratory device (reaction chamber)
- determination of critical bed shear stress points after different settling periods: (i) critical bed shear stress (τ_{crit}), to define the beginning of an erosion event and (ii) a minimum required bed shear stress (τ_{100}) that relates to particle transport without sedimentation effects
- evaluation of the erosion behaviour by calculating the erosion rate.

4.1.1 Literature review

A large number of experimental designs for the assessment of erosion characteristics have been presented in the past. These designs split into in situ and laboratory designs. In situ designs are application dependent, e.g. modified for channel flow systems [52]. Original in situ devices have been presented by [53] (cohesive strength meter). Laboratory devices can be split into: (i) reaction chambers, as used in this work and (ii) flumes. The reaction chambers largely originate from [54]. In adaption to their EROMES-system, various designs have been developed specific for each targeted application, e.g. a laboratory design by [55], but also in situ devices, as EROSIMESS by [56]. An overview of different in situ devices is given by [57] and a comparison between in situ and laboratory design by [52, 58, 59].

4.2 Methods

4.2.1 Study site

The investigated PS is located in northern Germany in the city of Rostock. PS Rostock-Schmarl receives untreated domestic, industrial and commercial wastewater from approximately 40 000 inhabitants by a separate sewerage system of 80 km length. Additional surface runoff from main roads discharges to the PS, while roof runoff discharges into a storm water system. Four pumps, each with a power of 55 kW, raise the wastewater to the central WWTP in two cast iron pipelines (DN 600, each of 4100 m length).

Within the case study, two pumps were equipped with an energy saving pump control mode over the period of one year. The energy savings were achieved by reducing the flow with frequency controllers during nominal conditions (dry weather inflow) to an energy optimum. However, the reduction to an energy optimum results in reduced flow velocities and bed shear stresses.

To assess the erosion behaviour of the transported raw sewage of PS Rostock-Schmarl, samples were collected at the inflow channel (DN 1200) to the pumping well with a ladle during dry weather inflow. In total six samples, each with a volume of 25 L, were collected during the case study. Due to the mechanical treatment at the inflow, in the form of a rake with a wide-space bar opening (20 mm), coarse material was removed from the samples before processing.

4.2.2 Experimental design for erosion measurement

The presented experimental design is based on the work of [52, 60], both of which reference their constructions to [56]. The applied device for measuring erosion events (see Figure 11), consists of the following components:

- polyvinyl chloride (PVC) cylinder (diameter = 125 mm) as erosion chamber
- PVC fixed flange (diameter = 125 mm) as mounting fixture for the PVC cylinder
- PVC blind flange (diameter = 125 mm) as bottom component
- six PVC baffles for axial direction of flow conditions
- speed controlled stirrer motor (Heidolph RZR 2102) and a pitched blade propeller for applying bed shear stress
- extinction sensor (Semitec Dynamic Extinction Probe) for continuous erosion measurement.

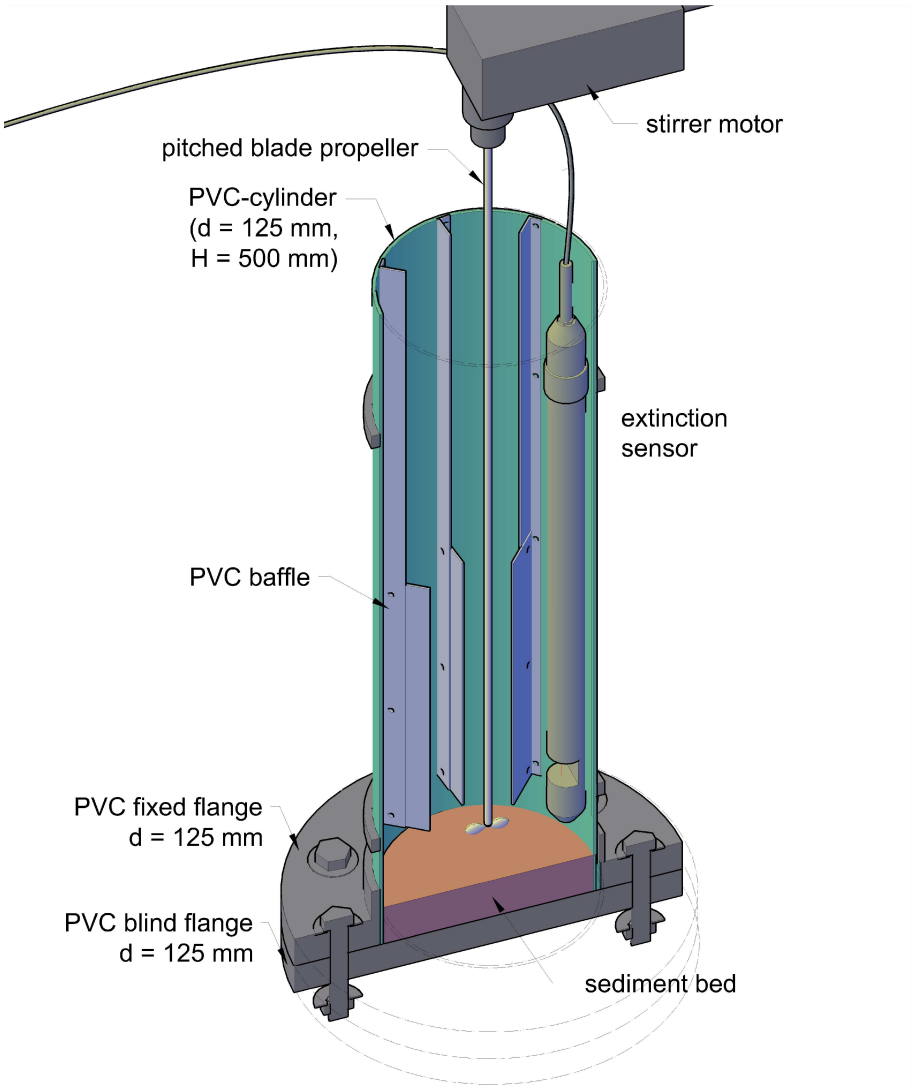

Figure 11. Experimental design for wastewater erosion measurement.

The transparent PVC cylinder (V = 6.14 L) is fixed to a revolving metal frame rack, which ensures stability during the stirring process. The stirrer motor is fixed above the PVC cylinder on the metal frame rack as well. Motor speed can be adjusted up to a maximum of 2000 rpm and is controlled by defined sequences using MatLab. The blade propeller is located 5 cm above the bottom. Six PVC baffles are attached to the PVC cylinder, which are constructed in two pieces (beam and baffle) to allow for adjustment of flow conditions.

The erosion of the sediments was measured continuously with an extinction sensor (Semitec Dynamic Extinction Probe). The extinction itself is defined as the negative logarithmic ratio between emerged and entered radiation. Thus, the erosion was measured as a light attenuation. The sensor is fixed vertically to the PVC cylinder and is located equal to propeller height. So, the extinction laser measures vertically, near to the sediment bed. Sensor and motor data have been logged in a time interval of 3 s.

4.2.3 Stirrer motor calibration

The device cannot directly measure shear stress (N/m^2). Hence, values of shear stress are derived from applied motor speed (rpm). For this, experiments of [61] (erosion of defined sand particle sizes) serve as the basis to relate present shear stress to applied motor speed. Within a mathematical approximation of Shields experiments from [62], critical bed shear stress τ_c (N/m^2) is calculated for each grain size d_m (mm) eroded by a specific Shields bed shear stress $\tau_{c,shields}$ (N/m^2), the density of applied sand ρ_S (kg/m^3), fluid density ρ (kg/m^3) and gravitational acceleration g (m/s^2), see Equation (15):

$$\tau_c = \tau_{c,shields} \cdot (\rho_S - \rho) \cdot g \cdot d_m \tag{15}$$

The calibration process itself was conducted by four observers and 11 different sand particle classes (d_m between 0.1 and 8 mm). After filling and complete settling of each individual class in the erosion cylinder, stirrer speed was increased stepwise. The erosion of each class was then detected from each observer when 10 % of the settled sediment bed eroded. The critical bed shear stress τ_c for the erosion of each class was calculated applying the approximation of [62] (Equation (15)). The respective stirrer speed noted at 10 % erosion then marks the calculated critical bed shear stress τ_c. Equation (16) shows the resulting calibration function.

$$\tau_{rpm} = 8 \cdot 10^{-6} \cdot rpm^{1.96} \tag{16}$$

4.2.4 Experimental procedure

Each experiment starts by filling the erosion cylinder with homogeneous raw sewage (V = 6 L) from PS Rostock-Schmarl. The subsequent settling sequence ends after one of the following periods: 20 min, 1 h, 4 h, 7 h, 14 h, 17 h, 24 h or 72 h. Once settling is completed, the erosion sequence with the stirrer motor starts at 20 rpm (0.003 N/m^2), increasing every 60 s by 10 rpm (0.0007 N/m^2) and ends at 400 rpm (1 N/m^2) automatically. In parallel, the extinction sensor measures continuously the light attenuation, caused by the eroded particles in the fluid section. It is assumed that the light attenuation is lowest at the beginning of each experiment, varies by a certain amount within each bed shear stress level and increases with each level up to a maximum value.

4.2.5 Determination of erosion data

The erosion behaviour of transported wastewater inside the pipe is described by three parameters: (i) the critical bed shear stress at beginning of erosion, described by τ_{crit} (N/m^2), (ii) erosion rate a (kg/(m s)) describing the dynamic of an erosion event per pipe length, (iii) bed shear stress value when all particles are completely resuspended, described by τ_{100} (N/m^2).

4.2.6 Determination of the critical and complete resuspension bed shear stress

The most common applied methods to identify critical bed shear stress points τ_{crit} have been presented by [63] (erosion events from dredge material) and [64] as well as [65] (erosion from river delta and tidal flats sediments). Following these methods, the course of measured erosion is expressed by either two power functions [63] or as a linear and a logarithmic function [65]. τ_{crit} is then defined as the point of intersection of the respective function set. Here, the latter method of [63] was chosen, due to smaller standard deviations for the reproduction of the erosion results τ_{crit} and τ_{100}.

The continuous extinction measurement provides information about the influence of any bed shear stress value to resulting erosion behaviour. So not only τ_{crit} can be calculated, but also τ_{100} by the same method. Similar to assessing τ_{crit}, τ_{100} is the result of the point of intersection of the equal function set, only shifted to the right on the measured extinction curve. Errors from the continuous extinction measurement were removed by Chauvenet's criterion.

As an example, Figure 12 shows the results for assessing τ_{crit} and τ_{100} for an erosion experiment after 4 h settling. If the left and right plot are joined, the measured extinction forms an s-curve, where four power functions were fitted. Following the respective functional expression, the points of intersection were calculated as 139.3 rpm and 224.3 rpm. τ_{crit} and τ_{100} are now calculated by the help of Equation (16) as 0.128 N/m^2 and 0.325 N/m^2.

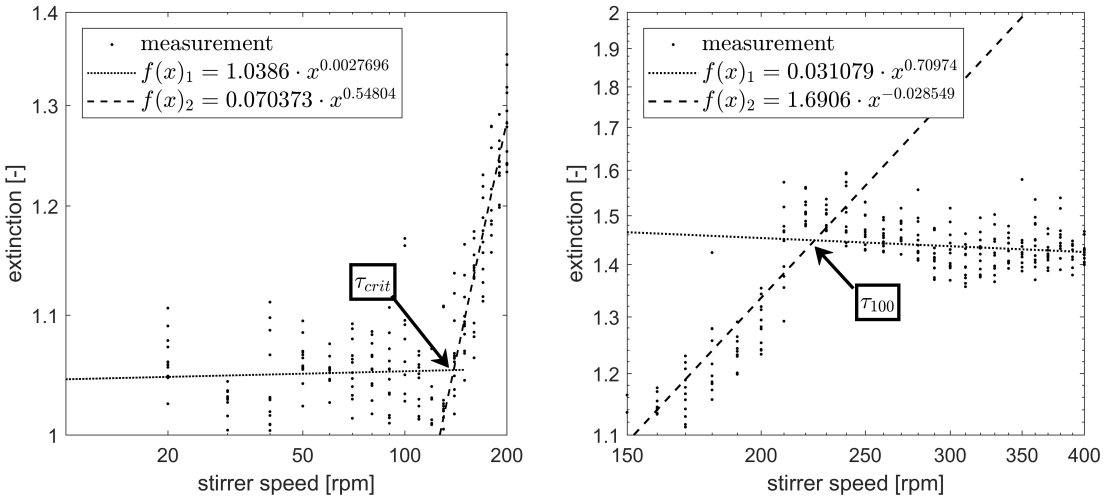

Figure 12. Extinction measurement, power function fit and τ_{crit} for an erosion experiment after 4 h settling (left) and for the same experiment τ_{100} (right).

4.2.7 Determination of the erosion rate

In order to calculate the erosion rate a (for the activation of sediments) (kg/(m s)), the particle concentration profile must be derived from the measured extinction curve for each procedure. This curve can be idealized in the form of a sigmoid function (Equation (17)), where the upper limit ex_{max} marks the maximum light attenuation (all particles are resuspended) and the lower limit ex_{min} the minimum light attenuation (certain proportion of particles settled), see Figure 13. The function itself can easily be adjusted using the least squares method with fitting parameters c (-) and p (s).

$$f(rpm) = \frac{ex_{max} - ex_{min}}{1 + c \cdot e^{-p \cdot rpm}} + ex_{min} \tag{17}$$

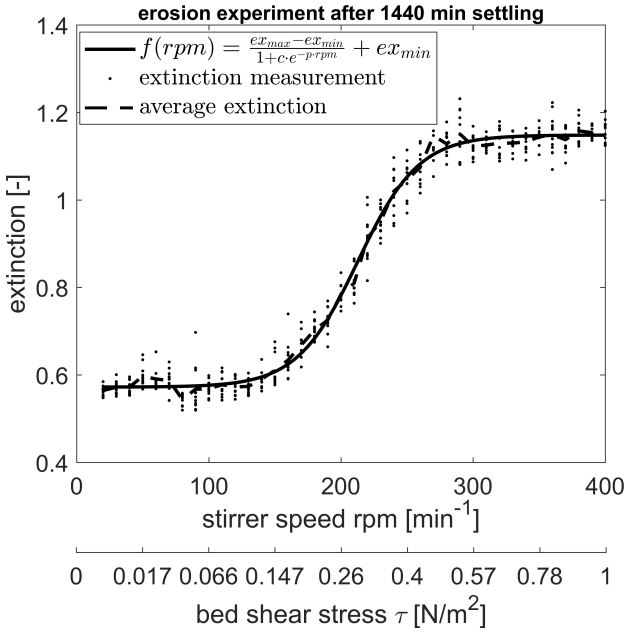

Figure 13. Exemplary extinction measurement for an erosion experiment after 24 h settling including sigmoid function fit.

When all particles are resuspended, the particle concentration inside the fluid is equal to the initial particle concentration of the raw sewage sample. Thus, the TSS profile of the erosion experiment can be displayed, if the initial TSS (kg/m^3) of the raw sewage sample is known. The initial TSS of the six collected samples was determined as 0.28, 0.33, 0.3, 0.3, 0.29 and 0.18 kg/m^3.

The erosion of the sediments is then described by Equation (18),

$$a(\tau) = d \cdot (\tau - \tau_{crit}) \tag{18}$$

with d (s), the erosion parameter, which indicates the strength of an erosion event, τ (N/m^2) the current bed shear stress value and τ_{crit} (N/m^2) the critical bed shear stress after a specific settling duration.

The value of a itself is obtained by solving the optimization problem in Equation (19). Here, d and additionally τ_{crit} are obtained by fitting a to the measured erosion of particles inside the erosion cylinder e_a (kg/(m s)).

$$\min_{d,\tau_{crit}} \sum_{i=1}^{n} e_{a,i} - a_i \cdot w_i \tag{19}$$

where n is the number of applied bed shear stress intervals (n = 39), $e_{a,i}$ the measured erosion rate at the interval i, w_i (kg) the particle mass on the bottom of the cylinder at the interval i (calculated as difference from the TSS concentration profile multiplied by cylinder volume). e_a itself is derived from the TSS difference by Equation (20), where Δt is the time difference of the bed shear stress increase interval (Δt = 60 s) and A_s is the surface area of erosion (m^2).

$$e_a = \frac{TSS_{i-1} - TSS_i}{\Delta t} \cdot A_s \tag{20}$$

4.3 Results and Discussion

4.3.1 Critical and complete resuspension bed shear stress

To ensure safe transport under energy-efficient control, the methods to determine bed shear stress points must be reliable. Since two different methods were used to determine τ_{crit} (power function set and erosion rate), reliability can be tested. If the results of both methods differ significantly, at least one of the methods is not applicable. If the results are similar, then the power function set is applied to determine τ_{100} as well. The results are illustrated in Figure 14. The boxplot on the left shows the bed shear stress values of the critical parameters, depending on used method and settling duration. The τ_{crit} values of both methods are in a similar region.

The mean-difference plot on the right shows the difference for each determined bed shear stress point in relation to the average of both methods. There is a maximum difference of 0.0928 N/m^2 (60 min settling) and an average of 0.01964 N/m^2 between both methods. The positive mean average shows that τ_{crit} is tending to slightly lower values when the erosion rate is applied. Next to this, only one point is located outside the confidence interval. Based on these facts, both methods are considered as applicable.

Figure 14 on the left also shows the average τ_{crit} and τ_{100}. A large τ_{crit} or τ_{100} value is the result of a long settling period with both settling (TSS increase) and consolidation effects (cohesion/compaction/biological solidification).

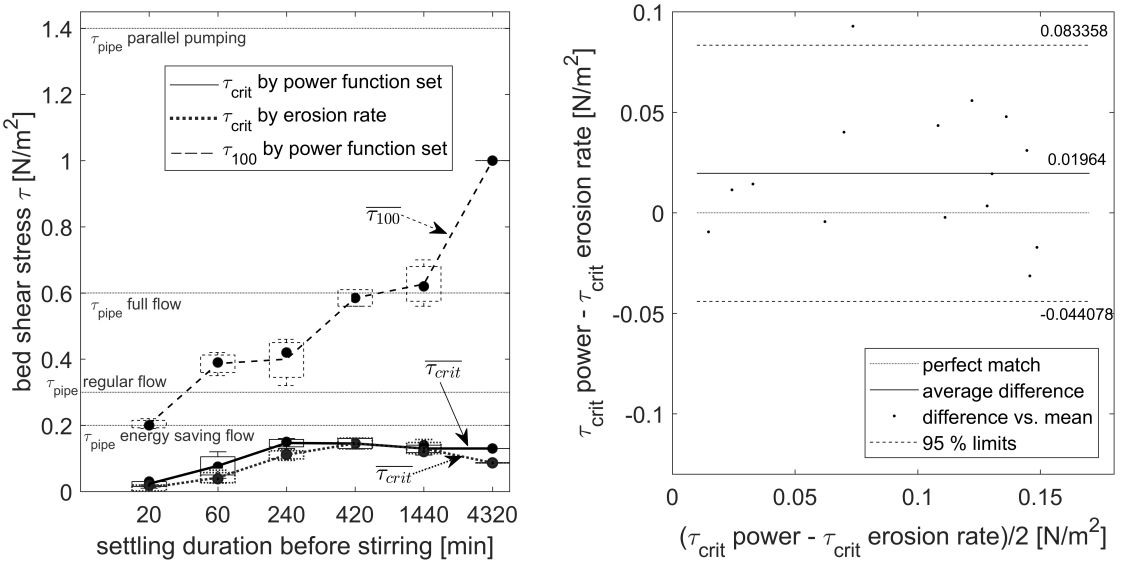

Figure 14. Resulting τ_{crit} and τ_{100} by laboratory erosion measurement, for different settling periods with raw sewage samples from PS Rostock-Schmarl (dry weather inflow) including the bed shear stresses inside the pipe under energy-efficient control, regular control, full flow and parallel pumping (left plot) and mean-difference plot of power function and erosion rate method (right plot).

Table 5 shows the maximum, mean and minimum shear stress values and standard deviation determined by the experimental procedure. Here, σ indicates the deviation of the critical parameter of the different sewage samples. Both critical parameters increase with settling duration. Especially after 20 and 60 min settling, a strong increase of τ_{crit} was detected (τ_{crit} from 0.02 N/m^2 at 20 min to 0.146 N/m^2 at 240 min). τ_{100} increases after 20, 240 and 1440 min strongly (from 0.2 N/m^2 at 20 min to 0.4 N/m^2 at 240 min up to 0.6 N/m^2 at 1440 min and 1 N/m^2 after three days settling). The TSS increase of sediments up to a settling duration of 240 min seems to have a decisive influence on τ_{crit} and τ_{100}. This increase seems completed after 420 min settling. From 420 min up to 1440 min, τ_{100} remains at a level of $\approx$ 0.6 N/m^2 and τ_{crit} remains constant also (0.13 to 0.146 N/m^2).

Progressive settling (TSS increase) is negligible after 420 min and does not yield further increase of τ_{crit} and τ_{100}. Subsequent effects responsible for further increase of τ_{crit} and τ_{100} are slower processes: cohesion, compaction, biological solidification. These consolidation processes become effective after 420 min, where τ_{100} increases up to 1 N/m^2. τ_{crit} is still small since even lighter and smaller particles settle on the surface of the sediment bed, which can therefore be eroded even more easily. This was also recognized as ‘first foul flush’ by [66, p. 5228]. In summary, the TSS increase is the first effect that increases τ_{crit} and τ_{100} and occurs in the first 4 h of the settling process. Cohesive interaction (particle–particle, particle–surface), gravitation (compressing in lower sediment layer) and biogenic changes of the sediment (conversion of organics by bacteria) work decisively slower and appear to be the main effects after 4 h settling.

Table 5. Results for critical shear stress measurement of raw sewage samples from PS Rostock-Schmarl after specific settling durations determined by power function method

		Settling duration (min)					
		20	60	240	420	1440	4320
max τ_{crit}	(N/m^2)	0.03	0.12	0.16	0.16	0.14	-
mean τ_{crit}	(N/m^2)	0.02	0.08	0.146	0.145	0.13	0.13
min τ_{crit}	(N/m^2)	0.01	0.04	0.13	0.13	0.11	-
σ		0.02	0.03	0.01	0.02	0.02	-
max τ_{100}	(N/m^2)	0.22	0.42	0.46	0.61	0.7	-
mean τ_{100}	(N/m^2)	0.2	0.39	0.4	0.58	0.62	1
min τ_{100}	(N/m^2)	0.19	0.35	0.32	0.56	0.56	-
σ		0.01	0.03	0.07	0.02	0.06	-

Both shear stress points decide on the energy saving intentions of PS Rostock-Schmarl. If the operational bed shear stress is smaller than τ_{crit} and τ_{100}, the pump control needs adjustments to guarantee a resuspension of the settled particles after a pump pause. Within the energy saving control, the flow rate and flow velocity decrease, from 90.3 L/s and 0.32 m/s in regular control, down to 75.3 L/s and 0.27 m/s respectively. The bed shear stress inside the pipe τ_{pipe} (N/m^2) is then calculated as 0.2 N/m^2 (while 0.3 N/m^2 in regular control, see Figure 14), based on the fluid density ρ (kg/m^3), the flow velocity v (m/s) and the friction factor λ (calculated after the Colebrook–White equation), with Equation (21).

$$\tau_{pipe} = \rho \cdot \frac{v^2}{2} \cdot \frac{\lambda}{4} \tag{21}$$

With a reduced flow rate, the pump pauses decrease as well. The average pump pause reduces from $\approx$ 64 min (regular control with higher flow rate) down to $\approx$ 20 min. As τ_{crit} and τ_{100} for 20 min settling are below the bed shear stress level of the energy saving pumping mode, a resuspension of the settled particles after the pump pauses is guaranteed, as well as a complete transport.

Larger pump pauses should be kept below 4 h. Especially at night (12:00 a.m. to 6:00 a.m.), with low inflow rates, the pump pauses increase. In regular control mode, these pauses last on average 2.5 h. These could be reduced by the energy-efficient control down to 40 min, so the bed shear stress of 0.2 N/m^2 is still higher than the respective τ_{crit} value. However, a total resuspension is not reached by the energy-efficient control. To tackle this problem, pumps should start-up to maximum power, in the case of PS Rostock-Schmarl with a flow of 137 L/s and a flow velocity of 0.5 m/s (respectively 0.6 N/m^2 bed shear stress, see Figure 14), before regulating the flow rate down to the energy saving flow. The deposited sediments by pump pauses over 7 h are only resuspended by parallel pumping, with a bed shear stress of 1.4 N/m^2 (respectively 212 L/s flow and 0.75 m/s flow velocity).

4.3.2 Erosion rate

In contrast to the single value of τ_{crit} or τ_{100}, the erosion rate $a(\tau)$, as a mathematical function, serves as a continuous description of an erosion event and contains information about its dynamics inside the pipe. The erosion rate in literature is always applied to a non-limited sediment bed [55, 66, 67], see Equation (18). Therefore, all erosion rates found in literature permanently increase with the bed shear stress. However, since the mathematical approximation of the erosion rate by Equation (18) neglects the available sediment bed (nonlimited sediment bed), it is expected that for a limited sediment bed, the actual eroded mass per time will be higher after longer settling durations than for shorter durations. This limitation is therefore defined as the available particle mass at the bottom, settled within the respective settling duration.

By solving Equation (19), the erosion rate $a(\tau)$ from Equation (18) is fitted to the measured erosion rate e_a from Equation (20) by multiplication with the available (limited) sediment bed on the bottom of the erosion cylinder (w). Here, additionally τ_{crit} is received. The resulting erosion rates e_a and $a(\tau, w)$ inside the erosion cylinder (limited sediment bed), as well as $a(\tau)$ for a non-limited sediment bed (Equation (18)), are shown in Figure 15 (one erosion rate as an example for each settling duration). Additionally, bed shear stress values for different control strategies as well as τ_{crit} and τ_{100} values are illustrated.

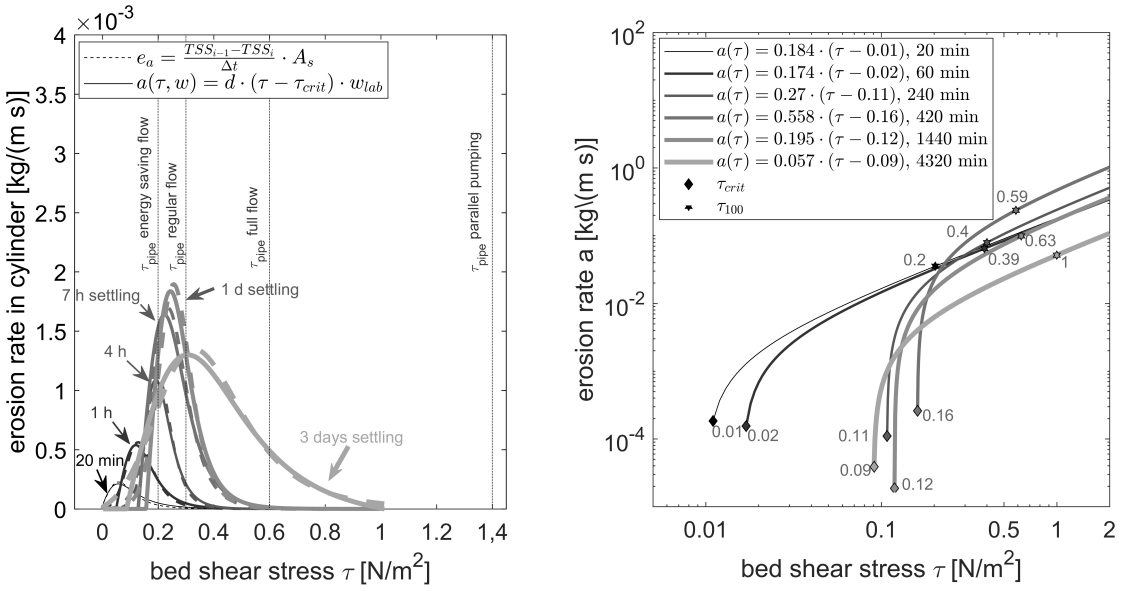

Figure 15. Measured erosion e_a (Equation (20)) and fitted erosion rate $a(\tau, w)$ (Equation (19)) inside the erosion cylinder (limited sediment bed) including the bed shear stress inside the pipe under energy-efficient control, regular control, full flow and parallel pumping (left plot) and erosion rate $a(\tau)$ (Equation (18), non-limited sediment bed on the bottom) for settling periods up to three days with raw sewage samples from PS Rostock-Schmarl, including erosion parameter d, τ_{crit} and τ_{100} (right plot).

With increasing bed shear stress inside the cylinder, more particles resuspend in the same time interval, until the erosion collapses at its peak (see Figure 15, left plot). The raw sewage represents a mixture of particles with different size. So, each peak shows the critical bed shear stress for the dominating particle fraction of the raw sewage. The peak is always located at the inflection point of the sigmoid function (Equation (17)). After the collapse, the erosion decreases and tends slowly to zero.

Comparing the curves with each other, it becomes clear that with an increased settling period, the function changes significantly. While the maximum erosion is initially located at 0.05 N/m^2 (for 20 min settling), the peaks shift towards larger bed shear stresses with increasing settling duration (up to 0.33 N/m^2 for three days settling). Here, the increase in erosion resistance of the sediment bed becomes visible as the peaks shift to the right. It is the result of the already mentioned TSS increase as well as effects of cohesion, gravitation and biological solidification. The different heights of the peaks can be related to the TSS increase as well. Since the erosion rate is linked to the available particle mass w on the cylinder bottom, the peak height increases with the settling duration. The highest peak was measured for 1440 min settling (1.8 g/(m s)). It represents an unconsolidated state with a high particle mass on the bottom. This, in turn, explains the smaller peak after three days settling (1.3 g/(m s)), where cohesion, gravitation and biological solidification have already contributed to the further increased mass on the bottom. Next to the lower peak, the larger spread of the three days curve can be explained by this as well. The structure of the sediment bed has changed. Previously easily erodible particles are now released from the bottom slowly.

The energy-efficient control of PS Rostock-Schmarl is not influenced by these effects, since the average settling durations between the pump pauses were reduced to $\approx$ 20 min (formerly 64 min in regular control). The bed shear stress for the reduced flow rate is above the 20 min τ_{crit} and equal to the τ_{100} value. The erosion rate inside the pipe is then in the range of 0.04 to 0.08 kg/(m s). For settling durations $>$ 20 min, τ_{100} is not reached. Hence, after larger pump pauses, the bed shear stress inside the pipe must be increased (start-up regular flow at 0.5 N/m^2), which ensures a higher and faster remobilization of the more resistant sediment bed.

Figure 15 on the right shows the erosion rates $a(\tau)$ for a non-limited sediment bed. The erosion rate increases in each case with bed shear stress. But at equal bed shear stress, $a(\tau)$ is smaller the longer the previous settling duration lasts. Especially the erosion rate for settling durations of three days is, above a bed shear stress of 0.2 N/m^2, significantly lower than others. For a bed shear stress of 0.2 N/m^2 (energy-efficient control), the erosion decreases from 15 g/(m s) after 20 min settling to 2 g/(m s) after three days settling by a factor of 7.5. This is due to an increased erosion resistance of the sediment bed, because of consolidation effects (cohesive interaction, compressing and biogenic changes).

It shows the rapidly changing erosion characteristics of raw sewage and the need to reduce pumping pauses to a minimum.

The idea of a non-limited sediment bed, as illustrated in Figure 15 (right plot), is incompatible with the erosion processes inside a pressure pipe. Due to the switch on/off regulation of PS, particles inside the pipe settle and resuspend alternately. The on/off regulation is regardless of the control mode. Thus, the sediment bed increases once in the switch-off sequences until a certain proportion of particles has been settled and decreases once in the switch-on sequences until the sediment bed is empty. When the sediment bed is empty, the erosion rate is zero, regardless of the bed shear strength. So the erosion process inside the pipe is more similar to the process inside the erosion cylinder (see Figure 15, left plot).

If the erosion rates $a(\tau)$ from Figure 15 (right plot) are now set as functions of the bed shear stress inside the pipe (τ_{pipe}) and the limited sediment bed on the pipe bottom w_{pipe} (kg), $a(\tau_{pipe}, w_{pipe})$ represents real-life conditions inside the pressure pipe. The sediment bed on the pipe bottom w_{pipe} was calculated similar to w (particle mass on cylinder bottom), assuming a TSS of 0.3 kg/m^3 (see Section 4.2). Figure 16 illustrates the calculated erosion rates $a(\tau_{pipe}, w_{pipe})$ over the complete pipe length (l_{pipe} = 4100 m) of PS Rostock-Schmarl after different settling durations of four different control modes in the pumps run-up phases: rule-based, modified rule-based, full power and parallel pumping. The run-up phases represent real values measured.

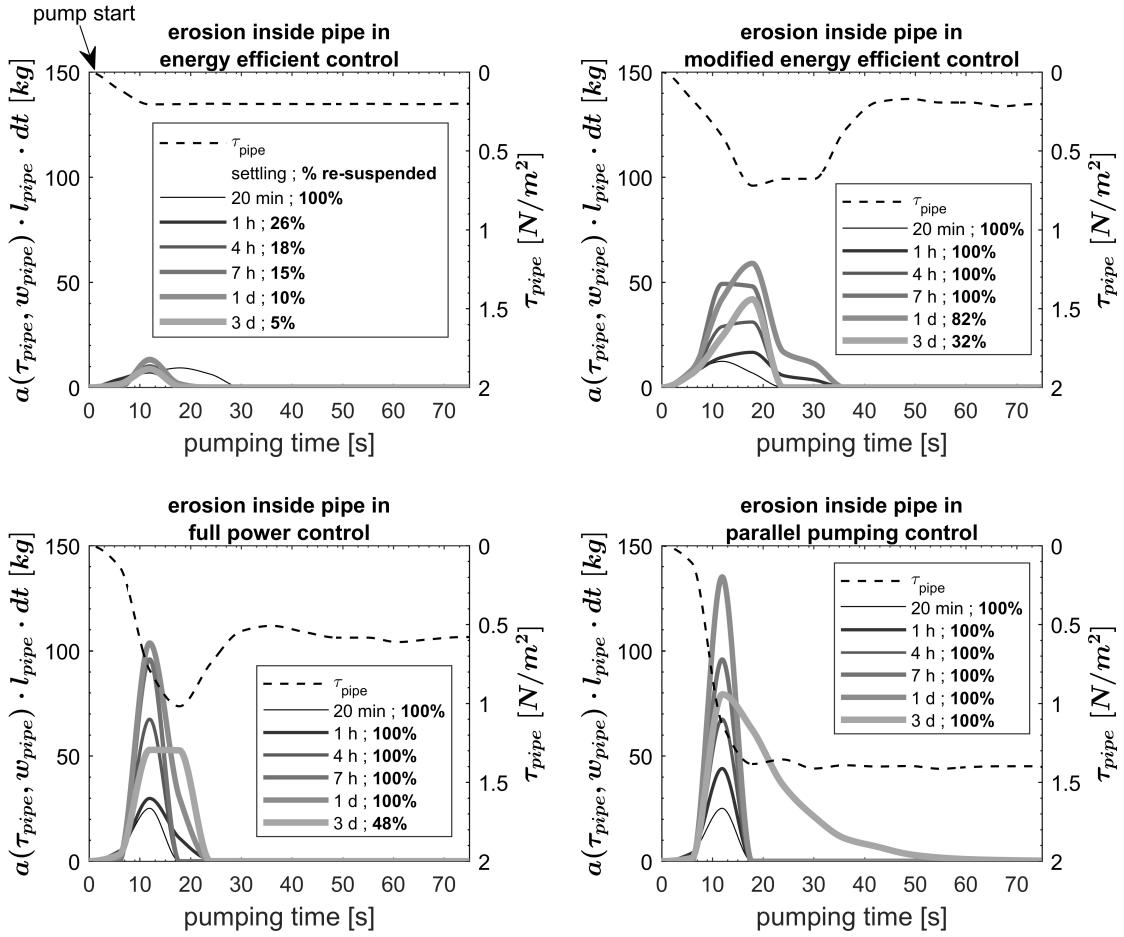

Figure 16. Calculated erosion of raw sewage inside the pressure pipe of PS Rostock-Schmarl in four different control strategies during pump run-up. Deposits erosion (solid lines, left y-axis) depends on previous settling duration. Resuspension of deposits (% values in legend) increases with the bed shear strength of the control mode (right y-axis).

Each pump start is followed by an erosion of the formerly settled sediments, if τ_{crit} is reached. The course of the erosion itself is similar to the erosion cylinder. The erosion is zero if the sediment bed is empty and also if the flow decreases before the sediment bed is completely resuspended. In usual energy-efficient control, pumps run up to the operation bed shear stress of 0.2 N/m^2 without a high-power run-up, see Figure 16 top left plot. The settled particles in a previous pump pause of 20 min (25.14 kg respectively) are then completely resuspended within 28.7 s. But in the case of larger pump pauses (e.g. at night, repairs, damages) the sediments are only resuspended partially. Adding a high-power run-up (up to 0.6 N/m^2) to the rule-based control enables complete re-suspension of settled sediments from pump pauses up to 7 h (top right plot). Deposits from 7 h settling are removed within $\approx$35 s (respectively 96 kg in sum). With settling sequences $\geq$24 h, full flow or parallel pumping is recommended. In parallel pumping control (1.4 N/m^2), a settled particle mass of 225.7 kg (three days settling) is completely resuspended after 75 s.

The results showing that a safe sewage transport and an energy-efficient control are not mutually exclusive. Due to the high erosion rates of the raw sewage, deposited sediments are resuspended fast (mostly < 30 s). A safe transport can always be guaranteed by adding a high-power run-up to the pump control, especially in energy-efficient controlled PS. In the case of PS Rostock-Schmarl the maximum pump pause duration is 40 min (night) under nominal inflow conditions. A pump run-up to full flow for 60 s followed by energy saving flow strikes a good balance between the energy saving intentions and a safe sewage transport.

4.3.3 Comparison with literature data

Erosion data from different investigations are mostly hard to compare, due to several reasons: sediments with different settling/consolidation times (minutes to years), different types of sediment (organic, cohesive, natural material), testing with different methods (cylinder, flume, ex situ, in situ). The critical values for incipient erosion of the raw sewage from PS Rostock-Schmarl is in the range of 0.01 to 0.146 N/m^2. The closest values were found in [66], with τ_{crit} values of 0.2 to 1 N/m^2 for deposited sewer sediment determined by a flume test and in [68], with τ_{crit} values of 0.44 to 1.02 N/m^2 by field tests under dry weather flow. As both tests were performed with already existing deposits, this might be the main reason for the differences.

Although test conditions differ greatly, the results from [68, 69], regarding the complete resuspension τ_{100}, are relatively similar. The critical values for a complete resuspension of the raw sewage from PS Rostock-Schmarl is in the range of 0.2 to 1 N/m^2. [68] have come to a range of 0.04 to 0.67 N/m^2, by a field test under dry weather inflow. [69] determined a value of 0.6 N/m^2, by field test in a combined sewerage system. Comparative literature data regarding the erosion rate are also hardly available: the erosion rate is determined either for different grain classes [70] or for different material (highly organically loaded like [55], admixtures of sediments like [67]). However, relatively comparable test conditions are provided by [66]. With up to 2.5 g/(m s) at 1 N/m^2 bed shear stress and up to 10 g/(m s) at 2 N/m^2 bed shear stress, the erosion rate is significantly smaller compared to the presented results. Depending on the settling duration, the erosion fluctuates at 1 N/m^2 between 8.6 g/(m s) (for long settling periods) and 40 g/(m s) (for settling periods < 4 h) and at 2 N/m^2 between 18 g/(m s) and 86 g/(m s) (see Figure 15). Decisively for the differences is the tested material. A general statement on the erosion properties of a wastewater, in the form of recommended values, is therefore hardly feasible.

4.4 Conclusions

The presented experimental procedure and its subsequent calculation methods allow a precise determination of erosion data for raw sewage (critical bed shear stress points, erosion rates). The published data are exemplary for a separate sewerage system in an urban region. This contributes to a more precise characterization of raw sewage and helps to further understand sewage and sediment transport processes in urban drainage systems. Todays tools to challenge increasing urbanization, energy optimization or storm water management, are often numerical simulations. The provision of precise data enables a more accurate calibration of urban water models and finally more sustainable solutions to be designed.

4.5 Advices for the reproduction of the erosion experiment

The experiences made during the entire laboratory experiment are listed below to facilitate a reproduction of the experiment. A major problem here is that, in contrast to the sedimentation experiments, there is no standardised procedure due to the complexity. A standardised procedure would help to make the results more comparable and thus provide better recommendations.

If the transport properties of the wastewater are to be determined, it makes sense to use the same sedimentation times as for the settling experiments, see Section 3.5. Furthermore, the settling periods can be adjusted to the expected duration of the pump pauses. This further increases the specificity of the results and saves time by avoiding unnecessary results. Additionally the following advices apply:

- Experimental design:
  - it is imperative that the test assembly is installed leak tight
  - especially the installation of the flow baffles requires the use of sealing tape
  - the cylinder must be attached to the fixed flange with PVC adhesive
  - a standard sealing ring between blind flange and fixed flange reduces further leakage
- Stirrer motor calibration:
  - the sand particle classes should have a small uniformity coefficient (commonly known as “well sorted”)
  - at least three observers should be used to calibrate the stirrer. The observation should be made individually
  - the horizontal and vertical positioning between the stirrer and the erosion cylinder cannot be changed after calibration
  - calibration procedure with final experimental setup (including sensor, sampling tubes, etc.)

- Experimental procedure:
  - fresh sample material should be used if possible. The remaining amount for further processing should be stored in the refrigerator. When taking samples, ensure that the sample volume is as high as possible
  - depending on the duration of the preceding sedimentation phase, it is recommended to repeat the procedure a maximum of three times with the same sample material. This prevents a change in the sample material
  - the step size of the speed increase also determines the accuracy of the measurement. A step size of 10 rpm is useful, since the test duration must also be taken into account here
  - each stirrer speed level should be held for at least one minute before further increasing. This guarantees a proper measuring process with sufficient measured values for later error calculation
  - thorough cleaning of the erosion cylinder, stirrer and sensor after a test procedure guarantees the validity of the calibration function.

5 Sediment Transport in Sewage Pressure Pipes, Part I: Continuous Determination of Settling and Erosion Characteristics by In situ TSS Monitoring Inside a Pressure Pipe in Northern Germany

5.1 Introduction

The physical characterization of sewage is indispensable for optimization efforts in all areas of wastewater management. Pumping processes are usually necessary in sewage and storm water transport. Because of their frequent use, all related processes offer high optimization potential, to name only a few: sediment transport, energy consumption and storm water management.

The main key to process understanding and optimization lies in data quality and quantity. Advanced optimization tools (e.g., numerical simulations) are especially data greedy. Quality and quantity varies with the data collection method: either ex situ or in situ. Ex situ methods are primary laboratory experiments. Experiments simulate real world conditions as accurately as possible and subsequently transfer the results into a representative model region. For example, most stream tests try to simulate more-or-less real-life conditions.

The advantage of in situ methods is the proximity to real life. Thus, an imitation is not required. To measure undisturbed processes, impacts on the system should be kept by a minimum.

Erosion and sedimentation of particulate matter in sewage are the dominating physical effects regarding the above-mentioned themes (sediment transport, energy consumption, storm water management). In the past, settling and erosion behaviour have been determined by ex situ experiments (Chapter 3 and 4 and [32, 33, 50, 55, 71]). In case of Chapter 3 and 4, several laboratory experiments were conducted to describe erosion and settling behaviour of the raw sewage inflow to a PS in an urban drainage system in Rostock (northern Germany). Consequently, the derived results are only temporal snapshots of continuous highly dynamic sewer processes.

A continuous description based on permanent (in situ) measurement allows, by far, more statements about raw sewage transport behaviour. In this study, the transport behaviour inside a pressure pipe is of interest. Therefore, the measurement is located directly inside the pressure pipe. Thus, the pipe itself serves as the reaction chamber for the experiments.

This work aims at an in-depth characterization of the erosion and settling behaviour of raw sewage by in situ TSS online measurement for the period of one year. Providing a large amount of data helps to increase the accuracy of transport simulations and improves the efficiency of the sewer system. The following three objectives are defined:

- determine applicability and quality of an in situ TSS online measurement system inside a pressure pipe
- characterize raw sewage erosion and sedimentation behaviour under dry weather inflow continuously by TSS online monitoring
- identify mechanisms changing the transport behaviour and characterize modified erosion and sedimentation.

5.1.1 Literature Review

In situ measurements in the field of urban drainage concentrate usually on non-pressure systems (open channel flow), often in the context of combined sewer overflows and pollutant loads in combined or storm sewers [72–77]. Continuous monitoring systems are almost exclusively used for the calculation of loads or fluxes. Further data analysis, regarding solids transport behaviour, is often not been conducted. An exception is provided by [76–78], all calculating mass curves from online data. An in situ monitoring study, dealing with continuous TSS measurements within pressurized systems, have not been published as known to the authors.

The characterization of sediments by continuous measurements is mostly applied within ex situ laboratory experiments: [50] performed ex situ tests with wastewater to determine the sediment accumulation in a pilot flume (diameter = 300 mm open channel flow, average discharge = 4 L/s) using the same TSS sensor as used in this study (Hach Lange Solitax). Another example is [71], where sediments were collected for flushing experiments in the laboratory, equipped with a continuous turbidity measuring system. Similarly to Chapter 4, where a continuous turbidity measurement was used to determine the erosion characteristics inside an ex situ laboratory device.

The same sensor (Hach Lange Solitax) was also used by [72] inside a combined sewer (in situ) to assess the dynamics of erosion and sedimentation events (load calculation).

Hybrids between ex situ and in situ are provided by [75, 76], where the monitoring sensors were mounted in external tanks or flumes supplied by a pump from a sewer.

The applicability of online sensor data for urban drainage problems and related uncertainty was investigated with large effort by: [74–76, 78–80]. The majority of the data processing methods in this study based on these publications.

One of the main differences to previous studies lies in the measurement interval (here 5 s). Sometimes, daily measurements were used as in [50], but with regard to systems dynamics, most studies used short intervals as in [75, 78] with a 2 min time step, [71] with 20 s, or [73] with 15 s.

5.2 Materials and Methods

5.2.1 Study Site

One of the main PS in the city of Rostock (≈ 200 000 inhabitants) is PS Rostock-Schmarl, conveying raw sewage from ≈ 40 000 inhabitants. A special technical feature of the upstream, usually separating sewer system is the connection to main roads storm water runoff. The storm water system itself collects runoff from roof discharge and secondary roads. Whatever the inflow condition to PS Rostock-Schmarl is, the incoming sewage is filtered at first by a rake with a wide space bar opening (20 mm) before it is transported directly to the central WWTP by four pumps (each of 55 kW) in two cast iron pipelines (diameter = 600 mm), each over 4500 m length. A schematic view of the catchment area and the PS in Figure 17 illustrates the study setup.

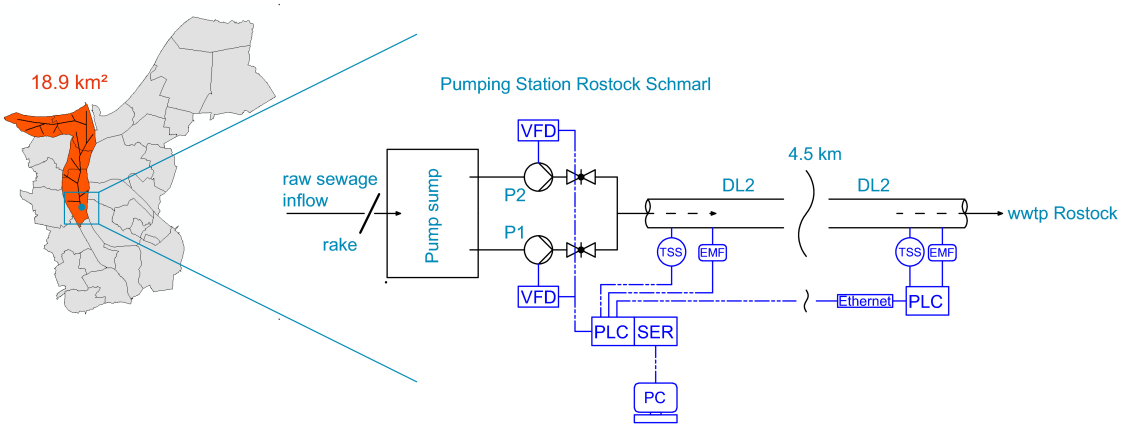

Figure 17. Visualization of the catchment area (18.9 km²) in Rostock (Germany) including a schematic view of the control and monitoring system during the study. The raw sewage inflow passes the rake and is collected inside the pump sump. Pumps P1 and P2 then conveying the raw sewage directly to the central WWTP in pressure pipe 2 (DL2). P1 and P2 are controlled over a variable-frequency drive (VFD) from a PC (connected over a serial port (SER) to the programmable logic controller (PLC)). The VFD adjusts pumps motor speed according to the control strategy (see Chapter 3 and 4 and [14]). All values from TSS sensors (TSS) and electromagnetic flowmeters (EMF) are stored in the PC.

5.2.2 In situ TSS Monitoring

For a studied period of one year, pumps P1 and P2 were controlled by a PC to perform a rule based, energy saving control strategy (see Chapter 3 and 4 and [14]). The sediment flux was monitored by online TSS measurements at the in- and outflow side of pressure pipe DL2. Table 6 shows the TSS sensors technical data. The sensors itself are shown in Figure 18.

Table 6. Technical data of TSS sensors

Sensor	Controller	Parameter	Measuring range	Installed and measured duration	Interval	Service	Num. of calibration processes	Wiper self-cleaning interval
Hach Lange Solitax inline Sc	Hach Sc 200 & Sc 1000	Turbidity, TSS	0.001-4000 FNU, 0.001-50 g/L	343 days installed, 292 days measured	5 s	1 per month	5 processes with 73 samples	15 min

Furthermore, the following parameters were monitored every 5 s over one year: pump sump level (m), inflow to the PS (L/s), pumps power input (kW), frequency F of the VFD (Hz), engine speed (1/min), pressure in DL2 directly after the pump (bar), flow Q_{pipe} in DL2 (L/s).

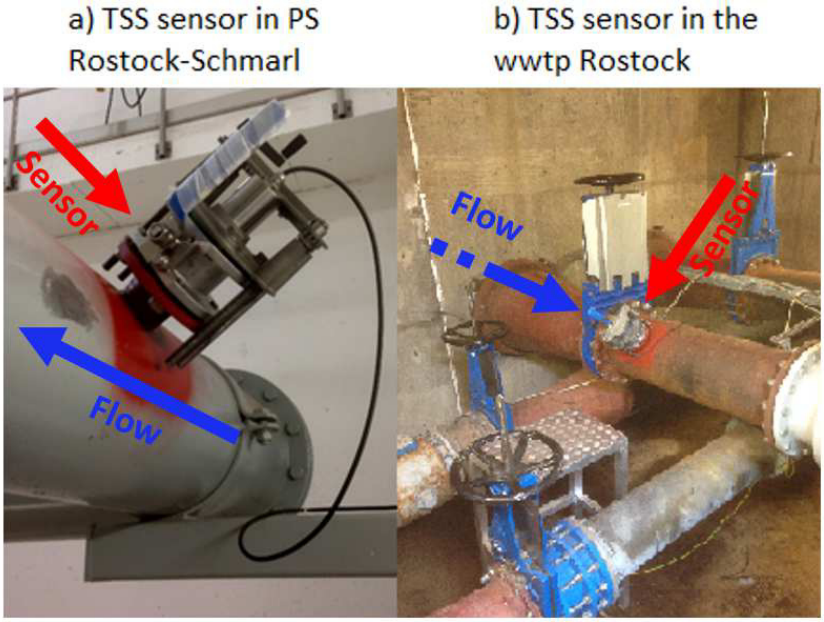

Figure 18. TSS sensors for monitoring sediment flux in pressure pipes. (**a**) TSS sensor in PS Rostock-Schmarl at the pressure side of the pump. (**b**) TSS sensor in the central WWTP Rostock at the outflow side of the pressure pipe.

5.2.3 Sample-specific Sensor Calibration

TSS eventually calculated from the turbidity by an internal factory calibrated formula. Commonly, diatomaceous earth is used for the internal calibration process.

To adjust the TSS sensor values to the local raw sewage composition of PS Rostock-Schmarl, a sample-specific calibration based on a correlation method was repeated five times, with 73 separate raw sewage samples in total. The samples are collected with a ladle from the inflow channel, just before the rake. Afterwards, the samples are filtered, according to the rakes space bar opening of 20 mm and subsequently separated into cylinders of a small volume (2.5 L). In the second step, the TSS concentration is artificially modified to obtain different cylinders with different TSS values. Therefore, the TSS concentration is decreased by mixing several dilutions using clear water, while settling increases the TSS values. This procedure provides a wide range of TSS values for calibration process. Thus, the resulting calibration function is applicable for a broad spectrum of TSS values without extrapolation. After that, a sample is filled into the calibration cylinder and continuously mixed by a magnetic stirrer. Next, the sensors are demounted from the pressure pipe and placed into the calibration cylinder. Subsequently, three sensor TSS values are noted from the controller board. Finally, each sample is analyzed for TSS by three-fold determination in the laboratory (analysis according to [47] by filtration and weight loss).

5.2.4 Fit Calibration Function and Analysis of Sensor Data

Sensor data must be validated before further processing into erosion and sedimentation behaviour. Various literature deals with error assessment and validation of sensor data to find a correlation function and at least a true area of measured values with respect to uncertainties [76, 79]. According to these publications, the determination of uncertainties was processed after the commonly used 'Guide to the Expression of Uncertainty in Measurement' [81]. Therefore, the following data analysis scheme was applied:

1. Fit calibration function (TSS to TSS) with errors in y and x direction using the total least-squares regression
2. Calculate function parameters uncertainties by Monte-Carlo simulation for 95 % confidence level
3. Transform original sensor data TSS_{sens} by the calibration function into calibrated sensor data TSS_{cal}
4. Remove TSS_{cal} values $>$ 1000 mg/L, based on local operator's expertise
5. Further error assessment by Walsh's outlier test

First, the calibration function is performed by the total least-squares regression. By this, errors in both directions, resulting from the TSS determination inside the laboratory (y) and the TSS measurement by the sensor (x), were accounted for the optimization problem. The resulting regression function is a first order polynomial function with the slope b (-) and intercept a (mg/L). The function calculates the calibrated TSS values TSS_{cal} (mg/L) from the original sensor data TSS_{sens} (mg/L), see Equation (22).

$$f(TSS_{sens}) = b \cdot TSS_{sens} + a \tag{22}$$

Second, the function parameters uncertainties are calculated for 95 % confidence level by Monte-Carlo simulation in MATLAB (see also [76]). The calculation of a combined uncertainty resulting from the sensor measurement itself and the field influences (i.e., installation site) has been omitted. It is assumed, that field influences are already included in the sensor output. It is furthermore assumed that the field influence occurring during the in-pipe measurement is equal to the field influence occurring during the calibration process outside the pressure pipe.

Third, the original sensor output TSS_{sens} is transformed into calibrated sensor data TSS_{cal} to obtain the estimated TSS values by Equation (22). Furthermore, the 95 % confidence interval is calculated based on the function parameters uncertainties.

Fourth, all TSS values >1000 mg/L are removed from the calibrated data set. The criterion based on the local operator's expertise.

Fifth, measurement errors are cleaned by the Walsh outlier test. The test requires no specific distribution, can easily be coded, enables fast computing and detects outliers greater and less than the remaining values.

5.2.5 Determination of Settling- and Erosion Data

After calibration and error assessment, the final data processing followed, before determination of settling and erosion data is conducted. The transport characteristics are analyzed based on TSS sensor values in PS Rostock-Schmarl. The TSS sensor values from the central WWTP are used in Part II as reference for the sediment transport model.

The data processing scheme is visualized in Figure 19 and is described below. To maintain the data for determination, the complete data set (Figure 19a) must be split up in two parts: (i) the erosion data-part (Figure 19b), containing data while one of the two pumps is working, (ii) the sedimentation data-part (Figure 19c), containing data logged while pumps are shut off. Each data-part (erosion-part and sedimentation-part) is further split up into separate erosion (Figure 19d) and sedimentation events (Figure 19e). This is necessary, because the characterization is at least a mathematical approximation of a single erosion and sedimentation event. These single events are now the basis the mathematical description.

The sedimentation of solid fractions inside a fluid can be described by a settling velocity distribution (see Chapter 3 or [33]). However, since the turbidity sensors are not able to detect single particle fractions, the following approximation is applied. The settling events are described as a decay process, modeled by a differential Equation (23).

$$\frac{dC}{dt} = -\alpha \cdot C \tag{23}$$

Its solution is an exponential decay, called settling rate $C(t)$ (mg/L), see Equation (24). With t (s), the settling duration in each pump pause, C_0 (mg/L), a fixed value relating to the first TSS concentration in each single sedimentation event, C_{rest} (mg/L), the final solids concentration at the end of each single setting event and the exponential decay rate α (1/s), which is the key parameter to describe the settling behaviour.

$$C(t) = C_0 \cdot e^{-\alpha \cdot t} + C_{rest} \tag{24}$$

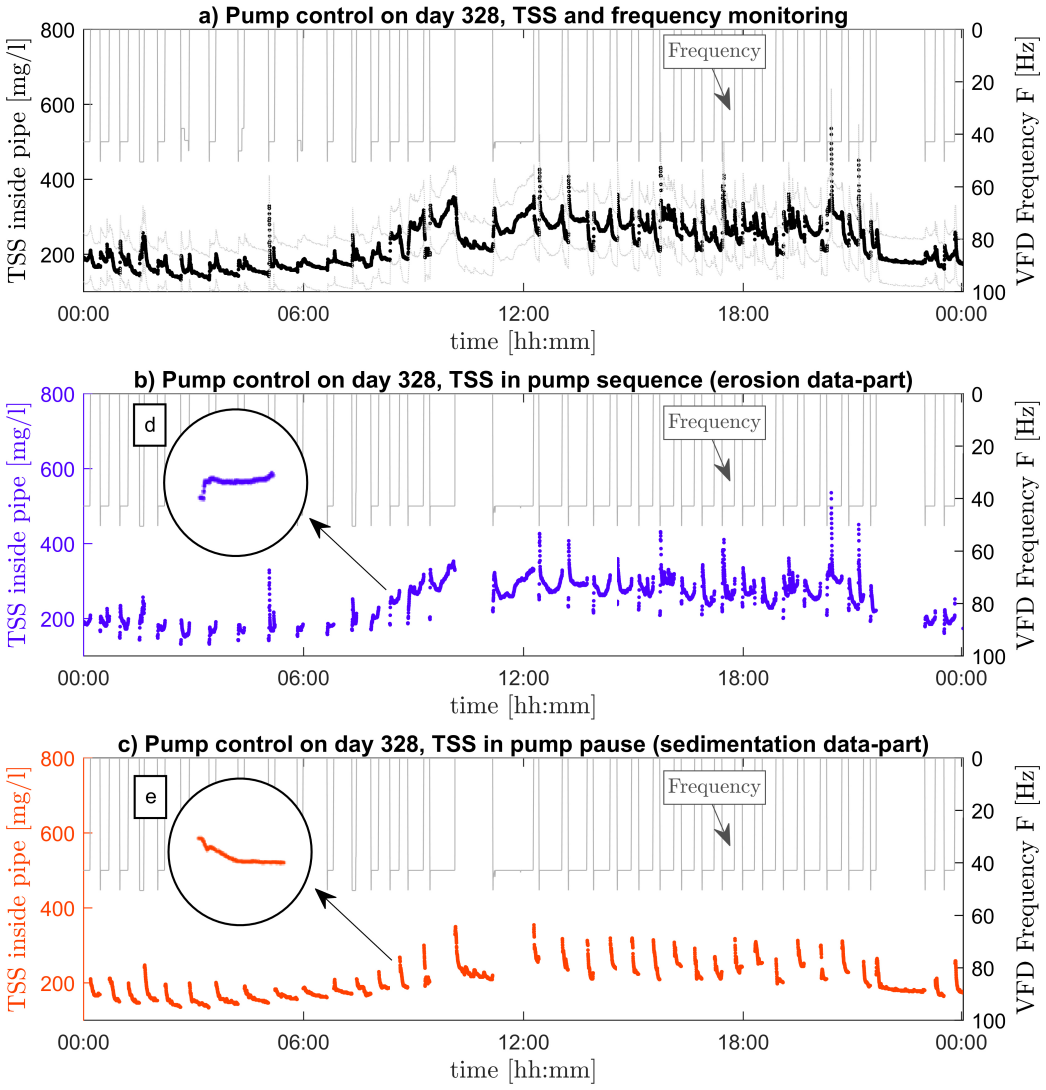

Figure 19. Data separation scheme: monitored TSS data (**a**) is split into an erosion- (**b**) and a sedimentation part (**c**). Frequency data from both VFD (for P1 and P2) is used as decision criterion for data separation (*if VFD1 and VFD2 = 0 then settling sequence, else erosion sequence*). The separation into single erosion (**d**) and sedimentation events (**e**) is based on a time difference between each value. If the time difference is larger the logging interval of 5 s (see Table 6), a single event is detected and separated.

Within each time step t, a proportion of the initial TSS concentration C_0 settles to pipes invert, according to the decay rate α, which is received by solving the optimization problem in Equation (25). With n, the number of values in each settling sequence and TSS_{cal} (mg/L), the measured and calibrated TSS concentration inside the pressure pipe.

$$\min_{\alpha} \sum_{i=1}^{n} (TSS_{cal,i} - C_i)^2 \tag{25}$$

The erosion events are described according to Chapter 4. The measured erosion rate e_a (kg/(m s)) inside the pipe is calculated from the TSS concentration after pumps start (shown in Figure 19d), by Equation (26). With $TSS_{cal,i} - TSS_{cal,i-1}$ (mg/L), the TSS difference between measurements, Δt (s), the time difference between measurements and A_s (m^2), the surface area of erosion (set to 1 m^2 for better comparability).

$$e_a = \frac{TSS_{cal,i} - TSS_{cal,i-1}}{\Delta t} \cdot A_s \tag{26}$$

The measured erosion rate e_a can be described as a function of the current bed shear stress, called erosion rate a (activation of sediments) (kg/(m s), see Equation (27). With τ_{pipe} (N/m^2), the current bed shear stress, τ_{crit} (N/m^2), the critical bed shear stress where erosion starts and d (s), the erosion parameter, which describes the strength of the erosion (equal to slope of the first order polynomic function).

$$a(\tau_{pipe}) = max\big(0, d \cdot (\tau_{pipe} - \tau_{crit})\big) \tag{27}$$

τ_{pipe} is calculated by Equation (28), based on the fluid density ρ = 1000 (kg/m^3), the flow velocity v (m/s) and the friction factor λ (calculated after the Colebrook–White equation).

$$\tau_{pipe} = \rho \cdot \frac{v^2}{2} \cdot \frac{\lambda}{4} \tag{28}$$

The height of τ_{crit} depends on several parameters, as the formerly settling duration (higher τ_{crit} values for longer settling duration) and the composition of the sewage (organic components raises τ_{crit} due to biogenic changes). For a detailed description of τ_{crit} see Chapter 4. The erosion rate a is adjusted to the measured erosion rate e_a by solving the optimization problem in Equation (29).

$$\min_{d,\tau_{crit}} \sum_{i=1}^{n} (e_{a,i} - a_i \cdot w_i)^2 \tag{29}$$

To consider real life conditions inside the pressure pipe, w (kg), the current particle mass on pipe bottom is multiplied with the erosion rate a. If the sediment bed is empty ($w = 0$), the erosion rate a becomes zero. By solving Equation (29), the function parameter d and additionally the critical bed shear stress τ_{crit} is received.

5.3 Results and Discussion

5.3.1 Sensor Calibration Results

The result of the calibration processes is shown in Figure 20. The laboratory TSS correlates to each sensor TSS by a first order polynomic function.

With the resulting calibration function, the sensor values are converted into the laboratory values, before further processing. The calibration functions are fitted with a R^2 value of 0.84 for TSS sensor PS Rostock-Schmarl and with a R^2 value of 0.85 for TSS sensor at the central WWTP Rostock. As found in literature, usual calibration functions used same functions with R^2 values between 0.83 and 0.92 [72] (calibration to turbidity) or, as already summarized in [79], between 0.80 and 0.95 [79] (calibration to turbidity). Reference [73] obtained a calibration function, for the same sensor used in this study, with a R^2 value of 0.94.

As one can see in the functions slope b, the measured values of both sensors are too high. Furthermore, we obtained two different calibration functions, although both sensors are identically and the same TSS samples used for calibration. A reason might be found in the differences to the internal calibration process. The used material for internal calibration differs from the raw sewage, as well as the calibration cylinder geometry. Another reason might be in the different controller devices used for the sensors. Differences in the internal signal processing may cause different values.

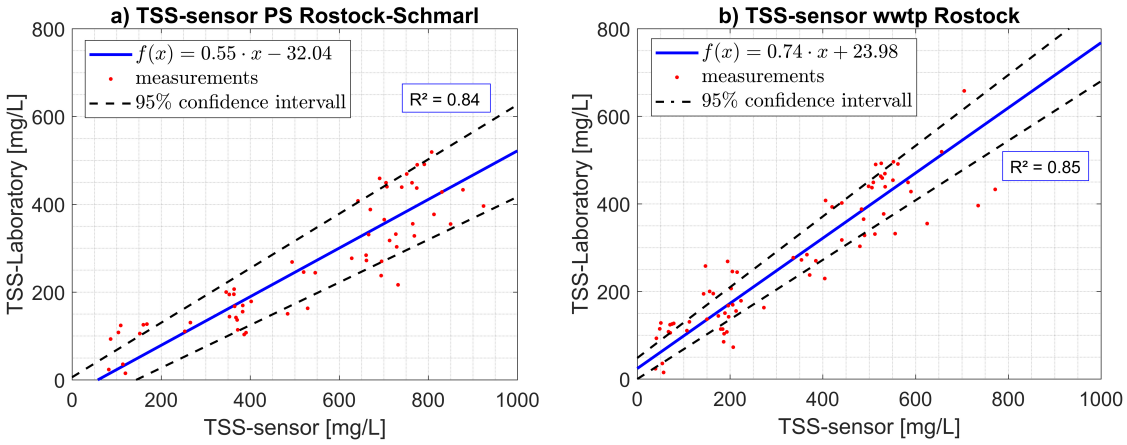

Figure 20. Calibration functions for calculating laboratory TSS values from in situ measured sensor TSS values, including goodness of fit R^2 and 95 % confidence interval. (**a**) For TSS sensor in PS Rostock-Schmarl. (**b**) For TSS sensor at the central WWTP Rostock.

5.3.2 Evaluation of the Erosion and Settling Approximation

The evaluation of the raw sewage erosion and settling characteristics is based on an enormous amount of data. In sum, the TSS sensor in PS Rostock-Schmarl recorded 4 238 121 values (5 s interval over one year). 2 203 618 values of them account for erosion sequences and 2 034 503 values for settling sequences. The total number of single erosion sequences amount to 6653, while 6733 single settling events are recorded. This leads on average to $\approx$ 24 erosion and $\approx$ 24 settling events per day. Hence, the pumps are working every half hour for 30 min.

For each single erosion and settling event, a mathematical function is adjusted to the measured TSS values, automatically by a MATLAB code. This enables a fast, uncomplicated and reproducible processing. The function itself is given by the settling rate $C(t)$, Equation (24) and by the erosion rate, written as $a(\tau, w)$ (following Equation (29)).

First, we will evaluate the approximations of the erosion and settling processes. Figure 21 evaluates the fit results graphically. In Figure 21a, all measured erosion rates e_a are plotted versus all fitted erosion rates $a(\tau, w)$. A perfect fit is given by $f(x) = x$ or $a(\tau, w) = e_a$. For the majority of erosion values, $a(\tau, w)$ follows the perfect fit course with deviations above and below. The fitting results are moderate. R^2 value of $\geq$ 0.9 having 7.3 % of the total approximations (n = 481 single events), 33.5 % (n = 2100) were fitted with R^2 values of $\geq$ 0.75, while R^2 values of $\geq$ 0.5 having 54 % (n = 3603). So the mathematical approximation by the erosion rate $a(\tau, w)$ is suitable to describe the real process of erosion. Because of the similar up- and downward deviation, a balance is assumed.

Figure 21b shows all measured TSS values in the pump pauses versus all approximations by $C(t)$. Here, the majority of the values are located just below the perfect fit line. Accordingly, the settling process is slightly overestimated. In contrast to erosion, a better fit is achieved for settling. R^2 values of $\geq$ 0.9 having 31 % of the total approximations (n = 2084 single events), 58.4 % (n = 3934) were fitted with R^2 values of $\geq$ 0.75 and R^2 values of $\geq$ 0.5 having 76 % (n = 5161).

Both models are able to describe real world conditions appropriately. The deficits in the erosion approximation may result from its dynamic process. If the TSS sensor measures a value immediately when the pump starts, it takes 5 s of pumping until the next value is recorded. Within these 5 s, some sediments are already eroded. This means that a shorter measuring interval is recommended for the erosion process in later studies. Furthermore, the limited flexibility of the erosion rate $a(\tau, w)$ itself, as it is based on a first order polynomic function (see Equation (27)), contributes to its moderate results. A transformation into a power function (e.g., $a(\tau_{pipe}) = d \cdot (\tau_{pipe} - \tau_{crit})^p$) leads to slightly better results but with larger computation effort, e.g., for a sediment transport simulation.

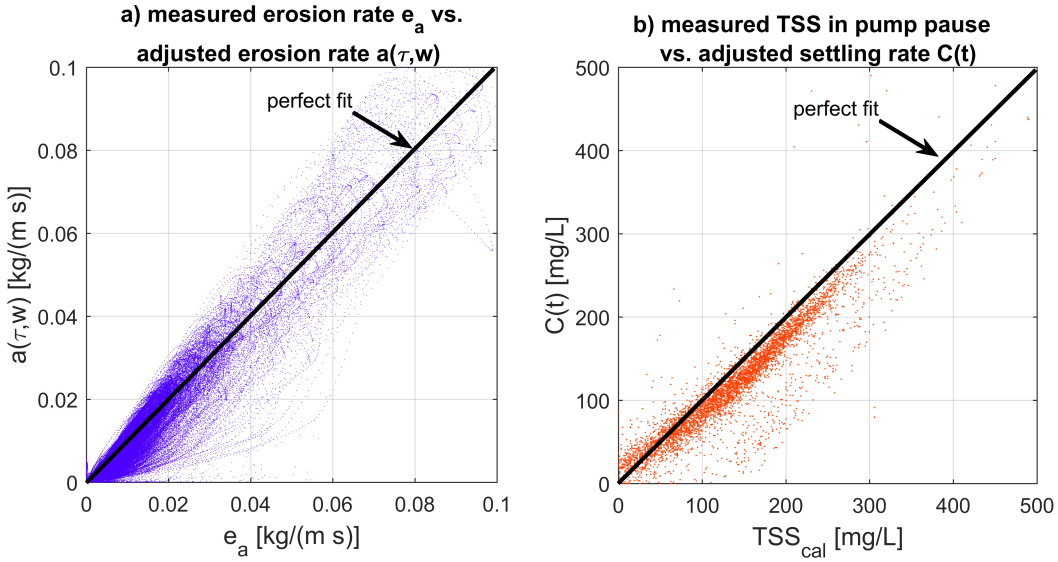

Figure 21. Evaluation of the erosion and settling approximation. (**a**) All measured erosion rates e_a vs. all mathematical approximations by $a(\tau, w)$. (**b**) All measured settling events inside the pipe vs. all mathematical approximations by $C(t)$.

5.3.3 Settling and Erosion Characteristics Inside the Pressure Pipe Under Dry Weather Inflow

Transport characteristics are essentially dealing with numerical simulation of sediment transport in open channel flow or dimensioning of facilities and treatment plants or solids transport inside pressure pipes. Hence, the in-pipe measurement helps to improve accuracy of the transport characterization and widen the spectrum of results substantially. Furthermore, it serves as a comparison to laboratory (ex situ) results, obtained in Chapter 3 and 4.

The example in Figure 22a shows a typical situation in PS Rostock-Schmarl, comparable to usual urban drainage PS. The diurnal course of TSS is separated, according to Figure 19, into erosion events (blue) and settling events (red). The diurnal course of the raw sewage inflow is presented by Q_{inflow} and the resulting pump flow by Q_{pipe} (right axes).

The TSS values during the night are relatively low. They reach a minimum of $\approx$ 200 mg/L at about 03:30 a.m. (in pump sequence) before starting to increase from 06:00 a.m. to 12:00 p.m. up to 400 mg/L. Peaks up to 600 mg/L may be the result of the sensor wiper, cleaning the sensor from heavy dirt (e.g., paper shreds). The TSS course follows the inflow course of Q_{inflow}. Hence, there is a relationship between TSS and Q_{inflow}. Low inflow results in low TSS values and vice versa. It results from the water usage and the hydraulic conditions in the upstream sewers. An increased solids amount reaching the PS by increased water consumption (stool, cooking, etc.). Furthermore, high water consumption raises the hydraulic performance in the upstream sewers and erodes deposits.

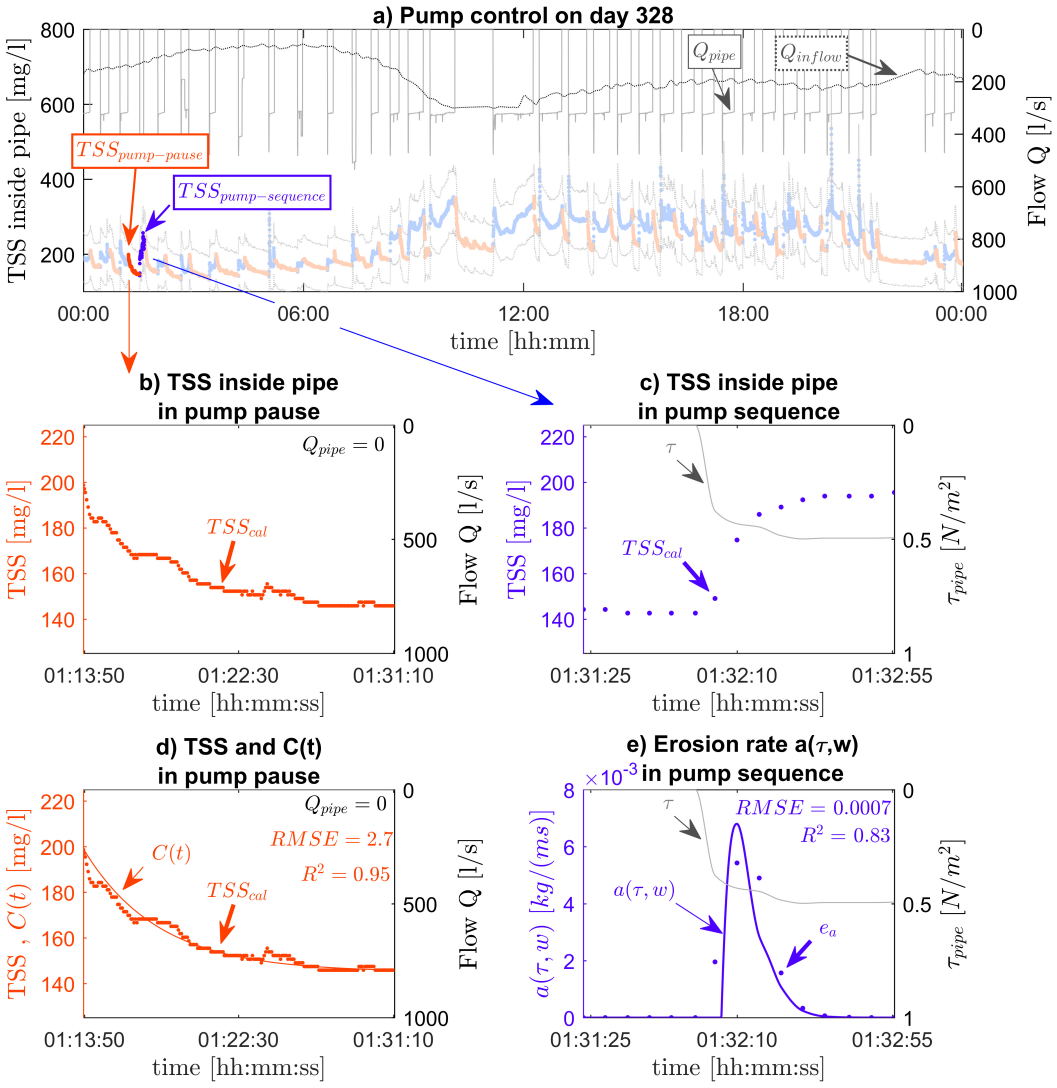

Figure 22. Monitored data in PS Rostock-Schmarl for day 328 (**a**) including exemplary erosion and settling determination scheme (**b–e**). (**a**) Q_{inflow} and Q_{pipe} (right axis) and TSS sensor data including 95 % confidence levels (left axis). (**b**) Settling event: TSS values (TSS_{cal}) after pumps stop in the night. (**c**) Erosion event: TSS values (TSS_{cal}) after pumps start at night. (**d**) Settling event determination: TSS values (TSS_{cal}) and approximated settling rate $C(t)$ including fit results. (**e**) Erosion event determination: erosion rate e_a and approximated erosion rate $a(\tau, w)$ including fit results.

The TSS course is characterized by two long settling periods. A specific settling characteristic becomes clear within these two periods. The TSS first decreases rapidly but then slows down. This is also addressed in Chapter 3, where the same characteristic was found. Accordingly, an exponential function (see Equation (24)) describes this process most appropriate. Consequently, the TSS never decreases to full extend in pump pauses.

Figure 22b shows an exemplary settling course in detail, while Figure 22d shows the resulting settling rate. Although the pump pause only takes ≈ 17 min, the TSS inside the fluid reduces from ≈ 200 mg/L at about 27.5 % to ≈ 145 mg/L. The effect of the exponential decrease shows the risk of forming a consolidated sediment layer inside the pressure pipe, even in short pump pauses. If sediments erode incompletely within the subsequent pump sequences, permanent deposits are likely to develop.

Figure 22c, e shows the subsequent erosion sequence and the determination of the erosion rate. The erosion process always forms an s-shaped curve (Figure 22c). This shape is characterized by a restrained start and is followed by an increased erosion. The inflection point of the s-curve marks the beginning of the decrease phase with a weakening erosion. The formerly settled solids are completely eroded from ≈ 145 mg/L up to ≈ 200 mg/L within 30 s. The resulting erosion rate (Figure 22e) shows an abrupt increase at the beginning, which is due to its moderate fitting results (R^2 = 0.83). Similar to the smoother decline at the end of the erosion event, a more gradual increase is assumed for the beginning. The maximum erosion appears at ≈ 0.43 N/m^2 and so, before the maximum shear stress level of ≈ 0.5 N/m^2 is reached. A further increase of shear stress (feasible by parallel pumping of P1 and P2) would not result in further solids erosion, as the maximum erosion level is already reached and the decline remarks the emptying of the sediment layer.

5.3.4 Comparison to Laboratory (Ex situ) Results

The results of the ex situ laboratory experiments in Chapter 4 are similar to the in situ measured erosion processes in this study. Both methods show the typical s-curve while eroding solids. Hence, the resulting erosion rates are quite similar. Especially the calculated duration for a complete resuspension in Chapter 4, with regard to similar hydraulic conditions (≈ 0.5 N/m^2 bed shear stress), is nearly equal to real world processes (duration ≈ 30 s). Thus, both methods (in situ and ex situ) are applicable to determine the erosion characteristics of raw sewage.

However, the in situ characterization of the erosion events is much harder compared to the ex situ method in Chapter 4, as the solids inside the pipe are moving in two main directions (upward and forward, micro-effects ignored). Therefore, next to the formerly settled solids directly under the TSS sensor, particles settled at the upstream section of the pressure pipe affecting the measurement. A closed reaction chamber, within the ex situ experiments in Chapter 4, simplifies the measurement extremely, as the erosion process of a controlled suspension is detected. This may be another reason for the moderate fitting results (see Section 5.3.2).

A direct comparison to the ex situ settling experiments in Chapter 3 is not possible. The in situ method measures the TSS reduction in the fluid phase (by a calibrated turbidity sensor) and the ex situ method measures the total mass increase at the bottom of a cylinder (by weight loss). Furthermore, the mathematical description differs from Chapter 3. However, by converting the cumulative growth from TSS into the fluids particle loss, an equal course to the settling rate is found (exponential shape). Furthermore, both methods counted approximately the same solids amount after similar settling durations. 25.4 % of solids mass settle in a laboratory test within 17 min while approximately 27.5 % of the solids settle within the same duration inside the pressure pipe.

A continuous measurement of solids decrease inside a fluid phase by a sensor is by far much easier and more worthwhile, than a manually ex situ determination of solids mass growth. The laboratory experiment lags behind the sensor determination, because of the high effort in designing and construction, sampling, the experimental conduction and mass detection. The continuous and automated in situ measurement scores by a unique installation, simple maintenance and calibration, high-resolution measurement (5 s interval) and automated data processing.

5.3.5 Effect of Storm Water Inflow to Settling and Erosion Characteristics

Due to the connected road runoff, a changed erosion and sedimentation behaviour is assumed by storm water inflow. Several storm events were measured during the study period. One example is shown in Figure 23. Figure 23a shows a rain event at 07:00 p.m. with 4.9 mm/h precipitation (right axis). The inflow curve shows the storm runoff slowly reaching the pump sump (see Q_{inflow}, left axis). The TSS course (left axis) is separated into erosion (blue) and sedimentation sequences (red). The TSS concentration increases significantly up to $\approx$ 600 mg/L after the peak runoff reaches the pump sump. Figure 23b compares a dry weather inflow erosion rate (1b) with a storm water erosion rate (2b). The maximum erosion increases with the storm inflow almost by a factor of five. One reason is the storm runoff composition. Solids (sand, tire abrasion, etc.) are washed off from roads and entering the sewer. Furthermore, the increased discharge erodes presettled and consolidated deposits and spills a mixture of runoff solids and sewer solids to the PS.

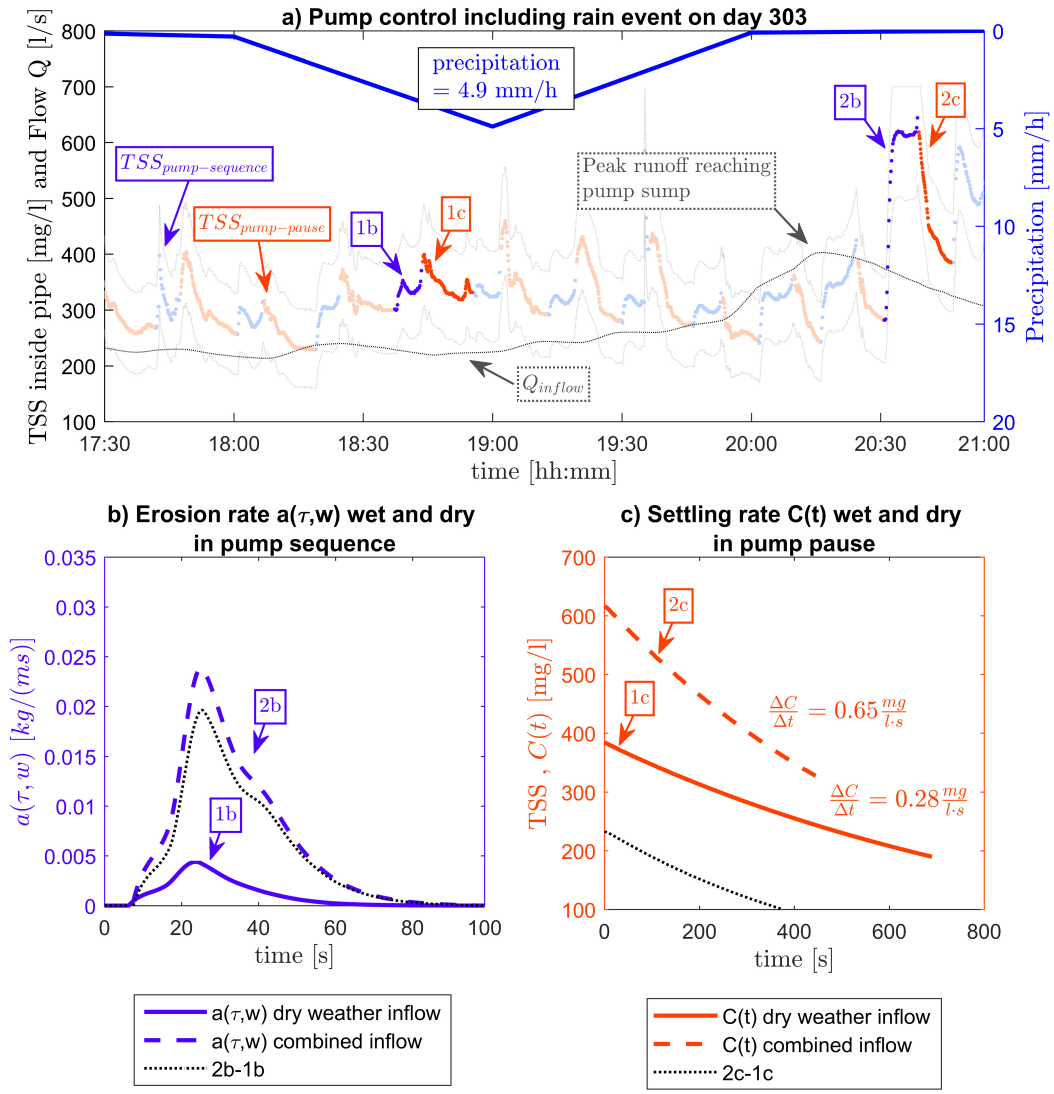

Figure 23. Effect of storm water inflow to erosion and sedimentation. (**a**) Q_{inflow} and TSS data (both on left axis) during rainfall event from 06:00 p.m. to 08:00 p.m. with a peak of 4.9 mm/h (right axis). (**b**) Erosion rate $a(\tau, w)$ during storm water inflow (2b) compared to dry weather inflow (1b). (**c**) Settling rate $C(t)$ during storm water inflow (2c) compared to dry weather inflow (1c) including mean decrease $\frac{\Delta C}{\Delta t}$. The German Weather Service (DWD) provides the precipitation data.

The following sedimentation process (2c) is significantly different compared to dry weather conditions (1c), accordingly. The increased TSS inflow raises the start value of sedimentation (C_0) from $\approx$ 400 mg/L up to $>$ 600 mg/L. A better comparison of the settling processes is provided by the mean decrease, which is defined as the difference quotient in the interval $[t_1; t_{end}]$, see Equation (30).

$$\frac{\Delta C}{\Delta t} = \frac{|C(t_{end}) - C(t_1)|}{t_{end} - t_1} \tag{30}$$

In this example, the TSS concentration decreases under dry weather inflow (1c) with 0.28 mg/(L s), while under storm water inflow (2c) twice as fast with 0.65 mg/(L s). Hence, next to the solids concentration, the solids composition changes as well. This indicated an increased inflow of heavier particles (runoff- and sewer solids). The total mean decrease under dry weather inflow, calculated over 4520 settling events, is 0.23 mg/(L s), while under storm water inflow 0.9 mg/(L s) (calculated over 9 rain events). So, a more than 3.5 times faster settling can be assumed under storm water inflow. This increases the risk of blockages significantly. The risk is highest when the solids entering the pressure pipe. The storm runoff reaches the pump sump 1 h after the rain event and enters the pressure pipe usually 1.5 h after the rain event. The accumulation of particles on roads and the deposition of solids inside the sewers increases with longer dry periods. This is due to missing wash-off and limited discharge. Hence, the risk of blockages in the pressure pipe increases for short but intensive rain events after long dry weather periods. However, this effect is not investigated within this study.

5.3.6 Comparison to Laboratory (Ex situ) Results

A changed sedimentation behaviour is already recognized in Chapter 3. Samples, collected under storm water inflow settling significantly faster. Comparable laboratory tests showing a mean decrease for storm water samples by 1.1 mg/(L s), while 0.18 mg/(L s) for dry weather samples.

5.3.7 Diurnal Variation of Settling and Erosion

Settling and erosion characteristics are changing not only with storm water inflow. As already mentioned previously, TSS follows the inflow course. As settling and erosion depends on TSS, their behaviour follows TSS and consequently inflow. Hence, changes are also assumed due to the diurnal variation of inflow. This relation is shown in Figure 24 and Figure 25. Both showing the average diurnal variation of inflow (black line), including boxplots for hourly mean decrease (Figure 24) and hourly maximum erosion per event (Figure 25).

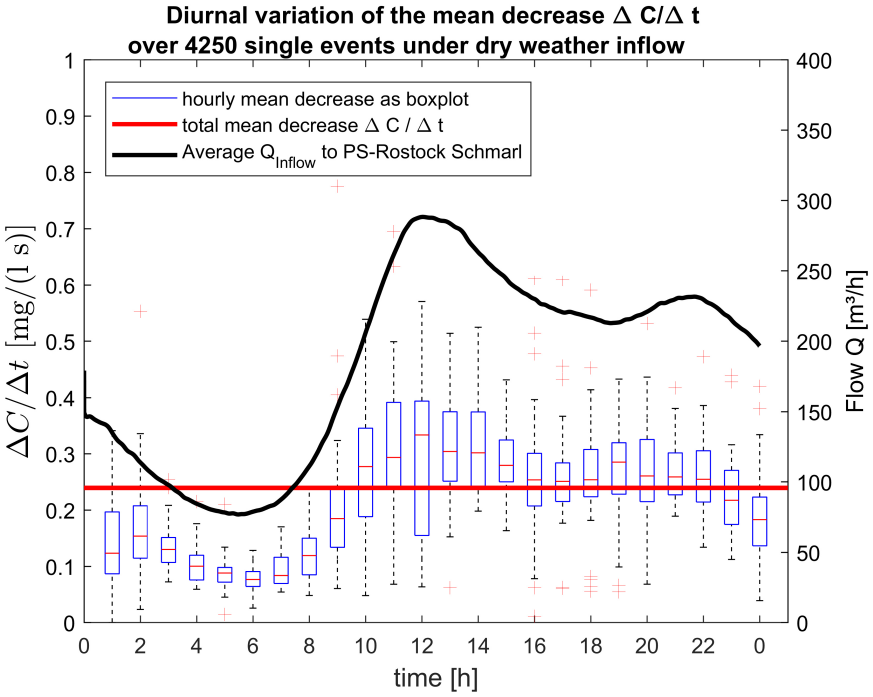

Figure 24. Diurnal variation of the mean decrease $\frac{\Delta C}{\Delta t}$ (boxplots) including total mean decrease over 4250 single settling events (red line) and the average Q_{inflow} for dry weather conditions (black line).

Both indicators (mean decrease and maximum erosion) follow the up- and downward course of inflow. Especially in the morning, the sewage is characterized by slow settling processes ($<$ 40.1 mg/(L s)) and low erosion rates ($<$ 0.0025 kg/(m s)). This can be explained by the reduced water usage in the night (reduced solids input, reduced hydraulic performance in upstream sewers). Vice versa, due to a high water usage in morning hours, peak inflows reaching the PS at lunch and changing the sewage to a faster settling mixture (up to 0.5 mg/(L s)). Accordingly, the erosion rate increases up to 0.02 kg/(m s). The increased erosion rate is a result of a faster settling process. The more solids settle within the pump pauses, the more solids can be eroded in the pump phases. Hence, the erosion rate depends on the pump pause duration. Longer pump pauses generally occur in the night or in the morning with low inflow rates (see Chapter 3). Nevertheless, due to a slow settling sewage, the erodible amount of solids is low. The erodible amount is at its peak, when the settling process is fast (usually at midday), irrespective to pump pause duration. Concluding, the sewage settling characteristics (slow or fast) determine the deposits formation more than the duration of the pump pauses.

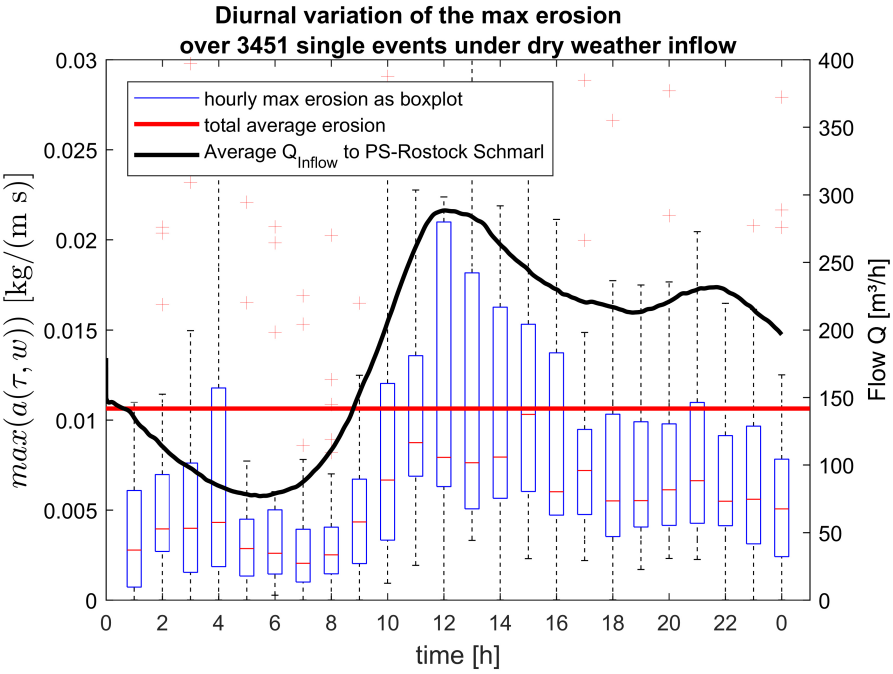

Figure 25. Diurnal variation of the max erosion (boxplots) including total average erosion over 3451 single erosion events (red line) and the average Q_{inflow} for dry weather conditions (black line).

5.4 Conclusion

The paper presents a continuous in situ TSS measurement system for raw sewage inside a pressure pipe and the determination and characterization of settling and erosion behaviour based on high-resolution sensor data. Ultimately, the following findings are concluded:

- the installed sensors are suitable for supervision of TSS fluxes inside sewage pressure pipes
- periodically calibration and maintenance of TSS sensors result in reliable data
- TSS sensor data allow for a characterization of solids sedimentation and erosion behaviour
- measured in situ erosion and settling results are similar to ex situ (laboratory) results
- settling accelerates with high inflow rates (storm water inflow, diurnal inflow peaks) and decelerates with low inflow (reduced TSS inflow in night phases)
- erosion rate increases and decreases based on the available amount of solids, hence, with changing settling behaviour
- solids are eroded before maximum shear stress level reached.

Within continuous sensor measurements, a huge amount of data is generated. Especially with regard to urban water simulations, this provides the opportunity for precise calibration up to specified scenarios. Hence, changes of solids erosion and sedimentation caused by storm water inflows of various intensity or by the diurnal inflow can be dynamically implemented into hydraulic models by providing a wide spectrum of appropriate calibration parameters. The presented results are primarily used for a sediment transport simulation inside the pressure pipe of PS Rostock-Schmarl, presented in Part II of this publication: “Sediment Transport in Sewage Pressure Pipes, Part II: 1D Numerical Simulation”.

5.5 Advices for in situ TSS monitoring in wastewater pressure pipes

The supervision of solid fluxes by In situ turbidity/TSS measurement directly inside wastewater pressure pipes is not part of todays scientific literature (according to the author’s knowledge). Hence, the experiences gained within this study are extremely useful. Table 6 already shows some technical data and settings for the sensor measurement. The following list gives further recommendations for the successful implementation of a TSS monitoring programme (in addition to the manufacturer’s recommendations):

- Installation:
  - to ensure long functionality (protection against weathering and corrosion), the sensor should be installed e.g. inside an extra manhole
  - the installation site of the sensor should be easily accessible and provide sufficient space for calibration processes
  - sensor preferably with wiper. Wiper settings must be adapted to the conditions (a lot of fibres = more frequent wiping)
  - transmit measured values to the process control system via remote data transmission
- Service and calibration:
  - depending on the wastewater composition and mechanical pre-treatment, remove the sensor at least once or better twice a month to clean the sensor and wiper
  - change wiper blades half-yearly
  - calibration processes one time per quarter
  - standardize the calibration process as much as possible. This applies above all to the reference measurement in the calibration cylinder (e.g. magnetic stirrer settings)

  - magnetic stirring: avoid stirring too fast (prevent whirl formation) and too slowly (keep particles in suspension). Always use the same magnetic stir bar size
  - one person can easily carry out all processes. The duration of the whole procedure for two sensors is about 1.5 days (including sensor maintenance and full calibration procedure)

- Monitoring:
  - short measuring intervals, if possible below 10 s (here $\approx$ 5 s). The smaller the measuring interval, the better the transport parameters can be investigated and determined
  - pump data are essential for evaluation. These should be as comprehensive as possible (inflow rate, flow rate in pressure pipe, pressure, power input, frequency of VFD, motor speed, etc.) and should be recorded at the same interval, see Section 3.2.1
  - data from existing rain measurements in the catchment area are also advantageous. If no rainfall measurements are available, an appropriate measuring device should be installed in the catchment area (combined sewer systems)
  - daily checking of the values, for example by connection to the process control system with automatic error messages. This is recommended to detect heavy contamination at an early stage

- Data analysis:
  - with shorter measuring intervals the amount of data increases. Standard evaluation routines should be designed to evaluate the amount of data efficiently but safely (preferably as a script, macro or function, etc.)
  - parallel recorded data on pump operation and rain should be included in the evaluation routines. For example, sedimentation and erosion phases can be separated and investigated, see Section 5.2.5
  - plausibility checks with experience and data of the sewer system operator with subsequent error calculation (e.g. Walsh test), see Section 5.2.4.

6 Sediment Transport in Sewage Pressure Pipes, Part II: 1D Numerical Simulation

6.1 Introduction

Numerical simulations are state of the art in challenging problems in urban water management. Whether in wastewater treatment, trying to optimize single or multiple treatment processes, or in sewer systems, for hydraulic optimization or planning and design. Modelling is today's tool to solve complex problems efficiently.

Dealing with hydraulic problems, modelling focus lies on non-pressure systems (open-channel flow), mainly driven by heavy rain events, combined sewer overflows (CSOs), pollutant loads, etc. Hence, the main effort of scientific research concentrates on gravity sewers. Certainly, hydraulic simulation of pressurized systems is mostly a part of urban drainage modelling software, but this becomes almost insignificant in engineering science. Currently, a reason might be due to more relevant problems occurring in gravity sewers such as overload, flooding, CSO, or fat deposition. All these issues provide opportunities for research. Whereas pumping systems are considered to be safe and trouble-free systems, which may be due to their controllability (flow control by speed regulation, pumps in series or parallel, pumps switching, etc.). The possibility to control results in an almost absolute steady operation, thus, equal flow processes and subsequently the assumption of a uniform and unchanging environment inside the pressure pipe.

However, there are several disadvantages of pumping systems. One main drawback is the use of energy. For the transportation of fluids, pump power has to overcome, beside the geodetic height difference, the sum of friction losses. This sum increases with the square of the flow velocity (according to the calculation of friction losses by Darcy–Weisbach). Conversely, reducing the speed by half, quarters the dynamic friction losses and subsequently reduces energy consumption. Therefore, a large energy saving potential in urban drainage is related to the operation of sewage pumps. So, reducing flow velocity is the key to energy optimization. The reduction has several benefits (next to energy saving): It increases the pump duration, reduces the off/on switching frequency and homogenizes the flow to the downstream sewer system. But it also comes with a significant disadvantage. It might increase the risks of sedimentation and subsequently blockages, as solids are settling when velocity and resulting bed shear stress is below a critical level.

Another disadvantage may occur due to the increased retention time inside the pressure pipe. The decomposition of sewage may be increased, leading to the formation of toxic and corrosive gases (e.g., hydrogen sulfide). This problem can be engaged by a chemical precipitation.

Especially with regard to sedimentation and erosion, a numerical simulation is now of interest. Within a case study in an urban region in northern Germany (city of Rostock), solids transport inside a pressure pipe was investigated within several ex situ (laboratory) experiments in Chapter 3 and 4 and continuously monitored by in situ turbidity measurements for one year under energy-efficient pump control in Chapter 5. However, the energy-efficient control was only permitted in certain range of operation conditions. Especially low flow velocities could not be realized due to the risk of blockages. Monitoring of solids transport under low flow velocities, or after longer pump pauses, could not be investigated. Hence, a sediment transport model was developed and calibrated, to extrapolate the observed data into the restricted range of operation.

In this work, the sediment transport model is introduced, calibrated and used to simulate the above mentioned conditions. This publication implies the following main objectives:

- derive a physical, but still simple, numerical model for solids transport inside sewage pressure pipes
- calibrate the model based on ex and in situ determined sedimentation and erosion characteristics
- determine the accuracy of the transport simulation
- investigate and evaluate solids transport under various flow regimes.

6.1.1 Literature review

The simulation of non-cohesive sediment transport in sewers can be split up into morphological and mathematical models. Morphological (or detailed sediment transport) models uses, as the name suggests, the (mostly abstracted) morphology of the particles to be transported. Common morphological models are the “Bagnold Model” [82], the “Engelund–Hansen Model” [83], the “Ackers–White Model” [84], the “Engelund & Frodsøe Model” [85] and the “van Rijn Sediment Transport Model” [86]. Several morphological models found their way into hydrological and hydraulic modelling, whether in river modeling (e.g., HEC-RAS) or urban water modelling (e.g., DHI Mike Urban). All these models are driven by the main physical force reacting to the particles, which is shear stress. Hydraulic data is received by a hydrodynamic simulation. The sediment transport is then uncoupled (water flow and sediment transport not interacting), semi-coupled (water flow and sediment transport interacting by iteration of uncoupled model, e.g., [87–89]), or fully coupled (simultaneous computation of flow and sediment transport, e.g., [90, 91]) to the hydraulic computation.

Mathematical models bases on the one-dimensional ADE, describing the mass conservation of substances transported in direction of the mean flow velocity. The use of the ADE is widely spread, e.g., for modelling the transport of dissolved substances in natural flow processes (e.g., inside ground water bodies or river flows) or modelling substances in urban drainage systems or water distribution.

Hydrodynamic urban drainage models are regarding 1 D channel flow by solving the Saint Venant equation. The ADE is then commonly used by urban water modelling software (DHI Mike Urban [92]) for modelling the transport of dissolved substances/pollutants (e.g., organic pollutions (biochemical oxygen demand)). Nevertheless, the ADE is not exclusively limited to the transport of dissolved substances. [92] mentioned the ADE "(...) can also be used for the simulation of suspended (fine) fraction of particulate pollutants and sediments." [92, p. 99].

However, irrespective of the substance to be transported or the transport formulation approach (detailed or mathematically), the sediment transport is usually described in literature/computed by software for non-pressure systems (open-channel flow, pipes). The transport of substances in urban drainage pressure pipes is commonly not computed by any transport simulation. Pumping systems are usually modelled without pressure mains, but rather as a direct connection between the sump and the end-node with a fixed pump capacity (see also [92]). As a result, the "(...) dissolved matter is routed through such a system with no time lag between the pump and the end of the conduit." [92, p. 108].

The application of ADE for modelling transport of dissolved/particulate substances inside pressure pipes is common for water distribution systems. Modelling water quality within the simulation software EPANET 2 provides possibilities to transport dissolved substances through a pressurized system [93] (also implemented in DHI Mike Urban WD tool). The basic idea of the substance transport within this study is similar to the water quality modelling idea in EPANET 2.

Next to numerical approximations, soft computing methods (e.g., artificial neural networks, fuzzy logic and evolutionary computation) also tried to approximate real-life problems and so used to estimate the sediment transport in urban drainage systems [94–99].

The presented 1 D sediment transport simulation in this publication is computed by an uncoupled mathematical model that is based on the ADE.

6.2 Methods

6.2.1 Study area, pump control and monitoring total suspended solids

The supervision of solids transport under an energy-efficient pump control was implemented in PS Rostock-Schmarl in the city of Rostock (northern Germany). PS Rostock-Schmarl conveys the raw sewage of $\approx 40\,000$ inhabitants directly, via two cast iron pipelines of 600 mm diameter and 4500 m length, to the central WWTP in Rostock, by four pumps of 220 kW total pump power. The incoming sewage is filtered by a 20 mm rake at the inflow side of the PS. Under dry weather inflow the TSS concentration usually ranges from 150 mg/L up to 350 mg/L. The upstream, usually separating sewer sums up to 80 km. Under rainfall, the main roads storm runoff is connected to the upstream sewer (total suspended solids concentration then increases to > 500 mg/L). A parallel storm sewer receives the residual surface and roof runoff. Additional information about the study area are provided in Chapters 3 to 5. Chapter 5 includes a detailed schematic view of the sewer system and PS Rostock-Schmarl.

The usual operation mode of PS Rostock-Schmarl is a conventional two-point operation, where pumps switch on and off at pre-defined water levels inside the pump sump (sloped, squared geometry with a volume of 178 m^3). When pumps switch on, the variable frequency drive guarantees a soft start of the pumps. After a one minute soft start, the pumps operate at a defined duty point. In full power mode, the pumps duty point is then at ≈ 166 L/s (head loss ≈ 18.3 m) by ≈ 0.6 m/s flow velocity, respectively. The usual operation mode is the reduced two-point control where the flow decreases down to ≈ 100 L/s (head loss ≈ 17 m) by ≈ 0.35 m/s flow velocity, respectively. For a studied period of one year, an energy saving operation was implemented, to control two pumps and enhance energy efficiency. At low inflow, the duty point decreases to ≈ 76.5 L/s (head loss ≈ 16.7 m) at ≈ 0.27 m/s flow velocity. Energy savings amount to 11 % compared to conventional operation. The following constraints mainly hindered additional energy savings: (i) minimum flow rate of ≈ 53 L/s (flow velocity ≈ 0.2 m/s) and (ii) pumps forced to start up to maximum flow in each pump sequence, before regulating down to energy-efficient flow. These rules are defined by the operator to ensure solids transport and to avoid blockages. For detailed information about the control modes, see Chapter 3 and [13, 14].

In parallel, measuring TSS by two turbidity sensors directly inside the pressure pipe (one at pumps pressure side and one at the outflow side in WWTP Rostock) ensured a continuous monitoring of solids transport. Furthermore, the measurements provided data for continuous determination of solids settling and erosion characteristics and subsequently data for model calibration. The monitoring system is explained in depth in Chapter 5. Figure 26 shows a simple schematic view of the study side.

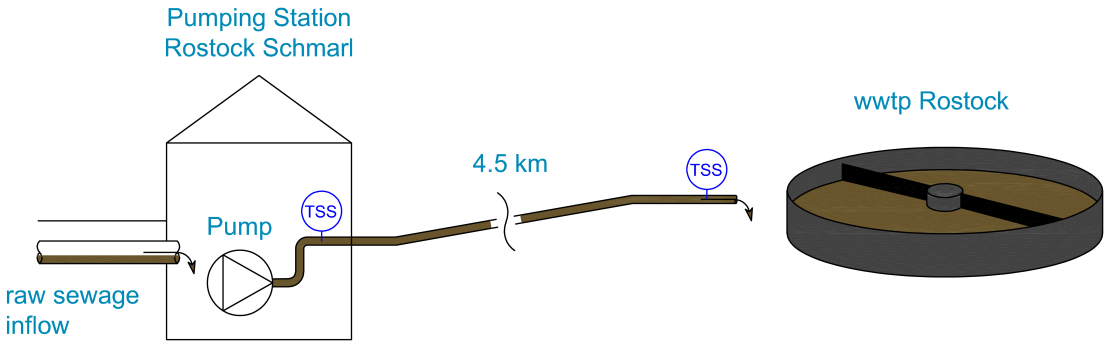

Figure 26. Schematic view of the study side. TSS are measured inside the pressure pipe in PS Rostock-Schmarl and at the outflow side in the WWTP Rostock after 4.5 km.

6.2.2 Sediment transport basics

The transportation of solids inside a fluid is mainly influenced by two main physical effects: (i) sedimentation and (ii) erosion. Equally to those two effects, two operation modes can be distinguished in pressurized flow: (i) pump pauses (shut off mode), where only sedimentation occurs and (ii) pump sequences (shut on mode), where solids eroded and subsequently transported under adequately hydraulic conditions.

In pump pauses, solids are settling according to their settling velocity at different speeds, mainly determined by their density and size. The sediment layer at pipes invert is then a superposition of different solid fractions. The settling behaviour of various particle fractions can be described as a settling velocity distribution, as conducted in Chapter 3. The computation of several particle fractions is useful for dealing with pollutant transport when specific fractions contain more pollutants than other components [100]. However, modelling various velocity classes also requires larger coding and computing effort. In contrast, pure mass growth of solids, when only TSS fluxes are of interest, can be modeled and calculated easily as an appropriate solution of a usual differential equation, e.g., as an exponential decay of solids concentration inside the fluid, as introduced in Chapter 5.

In pump sequences, solids eroding due to the force exerted by the turbulent fluid flow inside the pressure pipe (Reynolds number of 240 000 at 0.4 m/s flow velocity). The force is expressed by the shear stress τ (N/m^2) or indicated more exactly by the bed shear stress. When pumps speed up, flow velocity increases until τ reaches the critical shear stress level of the particles τ_{crit} (N/m^2). Because of the different densities of particles, solids are eroding successively after τ_{crit} level of the lightest particle fraction is reached, until all particles are eroded. Solids are then transported either as bed load (sliding, rolling and leaping of single particles) or suspended load, where particles are following the swirled streamlines of the turbulent flow. Suspended solids are then also moving transverse to the flow direction.

The physical processes within the erosion are by far more complex as pure sedimentation of particles. So, the implementation into a simulation results in high computation effort. If the flow is always turbulent (here Reynolds number of 120 000 by a minimum flow velocity of 0.2 m/s) and only a mass balance is required for a simulation, swirls and micro effects can be neglected.

6.2.3 Mathematical approximation

The solid transport is simulated for the above described pressure pipe (length l = 4500 m, diameter d = 0.6 m), conveying (mechanical pre-treated) raw sewage and sequentially combined sewage to the WWTP Rostock. The mathematical model is based on the ADE, Equation (31).

$$\frac{\delta u}{\delta t} = -v\frac{\delta u}{\delta x} + \frac{\delta}{\delta x}D_{xx}\frac{\delta u}{\delta x} + r \tag{31}$$

In Equation (31), the advective transport is represented by the first term $-v\frac{\delta u}{\delta x}$ (kg/(m^3 s)), the dispersive transport is represented by the second term $\frac{\delta}{\delta x}D_{xx}\frac{\delta u}{\delta x}$ (kg/(m^3 s)) and the reaction of a substance is represented by the third term r (kg/(m^3 s)). With u being the concentration of a substance to be transported (kg/(m^3)), t the time coordinate (s), v the flow velocity in flow direction (m/s), x the space coordinate (m) and D_{xx} the dispersion coefficient (m^2/s). The reaction of substances r is defined by Equation (32). With P being the production of a substance to be transported (kg/(m^3 s)) and S the sinking or degradation of a substance to be transported (kg/(m^3 s)).

$$r = P - S \tag{32}$$

The complex physical processes during sedimentation and erosion are unnecessary for pure modelling of the sediment flux. Hence, the following simplifications are assumed for the simulation. The sedimentation of different solid fractions, as described in Chapter 3, is not considered. The settling process is described as an exponential decay of solids, similar to Chapter 5. This minimizes the particle fractions to simulate and approximates the settling of solids adequately. The erosion of solids is described by a single particle fraction as well. Once eroded, the particles are distributed homogeneously over the pipes bottom, as the mean flow velocity is uniformly distributed over the pipes cross section in the model. As already mentioned in [93, p. 193] “Longitudinal dispersion is usually not an important transport mechanism under most operating conditions.” (with regard to dissolved substances). As a result, dispersion effects of contiguous grid sections is neglected completely (similar to [93, p. 193].

Further simplifications are: No attention is paid to biogenic processes inside the fluid or deposits phase, the pipes geometrical shape is ignored as the 1 D sediment transport is computed in longitudinal direction, the pipes negative or positive slope and curvature has been ignored too. As a result of the simplification, the ADE simplifies to the

one-dimensional advection equation with only the production and sinking left, Equation (33) (similar to [93, p. 193].

$$\frac{\delta u}{\delta t} + v\frac{\delta u}{\delta x} = P - S \tag{33}$$

The transportation of solids is simulated as a mass balance (conservation of mass) for the suspended load and bed load along the pressure pipe. Equation (34) describes the conservation of mass for suspended load transport. Equation (35) describes the conservation of mass for bed load:

$$\frac{\delta u}{\delta t} + v\frac{\delta u}{\delta x} = \frac{a(w,v)}{A} - s(u) \tag{34}$$

$$\frac{\delta w}{\delta t} = A \cdot s(u) - a(w,v) \tag{35}$$

The suspended load transport is defined as feeding minus loss. Therefore, the production P is replaced by the erosion of solids $a(w,v)$ (kg/(m s)) and the degradation S is replaced by the particle loss inside the fluid $s(u)$ (kg/(m^3 s)). Thus, eroded mass per pipe length and time $a(w,v)$ divided by pipes cross section A (m^2) minus the particle loss inside the fluid $s(u)$ represents the suspended load.

The bed load, Equation (35), is as well defined as feeding minus loss. Here, the feeding is described by the particle loss $s(u)$ multiplied by A minus the eroded mass $a(w,v)$. Erosion $a(w,v)$ is described by Equation (36), with $\tau_{pipe}(v)$ (N/m^2) the current bed shear stress inside the pressure pipe, $\tau_{crit}(w)$ (N/m^2) the critical shear stress level of the raw sewage dependent on the particle mass on pipes invert w (kg/m) and the erosion parameter d (s), which describes the strength of the erosion (see Chapter 4).

$$a(w,v) = max(0, d(\tau_{pipe}(v) - \tau_{crit}(w)) \cdot w) \tag{36}$$

The sedimentation is described as a first order decay process modelled by Equation (37).

$$\frac{du}{dt} = -\alpha \cdot u \tag{37}$$

The differential equation is approximated by the particle loss $s(u)$ by Equation (38), with the settling parameter α (1/s), which determines the exponential decay and the particle concentration inside the fluid section, u (kg/m^3) (see Chapter 5 and [101]):

$$s(u) = u \cdot \alpha \tag{38}$$

6.2.4 Numerical method

The partial differential equations are solved by a finite difference method (FDM) (partial derivatives are approximated as finite differences). FDM within water-quality modelling were i.a. investigated by [102]. The authors conclude, that the FDM method is, next to others, "(...) capable of adequately representing observed water-quality behavior (...)" [102, p. 146].

The FDM method applied here is an explicit/implicit finite difference scheme centered in time (discretization in time) and backward in space (discretization in space). The centered in time scheme taking the average value between time steps n and $n+1$ (also known as the Crank–Nicolson scheme). The first value n is calculated based on the previously computed value $n-1$ (explicit), while the second value $n+1$ is calculated based on the formerly computed value n within the same time step (implicit). The advective transport with the mean flow velocity results in the backward in space (or upwind) scheme, where only transport in the flow direction (from backward grid point) is allowed.

For the 1 D sediment transport model, the pipe is separated into 900 segments, with a length of Δl = 5 m. For a stable solution, the Courant–Friedrichs–Lewy condition is defined as $|\frac{v \cdot \Delta t}{\Delta l}| \leq 1$. The time increment Δt for a simulation step is then defined as $\Delta t \leq \frac{\Delta l}{|v|}$. Hence, the advective transport cannot be faster than one grid point per time step. Assuming a flow velocity of v = 0.5 m/s, the time increment of a simulation step is then calculated to Δt = 10 s.

The numerical simulation is realized in several Matlab functions. The pump control strategies of PS Rostock-Schmarl (several regular and energy-efficient control modes) are implemented into the transport simulation to investigate the particle transport under various control modes. Hence, the sediment transport simulation is based on the mean flow velocity, computed by a previous pumping simulation.

6.2.5 Calibration parameters

As described by Equation (36) and Equation (38), the parameters α, d and τ_{crit} are mainly responsible for the sedimentation and erosion behaviour and subsequently important for model calibration. The calibration of the transport simulation is based on two parameter sets: (i) ex situ parameters, resulting from laboratory experiments and (ii) in situ parameters, resulting from continuous turbidity measurement.

Ex situ parameters are provided by laboratory experiments, dealing with sedimentation and erosion of raw sewage samples from PS Rostock-Schmarl (see Chapters 3 to 4). Both experiments are explained in a few words: (i) the sedimentation tests are conducted in a vertical cylinder, the deposited mass is determined after various settling durations and the main outcome are growth curves for settled solids mass.

(ii) the erosion is tested in a vertical cylinder, the raw sewage is stirred until particles eroding from the ground level, the resulting erosion rates are detected by a continuous turbidity measurement and the calibration parameters are derived from the growth curves and erosion rates. Hence, the parameters are based on a great simplification of real-world conditions. For the settling parameter α, values between 0.0036 s^{-1} and 0.032 s^{-1} were determined, for settling periods of 24 h. The erosion parameter d was determined between 0.057 s and 0.56 s after settling for 24 h.

Another calibration parameter is τ_{crit}. The critical bed shear stress defines the erosion limit and depends on the previous settling duration (long settling periods resulting in high τ_{crit} values). The determination of τ_{crit} results in values of 0.08 N/m^2 for settling periods up to one hour and < 0.2 N/m^2 for settling periods of up to three days (see Chapter 4). The bed shear stress inside the studied pressure pipe is calculated by Equation (39), based on the fluid density ρ (kg/m^3), the flow velocity v (m/s) and the friction factor λ (calculated by the Colebrook–White equation).

$$\tau_{pipe} = \rho \cdot \frac{v^2}{2} \cdot \frac{\lambda}{4} \tag{39}$$

τ_{pipe} is calculated for the minimum flow velocity of ≈ 0.2 m/s to ≈ 0.1 N/m^2. Hence, the minimum flow velocity reaches the τ_{crit} value for one hour prior settling (0.08 N/m^2). At PS Rostock-Schmarl, pump pauses above one hour are prevented by a control regulation: At least one pump starts per hour to avoid blockages. But due to pumps soft start, the motor speed is regulated from zero flow up to full flow within 60 s, which results temporarily in flow velocities < 0.2 m/s. To always have the correct τ_{crit} value before pumps start, τ_{crit} is implemented into the simulation as a function of the prior settling duration. The present value of τ_{crit} is received during the simulation by an interpolation between the laboratory τ_{crit} results of Chapter 4.

The second parameter set are the in situ parameters, provided by a continuous turbidity measurement, as described in Chapter 5. Mass growths and erosion rates are determined inside the pressure pipe, as the pump pauses and pump sequences representing the settling and erosion experiments, respectively. By this, a wide range of calibration parameters are derived under real world conditions. After analyzing 6733 single settling events (or pump pauses), the settling parameter α is calculated to an average value of 0.0026 s^{-1}. The erosion parameter d is calculated to an average value of 0.018 s, after an analysis of 6653 single erosion events (or pump sequences).

However, due to the large number of events, a much more precise classification than pure average values can be achieved. In Chapter 5, a diurnal variation of the settling and erosion behaviour along with the variation of the inflow rate (and accordingly the TSS inflow) was detected. The changing settling and erosion behaviour are reflected by the settling parameter α and the erosion parameter d.

Hence, if the transport parameters dynamically change with the TSS inflow during simulation, the model always computes the appropriate settling or erosion process. After combining the settling parameter α of each single settling event (6733 in total) to the present TSS value, a simple linear function derives, Equation (40), with u_{inflow} (mg/L), the TSS inflow concentration.

$$\alpha(u_{inflow}) = 1.06 \cdot 10^{-5} \cdot u_{inflow} \tag{40}$$

The erosion parameter d changes proportionally with the settling parameter α. The ratio is determined to 1/0.1902. d is then calculated by Equation (41).

$$d(\alpha) = \frac{\alpha}{0.1902} \tag{41}$$

To illustrate the continuous adaptation of the model parameters, Figure 27 shows, exemplarily, the status bar of the sediment transport simulation. At the current simulation time 01:36 p.m. the pumps generate a flow velocity of 0.3 m/s. Figure 27a-d show the simulated values for suspended load (Figure 27a), bed load (Figure 27b), the settling parameter α (Figure 27c) and the erosion parameter d (Figure 27d) over pipe length (4500 m).

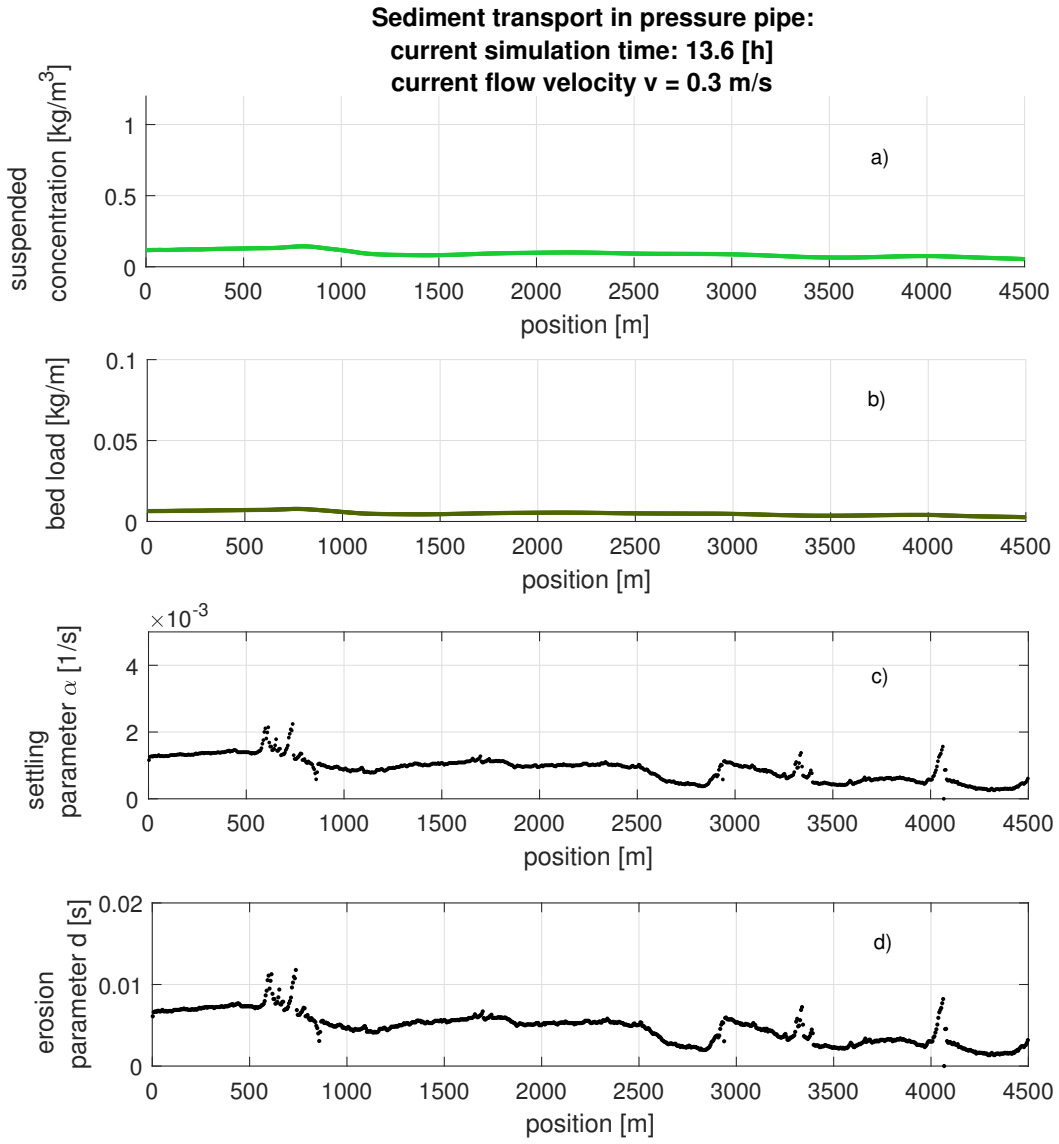

Figure 27. Status panel of the sediment transport simulation. Subfigure **a**) Present suspended load inside the pressure pipe at each grid position. Subfigure **b**) Present bed load inside the pressure pipe at each grid position. Subfigure **c**) Present settling parameter α inside the pressure pipe at each grid position. Subfigure **d**) Present erosion parameter d inside the pressure pipe at each grid position.

6.3 Results and Discussion

6.3.1 Evaluation of model accuracy

The evaluation of the numerical solution is based on a simple comparison. The reference values were compared to the simulation results. The best solution (minimal deviation to reference values) provides the best parameter set for later simulation of scenarios. The reference values were measured at the pipes end by the calibrated monitoring (see Chapter 5). The simulation was conducted with (i) static ex situ parameters, (ii) static in situ parameters and (iii) dynamic in situ parameters.

Figure 28 depicts the results of the sediment transport simulation for a typical dry weather inflow at PS Rostock-Schmarl. With the original particle concentration measurement at pipes end representing the reference values (black line). The simulation provides representative results after 13 h, as the pipe is filled with clear water at the beginning of the computation. All three simulations generally follow the measured TSS course. The variable parameter set (green line, $\alpha = 1.06 \cdot 10{-}5 \cdot u_{inflow}$, $d = \alpha/0.1902$) only differs marginally from the reference values. The simulation with in situ parameters (blue line, α = 0.0017 s^{-1}, d = 0.0189 s) and laboratory parameters (red line, α = 0.00033 s^{-1}, d = 0.0362 s) differ to larger extent. In particular, particles are transported too fast and reach the end of the pressure pipe too early. This is related to an underestimation of the settling process. The simulated TSS by laboratory parameters never decreases below 0.25 kg/m^3, while the original measurement decreases partially below 0.15 kg/m^3. So the particles, mostly settle more completely in real life than expected by the laboratory results from Chapter 5. One reason might be in the method (ex situ) itself, as several uncertainties overlay (sampling, experimental setup and laboratory analysis) and increase the measurement error.

The computation with in situ parameters resulted, by far, in better settling prediction, but contains a time shift as well. The simulated curve illustrates the advantage of the real-life measurement with less uncertainties, results in a more precise computation. With the variable parameter set (derived from all in situ parameter sets), a realistic particle concentration profile is simulated. This parameter set will further be used to compute several scenarios.

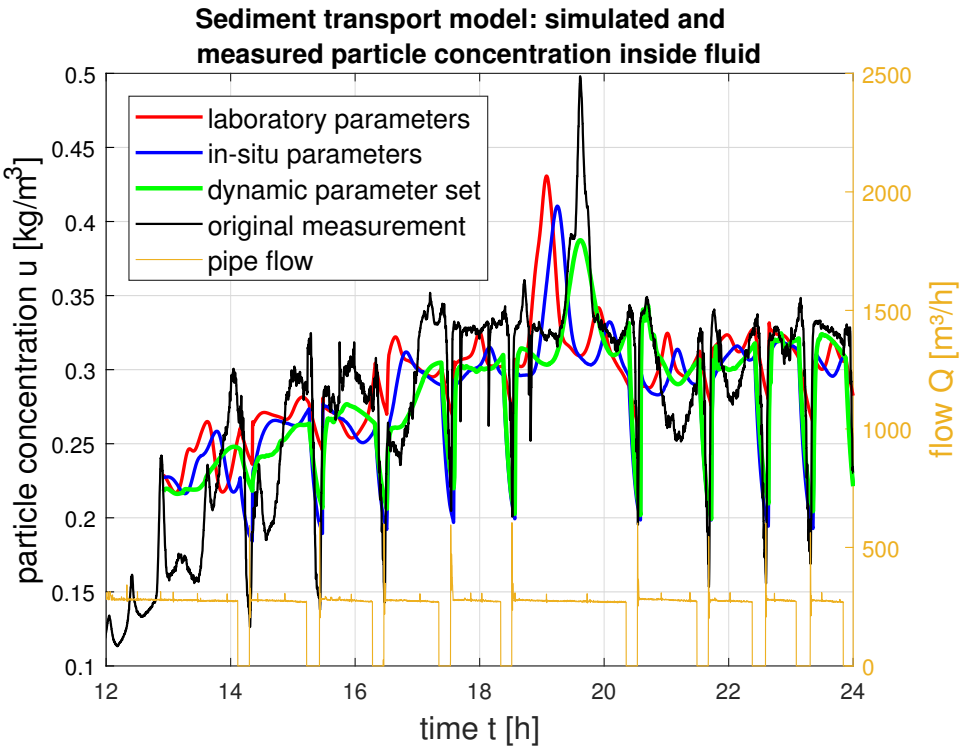

Figure 28. Results of the sediment transport simulation. Particle concentration measured and simulated with laboratory-, in situ- and dynamic parameters with slightest deviation.

The present deviation to the reference values are shown in Figure 29a and calculated as $(u_{model} - u_{reference})/u_{reference}$. A positive deviation within the settling sequences ($Q = 0$) remarks an underestimation of the settling process, while reversely a positive deviation within the erosion sequence remarks an overestimation of the real erosion process. Both, under and overestimation occurs within the settling and erosion sequences, with maximum values of $\approx +109$ % (for laboratory parameters) (underestimation of settling sequence). The variable parameter set simulation deviated at a maximum of +75 % (underestimation of settling sequence) at the beginning and reduced to $\approx +50$ % during the later simulation.

The largest deviations occur during settling sequences. The negative deviation at the beginning of the settling sequence (see Figure 29a) remarks an overestimation, the particles are settling too fast. Later they are settling too slow, remarked by the positive deviation. Figure 29b shows the simulated particle concentration for an exemplary settling sequence. As one can see, the real settling process (black line) seemed to be delayed. The settling process started significantly after pumps stop ($Q = 0$). This behaviour can be explained by the turbidity measurement. The reference values were measured only in the sensor section (in pipes central region). If the pump process stops, particles settled immediately over the complete pipe section. The particle concentration in the complete fluid section decreases, while it stagnated in the sensor section. Particles settling out of the sensor section were compensated by particles settling into this section. As a result, the reference particle concentration decreases later than expected by the computation.

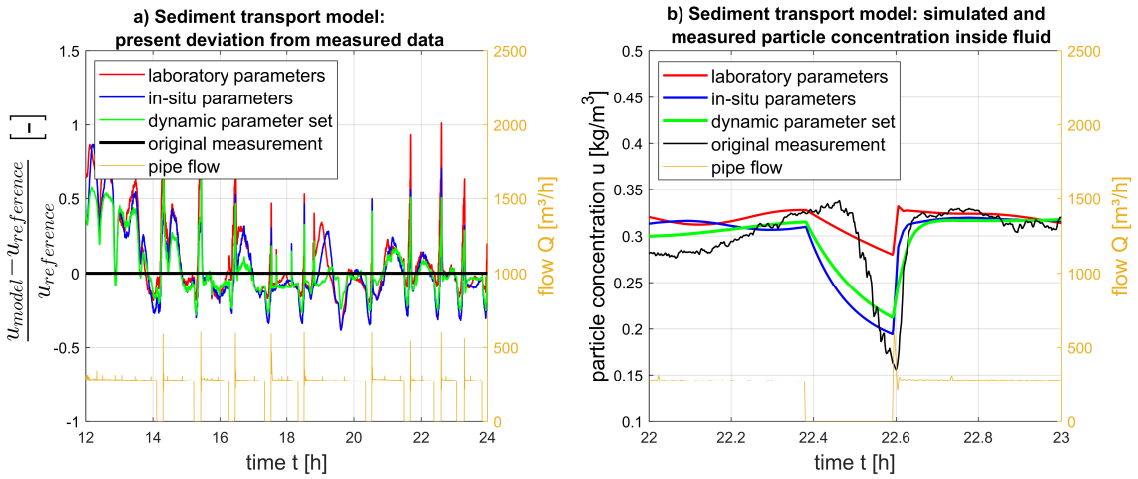

Figure 29. Results of the sediment transport simulation. Subfigure (**a**) present deviation from all three simulated parameter sets. Subfigure (**b**) settling sequence detail.

However, the simulated settling illustrates real life conditions, as the computed mass balance relates to the complete fluid section. This results, especially during the pump pauses, in a varying deviation. A trend cannot be detected visually. Therefore, Figure 30 shows the cumulated particle mass, calculated from the measurement and all three simulations.

The particle mass, transported through the pipe, amounts to 1164 kg (reference values). All three simulations were within a 10 % deviation (164 kg). The in situ and variable parameter sets were within 5 % deviation (82 kg). Hence, the sediment transport model can be used with the variable parameter set to simulate the particle fluxes inside a pressure pipe appropriately.

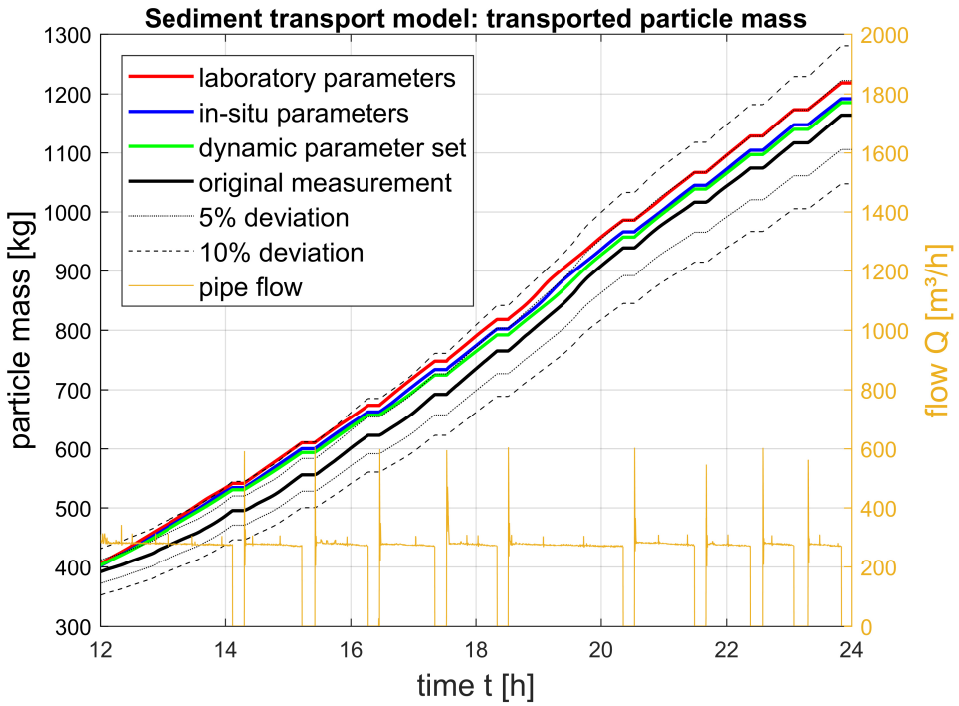

Figure 30. Results of the sediment transport simulation. Cumulative particle mass transport measured and simulated with laboratory-, in situ- and dynamic parameters.

6.3.2 Sediment transport under various regimes

The calibrated sediment transport model offers various possible applications in the field of urban drainage. We concentrate on the investigation of sediment transport inside pressure pipe under different flow regimes. Hence, the simulation of different pump control modes is the basis. Step one: We computed the mean flow velocity over a defined period, by a pump simulation. Step two: We computed the particle transport based on the previously simulated mean flow velocity, by a sediment transport simulation. The simulated pump control modes are summarized in Table 7.

Table 7. Simulated pump control modes with significant settings

	Simulated pump control modes				
	Full power 2-point control	Reduced 2-point control	Energy optimal 2-point control	Energy efficient control	Reduced energy efficient control
Flow in duty point (L/s)	166.5	100	76.5	76.5	76.5
Flow velocity in duty point (m/s)	0.6	0.35	0.27	0.27	0.27
Head loss in duty point (m)	18.3	17	16.7	16.7	16.7
Bed shear stress in duty point (N/m^2)	0.95	0.32	0.2	0.2	0.2
Power input in duty point (kW)	55	33.5	22.5	22.5	22.5
Power start-up*	yes	yes	yes	yes	no
Adjusted pump flow to inflow**	no	no	no	yes	no
Parallel pumping from critical sump level	yes	yes	yes	yes	yes
Forced operation at least 1/hour	yes	yes	yes	yes	yes

* Pumps start-up to maximum power over one minute before regulating down to duty point in each pump sequences

** If the inflow exceeds the present duty point, pump regulates up to the inflow rate

The main control rules from Table 7 represent real life pump control modes of PS Rostock-Schmarl appropriately. The control modes differ mainly in the reduction of the duty. Furthermore, some pump restrictions were added or left out, see Table 7. The measured inflow and TSS hydrographs at PS Rostock-Schmarl represent the incoming sewage and TSS flow for the pumping simulation. To compare the different pumping strategies, all five control modes were simulated over the same period of 30 days. The results were evaluated for bed load, suspended load and resulting energy consumption. The resulting bed load and suspended load transport is shown in Figure 31. Figure 31a shows the cumulative bed load while Figure 31b,c shows the cumulative suspended load over 30 days simulation. Table 8 summarizes the simulation results for all five pump control modes including the calculated energy demand.

Table 8. Resulting bed- and suspended load for five different pumping modes

	Simulated pump control modes				
	Full power 2-point control	Reduced 2-point control	Energy optimal 2-point control	Energy efficient control	Reduced energy efficient control
Total sediment transport (kg)	30 140 (100 %)	30 066 (100 %)	29 918 (100 %)	30 517 (100 %)	30 011 (100 %)
Bed load transport (kg)	360 (1.2 %)	546 (1.8 %)	750 (2.5 %)	757 (2.5 %)	841 (2.8 %)
Suspended load transport (kg)	29 780 (98.8 %)	29 520 (98.2 %)	29 170 (97.5 %)	29 760 (97.5 %)	29 170 (97.2 %)
Power consumption (kWh)	11 982	10 960 (-9 %)	9868 (-18 %)	9874 (-18 %)	7974 (-33 %)

The total transported sediment mass is similar in all five control modes and only differs by ≈2 %. In contrast, the ratio between bed load and suspended load varies between control modes. As to be expected, the least amount of bed load was transported within the strongest operation mode: Full power two-point control with ≈360 kg in sum. The suspended load amounts to ≈27 800 kg in full power mode. Hence, the bed load takes only ≈1.3 % of the total transported mass (= 28 160 kg) while ≈98.7 % are transported within the suspended load at a flow velocity of ≈0.6 m/s.

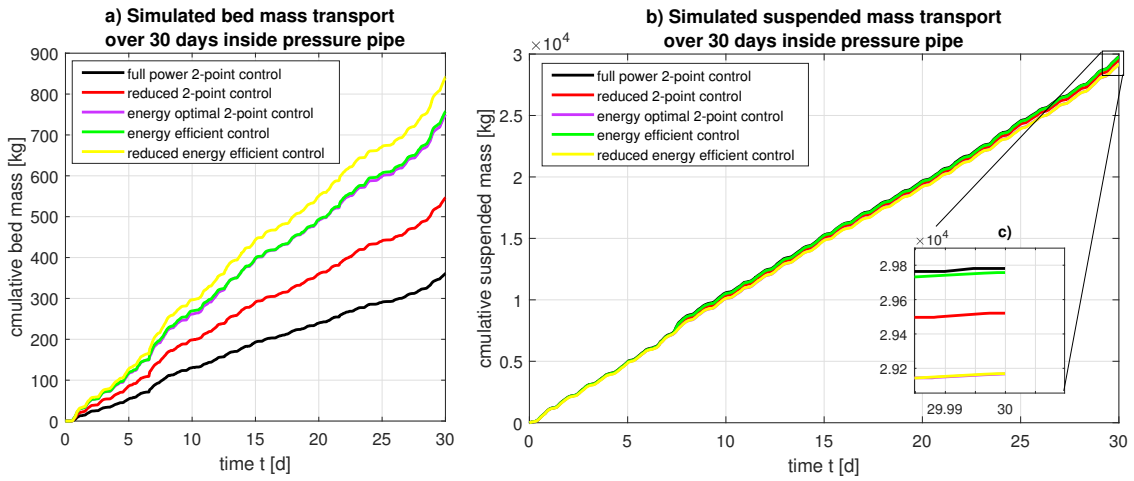

Figure 31. Sediment transport simulation for five different pumping modes over 30 days. Cumulative bed mass (Subfigure **a**) and suspended mass (Subfigure **b**) transport.

This ratio changes due to the weaker control modes on behalf of the bed load. The bed load transport increases with a decreasing duty point (compare to Table 7). However, even at very low flow velocities of ≈0.27 m/s within the energy-efficient control modes, the proportion of the bed load transport only amounts up to ≈2.8 % of the total transported sediments.

This means, a reduction of $>50\,\%$ flow velocity and a loss of $\approx 80\,\%$ bed shear stress (from full power two-point control down to energy-efficient control, see Table 7) does not results in significant changes of the bed or suspended load transport.

A critical transport limit is reached when the present bed shear stress falls below the critical bed shear stress for eroding sediments. The erosion rate then becomes zero. The least critical limit was calculated based on the results from Chapter 4 to $\approx 0.1\,\mathrm{m/s}$ flow velocity ($\approx 28\,\mathrm{L/s}$ flow rate) at a critical bed shear stress of $0.02\,\mathrm{N/m^2}$ after 20 min settling. This is below the technical minimum flow possible at PS Rostock-Schmarl of $\approx 53\,\mathrm{L/s}$, which at the same time represents the absolute mean inflow value to the PS. However, the simulation at a duty point of 0.2 m/s flow velocity showed that only 77 % of the total sediment mass is transported (compared to 100 % sediment transport in full power mode). Applying the calibrated model at a duty point below the technical limitation showed that having specific pure sewage flow velocities down to 0.1 m/s are feasible, but gradually lead to a decrease in transported sediment mass. Apart from this, such a reduction is not feasible for reasons of capacity loss. It is therefore recommended to set the duty point at least above the absolute mean inflow value, or even better to the energy-optimal value. In addition, a flow adjustment should be installed to compensate for inflow peaks, especially when storm runoff is connected. This guarantees both sediment transport and energy savings.

In order to put the sediment transport into context with the energy savings, these were recorded during pump simulation. The simulation of the energy consumption shows a good correlation of the pump simulation with the real system. The power consumption simulated for 30 days under reduced two-point control amounts to 10 960 kWh. In the same period, 11 179 kWh are measured in PS Rostock-Schmarl under reduced two-point control. The deviation is only -2 %. Concluding, the computed energy consumption can be used to make reliable statements for all five control modes.

Already 9 % energy savings were achieved in PS Rostock-Schmarl‘s usual operation mode (reduced two-point control) compared to full power two-point control. Further energy savings were obtained by the energy optimal two-point and energy-efficient control with 18 %. The maximum energy savings of 33 % could be achieved with the reduced energy-efficient control.

It should be noted that these energy savings were computed for a PS with a very flat system curve. The share of dynamic losses in total pressure losses was only 11 % in full power duty point (16 m static head to 18.3 m total head loss in duty point = 2.3 m dynamic loss). This proportion decreased with the energy saving control modes to 4 %. So, the energy saving potential was low and resulted in moderate energy savings compared to the usual operation mode. The ratio changes in favor of energy saving when greater friction losses occur in the usual duty point of a simple two-point control (e.g., with smaller pipe diameter).

However, the reduced flow regime in energy-efficient control contribute to the reduction of CO_2 emissions and operation costs without dangerously increasing the sedimentation of sewage solids.

6.3.3 Sediment transport under storm water inflow

Storm water inflow alter the transport characteristics of the raw sewage (see Chapter 3 and 4). Sedimentation and erosion are intensified. Storm water inflows are considered by the dynamical adjustment of calibration parameters α and d to the TSS inflow. Hence, the settled mass in the specific grid cell increases faster within pump pauses when storm water inflow enters the cell boundary. Subsequently erosion is intensified when the pumps start up. The critical bed shear stress τ_{crit} increases with the duration of the pump pause, but is not affected by the storm inflow. As the mechanical pre-treatment cleans the inflow from coarse material, it is assumed that the critical bed shear stress value after the pre-treatment is not modified by storm inflow. This assumption was supported by the results from Chapter 3. The laboratory experiments with raw sewage samples from PS Rostock-Schmarl have shown that "the particle spectrum did not change from dry- to wet-weather inflow (...), but rather the proportion of particles, especially in the medium speed fraction." [23, p. 10]. The proportion of the fastest particle class ($>$ 40 mm/s) only increased by 1.19 % from dry to wet weather sewage samples. An aggravated erosion was considered by the increased sediment amount on pipes bottom. The erosion process then simply takes longer. An example calculation is given in Chapter 4, where the erosion process is prolonged with increasing settling duration.

The effect of storm water inflow to sediment transport inside pressure pipe were evaluated for the same 30 days period as described in the previous section. Several rain events are recorded during this period in the catchment area of PS Rostock-Schmarl. Figure 32 shows the present amount of sediments inside the pressure pipe, simulated over 30 days for all five control modes.

The present particle mass was calculated as the total sediments quantity in all grid cells per time step (including both suspended and bed load). Figure 32 shows the present particle mass inside the pressure pipe for full power two-point control in detail (grey line) and for better visualization the 24 h simple moving average of the present particle mass of all five control modes (black to yellow lines).

The recorded rain events are shown on the right axis (blue line). Due to the size of the catchment area and the limitation of the connected areas on main roads (see Chapter 5), not all storm runoffs finally reach the PS. A good example was recorded at day 6. The storm runoff quickly enters the upstream sewer and subsequently the pressure pipe. The present particle mass increases up to $\approx$ 270 kg.

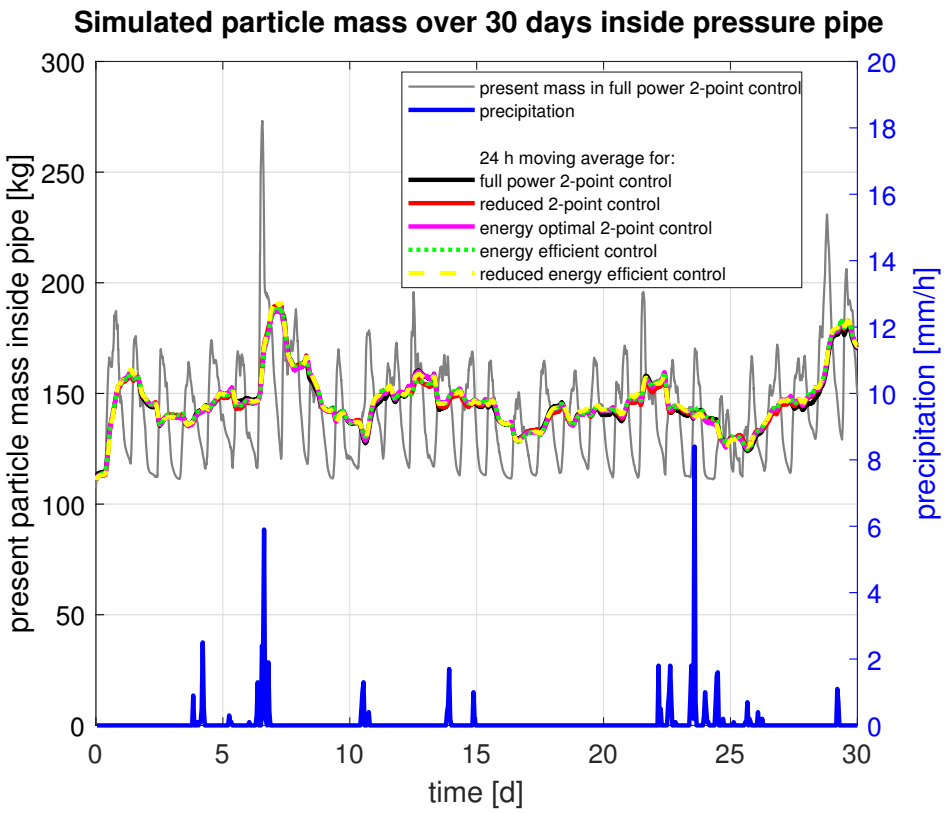

Figure 32. Sediment transport simulation for five different pumping modes over 30 days. Present particle mass inside pressure pipe on left axis and precipitation data on right axis (rain events are measured by a German Weather Service (DWD) meteorological station located inside the catchment area).

Under dry weather inflow, the peaks show the maximum sediment load inside the pipe during the day (at lunch) at $\approx$ 160 kg, while the sediment mass decreases in the night down to $\approx$ 115 kg.

Due to the 24 h average values, peaks were dampened but it provided the opportunity of supervision. It shows the results of long-lasting trends more clearly. If the moving average value increases constantly without decreasing, permanent deposits forming. However, such a trend cannot be detected. Even the increase in sediment volume due to storm runoff does not lead to a long-term formation of deposits. The sediments mass leveled out at $\approx$ 145 kg.

This is, off course, a result of the model calibration with settling parameters α, d and τ_{crit}. These parameters, calculated from in situ measurements in Chapter 5, representing real life conditions inside the pressure pipe. The simulation shows, that even under very low flow velocities, the sediments were transported safely. A permanent deposits formation is prevented by the continuous pump operation regardless of the control mode or the duty point.

6.4 Conclusion

The paper presents a transport model for 1D numerical simulation of the sediment transport inside a pressure pipe. The model aims at an exact description of the sediment transport by a limited but case-specific set of transport equations. It is quite simple from a physical point of view. However, an easy but descriptive assessment tool for sediment transport in pressure pipes is available, based on calibration parameter determination by in situ measurements.

The following fields of application are conceivable: Energy-efficient pump control, optimization of sewage disposal and treatment supply to WWTPs, pollution transport to urban drainage facilities, planning and design of urban drainage systems and optimization of pipe flushing.

The investigation of hydraulic boundary conditions in pressure pipes under dry weather and storm water inflow have shown in case specific that very low flow velocities and shear stress values are tolerable. Accordingly, the developed energy-efficient pump control with low flow velocities can guarantee the safe disposal of wastewater streams.

7 Final Discussion

The individual contributions are all driven by the same question: Can energy-efficient pressurized wastewater transport be combined with safe sediment transport? To answer this question, the individual contributions are discussed in sum. Finally, the results are structured and interpreted thematically regarding three categories: (i) technical, (ii) ecological and (iii) economic. This allows the evaluation of the actual benefit of the results, especially for the operation of pressure pipe systems.

7.1 Effects of the change in pump strategy

The strive for energy savings in wastewater pumping leads to a change from two-point control to energy-efficient control. Figure 33 illustrates both pump strategies for the same period (results are simulated based on calibrated pump simulation). The two-point pump control in Subfigure **a** shows surplus pump capacity for most of the time (see also Figure 1). Converted into power consumption, this proportion can also be seen as a potential for current energy savings. Under consideration of the operation restrictions (forced runs, transport limits, sump level limits, etc.), a part of this potential can now be obtained by means of the energy-efficient control. Subfigure **b** shows the energy-efficient strategy in energy optimal duty point. If the inflow rate to the PS exceeds the optimal flow rate, the flow rate is adjusted to the inflow rate. If the inflow rate falls below the optimal flow rate, the pump operates with the optimal flow rate until the stop level reached. Next to this, the following restriction always had to be respected: pumps are forced to start-up to maximum power for one minute before regulating down to energy optimal flow. At the energy-optimal flow, a significantly better adaptation to the current pumping demand is achieved. The proportion of surplus pump capacity is correspondingly lower.

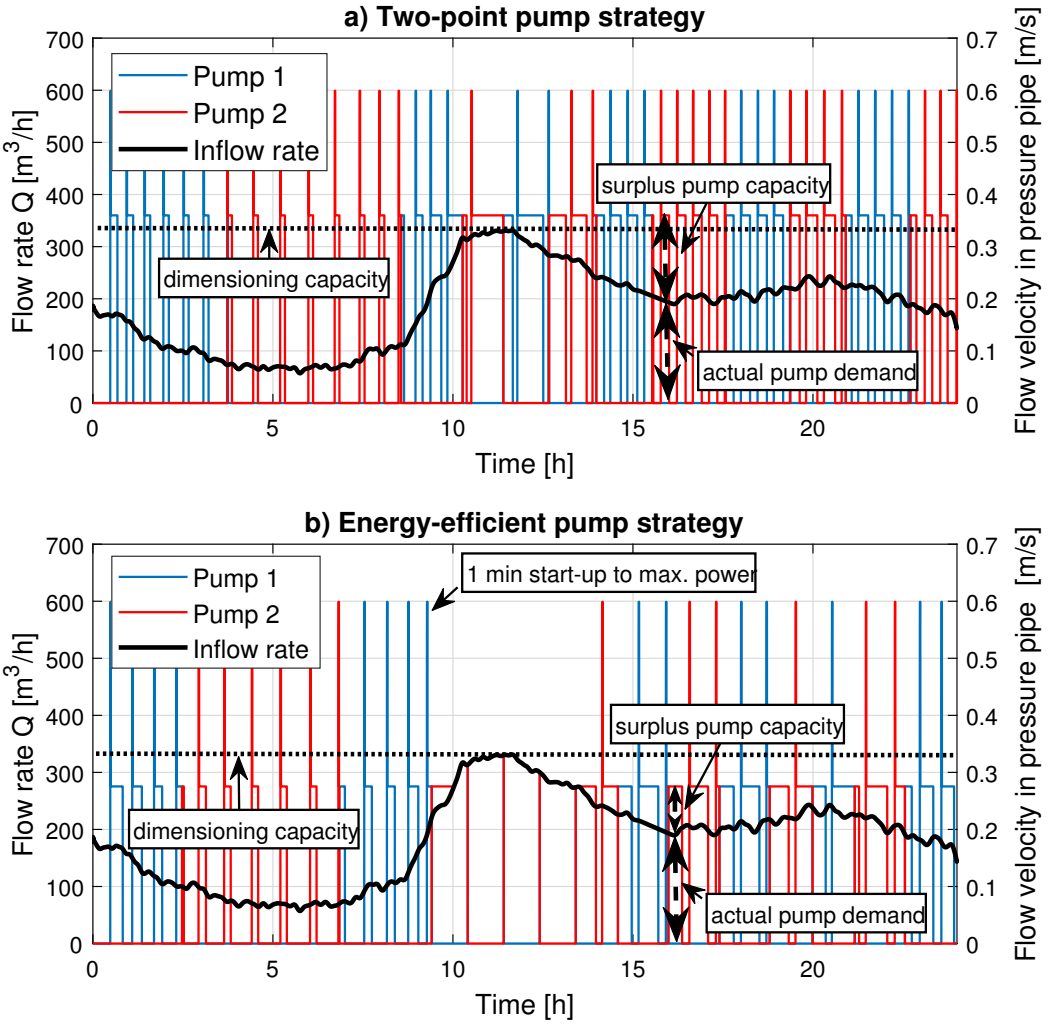

Figure 33. Pump control strategies in comparison and diurnal inflow rate to PS Rostock-Schmarl. Subfigure **a)** two-point pump strategy. Subfigure **b)** energy-efficient pump strategy in energy optimal duty point.

The resulting energy saving here amounts to up to 11 % compared to the common (reduced) two-point control of PS Rostock-Schmarl (18 % energy saving compared to full power two-point control, see Table 8). At the same time, the flow velocity decreased from 0.35 m/s to 0.27 m/s. This makes a decrease of the bed shear stress from 0.32 N/m^2 to 0.2 N/m^2, see Table 8. The total duration of the daily pump pauses has been reduced by ≈ 3.1 h, see Section 3.3.1. The longest pump pauses during the night partly decreased from 2.5 h to ≈ 40 min, see Section 3.2.3. On average, the pump pauses were reduced from ≈ 64 min to ≈ 20 min, see Section 4.3.2.

Vice versa, the duration of the pump sequences increased by the same amount the pump pauses decreased. The reason for this lies in the fact that exactly the same volume of wastewater has to be pumped. Hence, the time a fictitious volume element passes through the pipeline should be approximately the same when comparing different pump strategies.

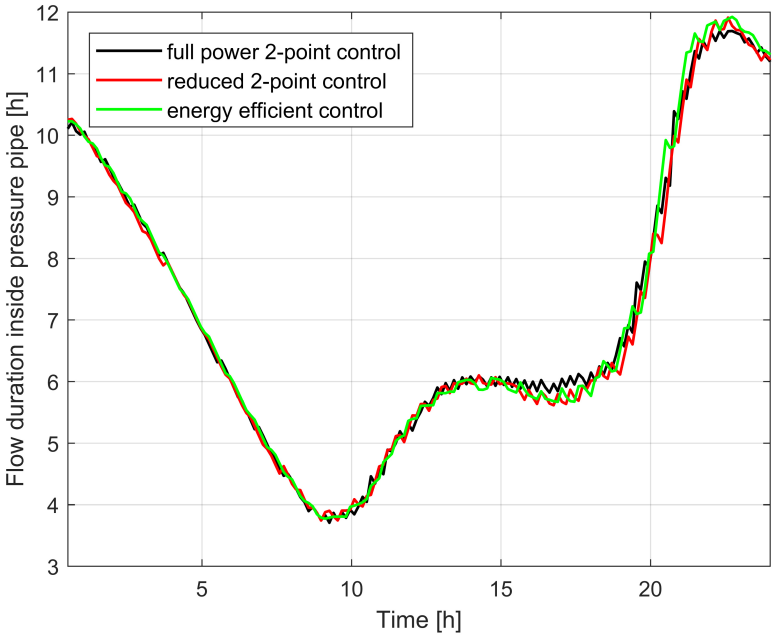

Figure 34. Simulated flow duration of different pumping strategies for PS Rostock-Schmarl. An example: a fictitious volume element entering the pressure pipe at 10 a.m. will arrive the WWTP Rostock after 4 h at 2 p.m. irrespective of the control mode.

Figure 34 illustrates the flow duration required by a fictitious volume element to reach pipes end (WWTP Rostock) when it enters the pressure pipe at a certain time. The flow duration fluctuates just as the diurnal inflow variation to PS Rostock-Schmarl (see Figure 33). It results in transport durations between 3.8 h starting at 9 a.m and 11.75 h starting at night. Most importantly, regardless of the pump strategy, the duration is almost identical. The distance covered in a shorter time in regular- or full power control is compensated by longer pump sequences in energy-efficient operation. An ”easily” transportable wastewater would thus be transported even more safely, since the settling sequences (pump pauses) have been reduced and the transport sequences (pump sequences) extended.

This is supported by the following consideration: PS Rostock-Schmarl and the connected pressure pipe were already built during the construction of the large housing estates in Rostock-Schmarl from 1976 to 1978. Thus, even before the study of the energy-efficient control from 2015 to 2016, a safe operation was guaranteed for decades. Even the installation of the VFD in 2001 and the adaptation of the control system had no negative effects on the operation. At least for the majority of the time, the transport characteristics must therefore be significantly below the recommendations here and thus case-specific. It is consequently necessary to define and evaluate the transport parameters exactly.

7.2 Ex- and in situ determination of the transport behaviour

Within this work, it was shown that the determination of transport properties with respect to sedimentation (see Chapter 3) and erosion (see Chapter 4) by means of ex situ laboratory experiments is possible with reasonable effort. Various plausibility calculations and finally the simulation of the transport of solids (see Chapter 6) have proven the reliability of the methods. Both ex situ methods were constructed from literature information and further developed and adapted.

In contrast, determining transport characteristics of raw sewage by in situ measurements directly inside the pressure pipe is a completely new methodology. Comparative literature was not found. Just like in modelling (see Section 6.1), this might due to the assumption of controllability and consistency of processes inside the pressure pipe. Research activities therefore tend to concentrate on gravity sewers. Furthermore, the scepticism of the sewer system operator (which is not unfounded) is certainly often opposed to the technical implementation of in situ measurement in a wastewater pressure pipe, especially when dealing with older pipes.

However, in Chapter 5 it was shown that the technical implementation of an in situ measurement provides above all very informative measurement results. In addition to the pure monitoring of the solid flux, transport parameters can also be determined using simple evaluation routines. The in situ measurement is particularly suitable for the observation and evaluation of sedimentation. Moreover, the in situ method can fundamentally enable the complete observation and characterisation of erosion process. However, the erosion measurement is technically delimited by the given minimum flow rate of 53 L/s, see Section 6.2.1. This results in a technical minimum bed shear stress of $\approx 0.1\,\mathrm{N/m^2}$. As the critical bed shear stresses are partly below this limit (see Table 5), it is impossible to carry out the tests in reality (especially the transition to erosion cannot be determined exactly). Concluding, the in situ measurement cannot replace the laboratory erosion tests here. This might be different in drainage systems with lower technical limitations or especially in combined sewers.

However, an exact determination of the case-specific transport behaviour is possible. This is the prerequisite for the evaluation of the solid transport under certain pump strategies. Furthermore, it can be proven that the transport parameters deviate significantly from recommendations.

7.3 Evaluation of the case-spefic transport characteristics

In the present work, the sedimentation was first described in Chapter 3 by means of a settling velocity distribution. The material is divided into different settling velocity classes (similar to a grain size distribution). This allows a good assessment of the sedi-

mentation dynamics and thus already first statements regarding the sediment transport and the behaviour in the pumping process, see Section 3.3.3.

A high percentage of rapidly settling particles with a small velocity distribution has a negative effect on the pump operation. In contrast, a rather broad velocity distribution with slowly settling particles is a good pumping medium. This is precisely the case for the dry weather-, raw sewage inflow to PS Rostock Schmarl, see Figure 10 Subfigure **b**. Based on the velocity distribution for dry weather conditions, it can already be concluded that there is hardly any risk of disturbance by sedimentation inside the pipe. The sewage samples also turns out to be a very slowly settling material in a literature comparison. The literature comparison from Section 3.3.2 is graphically presented in Figure 35 (only studies with the same methodology are presented).

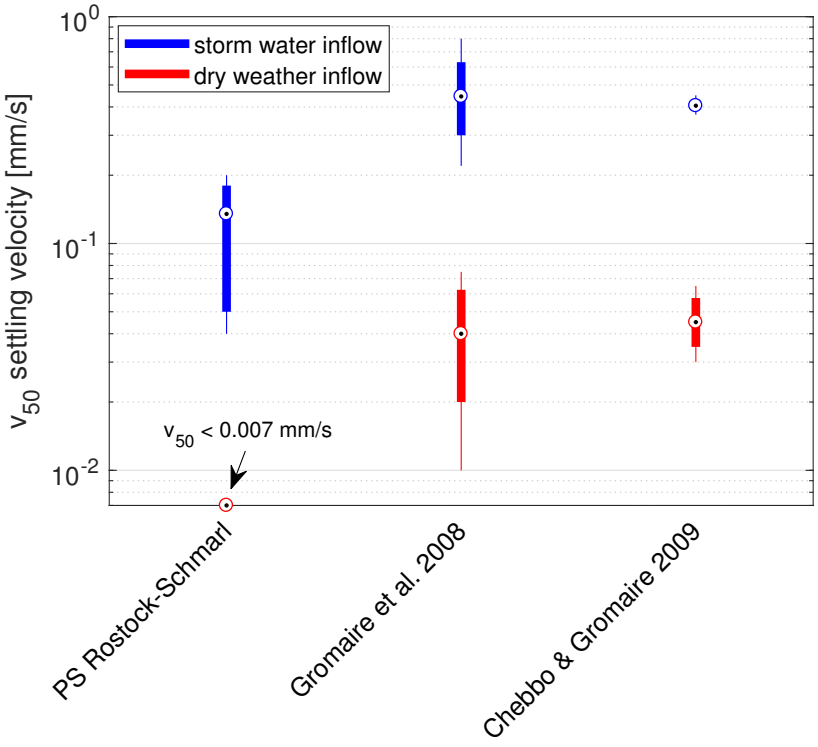

Figure 35. Settling velocity distribution in literature comparison under dry weather- and storm water inflow: settling velocity of 50 % of particles v_{50}.

To compare the studies, the settling velocity of 50 % of the particles, v_{50}, was chosen here, as this parameter is already used in the literature. The v_{50} value was not reached here under dry weather inflow, see Figure 10 Subfigure **b**. Nevertheless, compared to the literature values (which mainly originate from combined or storm water systems), the v_{50} values during dry weather inflow are significantly lower. This shows that the respective wastewater must be distinguished in each case.

The connection of the main road to the normally existing separation system in Rostock-Schmarl causes a temporal change of the sedimentation characteristics at storm runoff.

The storm water inflow changes the settling velocity distribution and thus increases the v_{50} value, see Figure 35. In comparison to the literature, the v_{50} values under storm water inflow are still significantly lower. This also supports the statement that the solid transport should be considered case-specific.

The situation is similar for the critical erosion limit τ_{crit}. In Table 9 the literature comparison from Section 4.3.3 was summarized and further comparative values were added. The results show that the determined transport limits for the pure sewage case here are clearly below the literature values, which were mainly performed in combined sewers. Furthermore, it can be seen that there are also considerable differences between the combined sewers itself. Both facts confirm to the case-specific consideration. However, it should not be ignored that these differences may have multiple causes: (i) settling duration: common settling durations for erosion tests in the range of 24 h up to several years. (ii) type of sediment: cohesive sediments (high organic loads) and large, heavy particles with increased mineral content in combined systems. (iii) method: variation of applied erosion measurements (open channels, cylinders, pipes, etc.).

Table 9. Comparision of critical bed shear stress values τ_{crit} with literature data

τ_{crit} (N/m^2)	Reference	Comment
5 - 7	Kleijwegt 1990 [103]	Ex situ laboratory test with cohesive sediments (combined sewer)
1.3 / 20	Kamphius 1990 [104]	Ex situ laboratory test with/ without grains of sand
1.8 - 2	Ashley 1992 [105]	In situ tests (combined sewer)
7 - 2500	Wotherspoon and Ashley 1992 [106]	Ex situ laboratory test with cohesive sediments (combined sewer)
2.2 – 5.6	Ristenpart 1995 [68]	In situ tests in combined sewer during storm water inflow
0.44 – 1.02	Ristenpart 1995 [68]	In situ tests in combined sewer during dry weather inflow
0.3 – 0.6	Gunkel 2017 [107]	In situ tests for combined sewage
0.015 – 0.16	Rinas 2018 [24]	Ex situ laboratory test with raw sewage (dry weather inflow)

An interesting fact here is that the particle spectrum hardly changes by storm water inflow. Only the particle distribution within the particle spectrum changes due to the storm runoff, see Section 3.3.2. This causes an increased rate of sedimentation (see Section 3.3.3) which subsequently causes an aggravation of erosion due to larger deposition rates (see Section 4.3.2). The problem is particularly apparent in two-point operation, when long pump pauses cause a high amount of deposits (see Figure 11).

Logically, it is safer for solids transport to keep the solids in suspension for a longer period of time at slow flow velocities than to allow them to settle more strongly during longer pump pauses caused by higher flow velocities. Since the particle spectrum has not changed during storm runoff, there is no change in the critical erosion parameter τ_{crit}. Consequently, the slower and prolonged transport in energy-efficient operation does not pose a safety risk.

If one considers the technical implementation, various restrictions have to be respected, especially during storm water inflow. In energy-efficient operation the pump capacity is adjusted to the inflow as soon as it exceeds the optimal flow, see Section 3.2.1.

This leads to permanent changes in the flow velocity and pump pauses. Since this also occurs briefly in dry weather inflow (see Figure 33), but above all with storm water inflow, only a rough evaluation of the transportation of solids by interpretation of the determined transport properties is possible.

A much more dynamic view is provided by monitoring the transport of solids by means of online TSS measurement. Since the direct effects on sediment transport of the change in pump control are permanently measured here, much more precise statements can be made. This is mainly due to the increased data volume provided by the continuous measurement, see Section 5.3.2. This allows the separation of the series of measurements into settling- and erosion phases, making the pressure pipe itself a test reactor.

Hence, the change of the transport properties by storm water inflow could be precisely observed and analysed here, see Section 5.3.5. Above all the in situ determination especially contributes to the detection and definition of the diurnal variation of the transport parameters, see Section 5.3.7. This results in a further level of detail in the evaluation of transport behaviour. In addition, the laboratory results could be confirmed, see Section 5.3.4 and Section 5.3.6.

The description of the sedimentation differs for in situ measurements. The formely used settling velocity distribution (see Chapter 3) is replaced by a settling rate. This settling rate is described by an exponential decay, see Section 5.2.5 and Section 6.2.3. This allows by far much easier analysis of the extensive data and also simplifies the description of the settling process. In spite of this simplification, good results were achieved in adapting the function, see Section 5.3.2. The process itself is described by a single parameter, the settling parameter α. This contributes especially for modelling. Since the aim from the beginning was to keep the model as simple as possible (no differentiation into settling classes), the number of calibration parameters had to be decimated. Hence, the settling process itself as well as its diurnal variation is described only by determining α. This simplifies the implementation into the model as well as the computation effort per time step.

The final level of detail in the evaluation of the transport behaviour is achieved by the development of the sediment transport model. The preceding investigations are to be regarded as direct input for the creation and calibration of the model, see Figure 3. The simulation enables the evaluation of the case-specific wastewater transport. Furthermore, a combination to a pump control simulation allows the evaluation of the resulting solid transport under different pump strategies.

7.4 1 D solid transport simulation

The presented sediment transport model is a one-dimensional numerical transport simulation. This means, the transportation of the solids (undissolved material) is only computed in one direction, which is the longitudinal direction here (along the pipe axis). The transportation itself is based on the ADE, see Equation (31), which is simplified to the one-dimensional advection equation, see Equation (33). According to this simplification (see also Section 6.2.3), the transportation is only permitted in positive flow direction.

The transport of materials is generally divided into the following three types (according to [108]): (i) bed load (particles glide, roll or jump on the bed), (ii) suspended load (particles that are kept above the bed by turbulence (according to [109]) and (iii) wash load (particles and substances floating always above the bed, no sedimentation).

As this classification was developed for running water bodies, it can more or less be transferred to the transportation of substances in sewers (see [110] and [111]). The solids to be transported here are always partitioned into the two fractions suspended- and bed load, see Equations (34) to (35) (conservation of mass). The simulation of the wash load is not performed here, since it generally only contains non-sedimentable and dissolved material. The partial differential equations are discretized by the finite difference method (FDM). By this, they are replaced (approximated) by difference quotients at finite grid points. The resulting system of equations is then solved stepwise by means of algebraic matrix operations within a computing environment (here Matlab). The solution gives the proportion of solids in the respective fraction at each time step and at the grid positions within the pipeline.

The formerly defined transport parameters α, d and τ_{crit} (see Chapters 3 to 5) determine the transport processes (sedimentation and erosion) modelled in the system of equations. The characteristic of the entire transport process is thus controlled by these three parameters. All three are non-static. They are changing, according to the inflow condition (α and d) and the settling duration within the pump pauses (τ_{crit}), see Section 5.3.7 and Section 6.2.5. The flow velocity required for the sediment transport computation is provided in advance by the simulation of the pump control. Together with the pump simulation, these models are uncoupled. It means that there is no change in the flow parameters in the pump simulation due to the effects in the sediment transport model (e.g. increase of the flow velocity by decreased pipe cross section due to increased deposits).

In principle, any number of different pumping strategies can be simulated, while five different pump modes were compared here, Section 6.3.2. In addition to pumps technical data (pump curve, performance curve, motors and pump efficiencies, etc.) and the sump geometry, the actually measured inflow curve is also used as input variable for the pump simulation. A wide range of measured inflow curves is therefore beneficial to

be able to simulate real scenarios. The simulation in Sections 6.3.2 to 6.3.3 is based on the measurement of the inflow to PS Rostock-Schmarl over 30 days in April 2016.

Due to the simplifications already mentioned from Section 6.2.3, the simulation results must be interpreted under the following aspects:

- **Flow formulation**: The previously executed pump simulation does not contain a hydrodynamic flow formula. The flows in the duty points (see Table 7) are calculated as mean flow velocities based on the continuity equation (one-dimensional stationary incompressible flow in a fully filled pipe). This represents the flow velocity required for sediment transport over the complete pipe cross-section (velocity distributions over the pipe cross-section are neglected). Transient flow processes, resulting from e.g. the closing of a gate valve or the switching on and off of a pump, are neglected here. This mainly concerns the pressure surges (water hammer) as they are not respected in the model when pumps switching on or off. Hence, settling starts immediately when the pump switches off. In reality, sedimentation may be delayed by the pressure waves.

- **Model coupling**: As already mentioned, both models (pump and sediment transport simulation) are uncoupled. The pump model only influences the sediment transport model. In reality, it is certain that increased power consumption due to increased frictional losses caused by increased sedimentation occurs. It is conceivable that a state of equilibrium is established in the case of extreme deposition formation in reality. Initially low flow velocities lead to the formation of permanent deposits which in turn increase the flow velocity. An equilibrium may be reached when the erosion caused by the increased flow velocity is equal to the rate of deposit formation. This might be a very important effect for the formation of deposits by sewage with high tendencies of settling. It should be noted that these effects are not considered here.

- **Settling formulation**: A potential deposit layer is distributed evenly on pipes bottom. No attention is paid to the pipes shape, see Section 6.2.3. In reality, deposits are probably more like normal distributed around the vertical pipe axis (the higher the sedimentation column, the higher the layer thickness). As already mentioned in Section 7.3, the settling formulation is simplified to an exponential decay. Hence, there is no separation into particle classes in the model.

- **Erosion formulation**: Since there is no separation into particle classes and the flow formulation leads to a mean velocity over the pipe cross section, eroded sediments are uniformly distributed over the pipe cross-section. In reality, there is certainly rather an increased proportion of the heavier particles near the bottom of the pipe depending on the flow velocity destribution, see [111].

  The critical bed shear stress increases with the pump pause. If sediments are incompletely eroded after the subsequent pump sequence, the settling period is not continued (see also item ”Transport processes”).

τ_{100}, the complete resuspension bed shear stress (see Section 4.3.1) was not included in the simulation. Pump pauses of 20 to 60 min (see Section 4.3.2) results in τ_{100} values of about 0.2 to 0.4 N/m^2 (see Section 4.3.1). These values are achieved in all applied control modes (see Figure 19 or Figure 25 **c** and **e**). Furthermore, the implementation would have made the model more complex, which would be in conflict with the actual objective of making the model as simple as possible.

- **Transport processes**: Particle transport can generally be divided into the processes erosion, transport, deposition and consolidation (commonly known as ETDC-cycle, see [110]). The definded transport parameters here describe the two processes erosion and sedimentation. The particles are transported at the mean flow velocity as soon as the critical bed shear stress is reached. If the bed shear stress falls below the critical bed shear stress sedimentation occurs. Special laboratory tests to determine the subsequent consolidation effects were not carried out. However, indications of initial consolidation effects could be found in the erosion tests (see Section 4.3.1). Sediments within the pipe consolidate when left in place. That is, when erosion is incomplete. This can occur when pumping with sufficiently high shear stress but only at short intervals. Hence, besides the force itself, the duration of the force effect on the sediment bed is also decisive. This is because, the force (bed shear stress) always acts only ”layer by layer”, see [27, p. 142]. The erosion rate is then not high enough to erode all sediments within the time slot (pump sequence) and consolidation occurs. Further considerations will be concluded in Chapter 9.

- **Topography**: As the pipes negative or positive slope and curvature are ignored, settling processes on slopes are not intensified (particles on pipes bottom do not glide or roll downhill) and erosion processes are not hindered (uphill) or intensified (downhill).

- **Status quo**: Simulation starts with new pressure pipe filled with clear water and without any deposits. All previous states cannot be simulated. The system has been in operation for over 40 years, see Section 7.1. This results in numerous difficulties: lack of knowledge about long-term control strategies, no technical data on the previously installed pumps, no information on modifications or additional installations, repairs and temporary shut-downs or cleaning work on the pressure pipe, no information on long-term upstream sewer connection situations that may have led to other operating conditions within the pipe, no long-term recorded inflow hydrographs as well as TSS inflow measurement, no information on long-term use of the rake, etc.

- **Sewage characteristic**: The modelled sediment transport is representative for a pure sewage from a separating system. Compared to the literature, the wastewater is easy to transport. The sedimentation tendency is very low (see Table 8) and it can be eroded easily (see Table 9). A change in the wastewater characteristics is caused by storm water inflow, see Section 5.3.5. The effects on the transport properties, however, are rather small. Hence, it is still easy to transport even under storm water conditions.

Considering the simplifications, the results of the simulations are sufficiently accurate for an assessment of the sediment transport in pressure pipes, see Section 6.3.1. This allows the simulation of a PS with different pumping strategies including sediment transport. In this way it can be examined whether energy-efficient pump control is compatible with a safe sediment transport.

7.5 Evaluation of the solid transport under reduced flow conditions

The results of the laboratory tests (Chapters 3 to 4), online monitoring (Chapter 5) and the pump- and sediment transport simulation (Chapter 6) have shown that it is possible to reconcile a reliable wastewater pumping with an energy-efficient control for an urban wastewater PS.

In the following sections, these results are evaluated from a technical, ecological and economic point of view. In parallel, case-specific recommendations for operation are derived. Evaluations and recommendations are based on the ex- and in situ tests and the pump and sediment transport simulation.

7.5.1 Technical evaluation and recommendation

Energy savings based on the reduction of dynamic energy losses are possible through active control of the pump system. Hence, essential for the implementation of an energy efficient control in a drainage system is a speed control of the pump motor. A sewage PS must be equipped with a VFD, if not already installed. The entire technical upgrade, the implementation of the pump control into the programmable logic controller and connection to the process control system results in technical, personnel and financial expenditure. Despite the expenditures it was shown that the amortization period is only a few years, see [15].

The non-invasive determination of the deposit height carried out in Section 3.3.4 can be used as a proven method to monitor the actual status of the pressure pipe. Thus, monitoring by means of online TSS sensors can be omitted [15]. An ex- or in situ determination of the transport parameters is not replaced by this, however. Further explanations have already been given for the determination of the deposition height by [13, 15].

On the other hand, there are primarily the savings resulting from the reduction of energy consumption. But there are also other positive effects. By using the VFD and the energy-saving control system, pump components are also protected by reducing mechanical stress (e.g., motor coupling, pump impeller, etc.). This contributes to extended life cycles and reduces service requirements. Furthermore, the use of VFD reduces waterhammers by a controlled stop of the pump. This protects the pressure pipe itself as well as its installation parts.

Changing the control system of a sewage PS also has an impact on the surrounding sewage network. Negative effects on the upstream sewers can be excluded here, since the original switch-on points of the pumps are retained within the energy efficient control. Even under extreme storm water inflow, forced control systems come into effect which trigger parallel pump operation. Thus, for example, possible intentions to use the storage capacity of upstream sewers in case of storm water runoff are not hindered.

The mechanical pre-treatment installed in the PS Rostock-Schmarl (rake) largely prevents the further transport of materials susceptible to clogging. This generally already reduces the transport load for the downstream system. It also has positive effects with regard to the pump sump. The effects of energy-efficient control on the sedimentation processes in the pump sump were not further investigated within the project. It can be assumed, however, that a reduction of the pump capacity does not necessarily lead to extended residence times in the sump. The extended pumping sequences in energy-efficient operation compensate for the short pumping sequences with high pumping power in regular operation, similar to Figure 34. However, due to the individual sump geometry, zones with different flow behaviour are formed. This can lead to longer residence times of individual fluid and solid particles.

Long residence times of wastewater in sewer systems are always associated with sewage fouling and the formation of gases. However, by proving the unchanged transport duration in Figure 34, this sewage fouling does not have to be given more importance than it already had. An increased formation of corrosive gases is therefore not to be expected.

It should also be mentioned that these effects, sewage fouling or pump clogging, were excluded as the investigations primaly focused on the sediment transport. There are two main reasons for this: (i) there are several technical solutions for solving these problems (e.g., sump geometry optimization, grinder pumps, chemical dosing systems, etc.). (ii) By far the greatest hazard potential within the study was assumed to be a blockage of the pressure pipe as a result of increased deposits formation.

A blockage of the pressure pipe, however, did not occur during the entire study period. Sediment transport is therefore not disturbed by the reduced flow conditions here.

But due to the locally very different conditions (PS, pressure pipe and above all wastewater composition) a generally valid statement about the sediment transport can hardly be made. So it is a fact that energy-efficient control can only be implemented if the transport properties of the wastewater allow safe transport. This is fully applicable for the present case. But it does not automatically apply to others as well. It can be assumed, however, that similar results can be found in structurally and technically similar drainage systems. At least, a differentiation must be made especially according to the composition of the wastewater. The methods developed here can be used to characterize and simulate the transport behaviour. Thus, the possibilities and limits of an energy efficient control can be determined in advance without risking dangerous conditions.

Nevertheless, experience shows that operators of sewage systems are often extremely sceptical about reducing flow velocity in favour of energy savings. Of course these concerns are not unjustified. The focus is then on a central problem. If the energy saving results in a permanent deposit formation which leads to a blockage and probably a failure of the wastewater pressure pipe, the costs and possibly also emissions for the repairs are perhaps higher than the savings itself.

On the other hand, however, it is a fact that the transport characteristics are mostly unknown. So even in regular pump operation a sediment transport is by no means guaranteed. It can be assumed that under certain conditions (mainly based on the wastewater composition), similar to those presented here, even an improvement in sediment transport can occur. This assumption is based on the following consideration: For the conveyance of an easily transportable wastewater, slower but longer lasting pump sequences with shortened pump pauses are safer than fast but short-lasting pump phases with long settling durations.

Irrespective of the control strategy, the primary objective for the operator is to ensure operational safety. Energy efficiency can then be optimized by continuously ensuring operation. Now this study has shown that operational safety and energy savings are compatible for a wastewater PS in an urban area. Especially for pure sewage PS with mechanical pre-treatment, the possibilities of energy optimization by means of frequency control seem to be the most appropriate.

But also for combined sewer systems it is possible to react to increased requirements regarding sediment transport by means of forced regulations within the control system. An exemplary solution are forced starting phases of the pumps up to maximum capacity before regulating down to energy efficient capacity. By determining the local transport parameters, the control limits can be determined and exact control specifications, e.g. for forced runs, can be given. In this way, operational safety can be brought in line with energy efficiency in pressured sewers.

Irrespective of the drainage system and the characteristics of the wastewater, the valid technical codes are to be applied in the first instance when dimensioning pressure

pipes and PS. However, this may results in operational problems. As already shown in Figure 2, the requirements can sometimes not be met. The recommended minimum flow velocity cannot be achieved here for technical reasons (max pump capacity not sufficient). This problem is further aggravated by the reduction of the flow velocity within an energy-efficient pump control.

If these values are to be achieved, other methods must be used (e.g., compressed air flushing). Otherwise, an increase in pump capacity would reinforce the already existing oversizing, see Figure 33. On the other hand, however, there is the functional efficiency over several decades as already mentioned in Section 7.1. The recommendations have thus already been ignored for longer periods without blocking the pressure pipe. The solid transport recommendations are obviously strongly safety-oriented, as they pursue a certain general validity.

This argues for a differentiation of the recommendations according to the composition of the wastewater or at least roughly according to the drainage method (separate or combined sewer). In addition, possible pre-treatment technologies should also be considered. Furthermore, it is possible to specify not only the minimum flow velocities but also the necessary durations and frequencies due to the sewage transport behaviour.

To meet the criteria, at least to some extent, the above-mentioned regular (at every pump start here), case-specific (depending on sewage settling and erosion behaviour) and short pump starts with a certain capacity (here one minute at nominal capacity) are a suitable instrument for a compromise between operational safety and energy savings. The subsequent main pump sequence can then be dominated by a reduced pump capacity to increase energy efficiency.

7.5.2 Ecological evaluation

If we recapitulate, the origin of the project lies in the reduction of greenhouse gas emissions by increasing the energy efficiency of wastewater PS, see Section 2.1.

Numerous contributions have already reported on the energy savings achieved [12–15, 26]. Table 8 shows the simulated energy consumption and potential energy savings of five different pump control modes of PS Rostock-Schmarl. The simulated energy savings deviate only slightly from the real measured savings, see Section 6.3.2. In energy-efficient operation there is a reduction in consumption of about 18 % compared to full power two-point control. Compared to the savings of 25 % originally assumed in Section 2.1, the efficiency is reduced, but is nevertheless still significant.

The extrapolation from Section 2.1 then changes as follows. Assuming an energy savings potential of 18 % for all PS of the water company in Rostock (347 PS in total), a reduction of the CO_2 emission of ≈ 330 t is achieved (for 2018, assuming a CO_2 emission factor of 474 g/kWh [11], originally ≈ 458 t assumed by energy savings of 25 %).

In addition to the savings from the pure reduction in consumption, there are also savings from the extended life cycles and smoother operation of the components: fewer repairs or replacements and maintenance intervals and the associated emissions from transport routes.

With the increasing use of renewable energies, the share of CO_2 emissions in the electricity mix is also decreasing. This logically reduces the savings potential here as well (which is generally a positive trend). However, this is in contrast to the expected increase in electricity costs, which can be counteracted by a continuous increase in efficiency.

7.5.3 Economic evaluation

Due to the general trend of increasing electricity costs, as already mentioned, there is a need to increase efficiency. It can be assumed that cost reduction is the biggest driver for an operator to increase efficiency.

In the sample from Section 2.1, the savings are reduced to 18 %, as mentioned above. With an assumed electricity price of 0.15 €/kWh, the current savings are $\approx$ 3800 € per year (for PS Rostock-Schmarl). The calculation is again transferred to all PS. This results in savings of $\approx$ 695 333 kWh and corresponding $\approx$ 104 300 € per year. Reinvesting the savings in energy efficiency can contribute to further optimization, see Section 2.1.

As already mentioned, the armotisation time for conversion to VFD operation is only a few years [15] and is almost completely omitted for already equipped systems. In addition, costs are reduced by the increased life cycles of technical plant components (pumps, motors, check valves, etc.).

8 Final Conclusion

The reduction of the flow velocity in sewage pressure pipes to achieve energy savings is countered by the generally assumed decrease in sediment transport.

The presented study showed for over a year of test operation that energy saving and operational safety are not mutually exclusive. By means of various laboratory and field measurements as well as simulation studies the transportation of solids inside wastewater pressure pipes could be described and a safe transport could be proven.

The study has shown that wastewater can be transported more easily than often assumed. However, it is often regarded as a problematic transport medium due to its spatial and temporal variability. Recommended minimum flow velocities often seem to be very safety oriented, at least for pure sewage PS. The energy saving control leads to reduced flow velocities and thus also to shorter pump pauses and lower critical bed shear stresses. Pure wastewater tends to very slow sedimentation processes. The critical bed shear stresses are significantly below $< 1\,\mathrm{N/m^2}$ in pure wastewater.

As already mentioned in Section 2.1 an individual case consideration is indispensable. The implementation of an energy-efficient control system should always be accompanied by strict supervision to ensure safe operation.

Ideally, laboratory tests are performed in advance to determine the specific transport properties of the wastewater. The determination is possible by means of simple laboratory tests. Online measurements do not replace laboratory tests. However, they are preferable for the direct recording of the transport properties. Within this study it was shown that online TSS measurements directly inside the pressure pipe are practicable and provide plausible results. Furthermore this work has shown that the transportation of solids in pressure pipes can be modelled quite simply by means of a case specific set of calibration parameters and suitable transport formulations.

9 Perspectives

Looking ahead, the first priority is to expand energy efficiency. A first step towards increasing the overall energy efficiency is to apply the energy-efficient control to other PS in a drainage system. The next step would accordingly be the intelligent control of a network of PS taking into account the total sediment transport.

For this purpose it is essential to further determine the transport characteristics. Especially due to the spatial (local wastewater composition) and temporal (fluctuation of the inflow hydrograph) variability of the transport characteristics, case-specific investigations are necessary. Especially sensor measurements are particularly suitable for this purpose. Besides the expanding of the characterization of various wastewaters, this can also contribute to an improvement in sensor calibration.

The further development of laboratory methods using camera-monitored measurements, laser or ultrasonic methods provides more detailed insights into the processes of sedimentation and erosion. This allows new conclusions to be drawn for the transport of wastewater.

Because the sediment transport simulation is kept quite simple, numerous extensions are conceivable. An improvement may be an upgrade into a semi-coupled model. This allows the interactions of the flow with the sediment bed to be modelled within the computation. Furthermore, the transport simulation can be enhanced by geometrical line routing and technical installations. This allows the spatial and temporal variability in sediment transport to be better taken into account.

Moreover, the transport model can be used to further detail the movement of solids by introducing settling velocity classes. Depending on the flow velocity distribution, the solids distribution over the pipe cross-section can be computed for each timestep and grid point. This would lead to more detailed results for the transport of pollutants, for example.

Ultimately, the developed transport model can also be implemented in existing hydrodynamic simulation models in which solids transport in pressure pipes has so far been excluded.

In the end, the results are at best included in the technical regulations. In the future, it will be conceivable to divide the required minimum flow rates into at least the type of drainage system and the type of pre-treatment technology. The ranges already given today could be further differentiated in order to expand the use of energy-efficient pump controls.

Bibliography

1. INTERNATIONAL ENERGY AGENCY (ed.). *Global Energy & CO2 Status Report 2019: The latest trends in energy and emissions in 2018*. Paris, 2019. Available also from: https://www.iea.org/reports/global-energy-and-co2-status-report-2019.
2. BUNDESMINISTERIUM FÜR WIRTSCHAFT UND ENERGIE (ed.). *Energiedaten: Gesamtausgabe*. 2019. Available also from: https://www.bmwi.de/Redaktion/DE/Artikel/Energie/energiedaten-gesamtausgabe.html.
3. UNITED NATIONS FRAMEWORK CONVENTION ON CLIMATE CHANGE (ed.). *Paris Agreement: FCCC/CP/2015/L.9/Rev.1*. Paris, 2015. Available also from: http://unfccc.int/files/essential_background/convention/application/pdf/english_paris_agreement.pdf.
4. CONINCK, H. de et al. *Strengthening and Implementing the Global Response. Global Warming of 1.5 ºC: An IPCC Special Report on the impacts of global warming of 1.5°C above pre-industrial levels and related global greenhouse gas emission pathways, in the context of strengthening the global response to the threat of climate change, sustainable development, and efforts to eradicate poverty*. Ed. by MASSON-DELMOTTE, V., P. ZHAI, H.-O. PÖRTNER, D. ROBERTS, J. SKEA, P.R. SHUKLA, A. PIRANI, W. MOUFOUMA-OKIA, C. PÉAN, R. PIDCOCK, S. CONNORS, J.B.R. MATTHEWS, Y. CHEN, X. ZHOU, M.I. GOMIS, E. LONNOY, T. MAYCOCK, M. TIGNOR, AND T. WATERFIELD. Genf: World Meteorological Organization, 2018. Available also from: https://www.ipcc.ch/sr15/.
5. NAIR, S.; GEORGE, B.; MALANO, H. M.; ARORA, M.; NAWARATHNA, B. Water–energy–greenhouse gas nexus of urban water systems: Review of concepts, state-of-art and methods. *Resources, Conservation and Recycling*. 2014, vol. 89, pp. 1–10. ISSN 09213449. Available from DOI: 10.1016/j.resconrec.2014.05.007.
6. DWA DEUTSCHE VEREINIGUNG FÜR WASSERWIRTSCHAFT, ABWASSER UND ABFALL E.V. (ed.). *DWA-Positionen: Positionen zur Energie- und Wasserwirtschaft*. Hennef, 2013. Available also from: https://de.dwa.de/de/thema-energie.html.
7. ARLE, J. et al. *Wasserwirtschaft in Deutschland. Grundlagen, Belastungen, Maßnahmen*. Ed. by UMWELTBUNDESAMT. Dessau-Roßlau, 2017. Available also from: https://www.umweltbundesamt.de/publikationen/wasserwirtschaft-in-deutschland-grundlagen.
8. LEMOS, D.; DIAS, A. C.; GABARRELL, X.; ARROJA, L. Environmental assessment of an urban water system. *Journal of Cleaner Production*. 2013, vol. 54, pp. 157–165. ISSN 09596526. Available from DOI: 10.1016/j.jclepro.2013.04.029.
9. VENKATESH, G.; BRATTEBØ, H. Energy consumption, costs and environmental impacts for urban water cycle services: Case study of Oslo (Norway). *Energy*. 2011, vol. 36, no. 2, pp. 792–800. ISSN 03605442. Available from DOI: 10.1016/j.energy.2010.12.040.
10. NORDWASSER GMBH. *Verbandsreport 2018 für das Gebiet des Warnow-Wasser-und Abwasserverbandes*. Ed. by WARNOW-WASSER-UND ABWASSERVERBAND. Rostock, 2018.

11. ICHA, P.; GESCHÄFTSSTELLE DER ARBEITSGRUPPE ERNEUERBARE ENERGIEN- STATISTIK; KUHS, G. *Entwicklung der spezifischen Kohlendioxid- Emissionen des deutschen Strommix in den Jahren 1990 - 2018*. Ed. by UMWELTBUNDESAMT. Dessau-Roßlau, 2019. Available also from: `https://www.umweltbundesamt.de/publikationen/entwicklung-der-spezifischen-kohlendioxid-5`.
12. ECKSTÄDT, H.; NEYMEYR, K.; KRAUSE, A.; FRICKE, A. *Untersuchung der Möglichkeiten eines energieeffizienten Betriebsmanagements von Abwasserfördersystemen: (Investigation of the possibilities of an energy-efficient operational management of wastewater transport systems): final report DBU research projekt 29356*. 2013. Available also from: `https://www.dbu.de/projekt_29356/01_db_2848.html`.
13. FRICKE, A. *Optimale Steuerung und ihre Anwendungen in der Abwassertechnik: (Optimal control and its application in wastewater technology)*. Rostock: Department of Mathematics, 2015. PhD thesis. University of Rostock.
14. KNUBBE, A.; FRICKE, A.; ECKSTÄDT, H.; NEYMEYR, K.; SCHWARZ, M.; TRÄNCKNER, J. Energieeffizienter Betrieb von Abwasserfördersystemen [Energy efficient strategies for wastewater pumping systems]. *gwf - Wasser—Abwasser*. 2014, vol. 155, no. 5, pp. 640–646.
15. TRÄNCKNER, J.; NEYMEYR, K.; FRICKE, A.; KOEGST, T.; RINAS, M. *Optimale Strategien zur Überwachung und Vermeidung von Sedimentation beim Einsatz drehzahlgeregelter Abwasserpumpen: (Optimal strategies for monitoring and prevention of sedimentation in the use of speed-controlled Sewage Pumps)*. Ed. by FINAL REPORT DBU RESEARCH PROJEKT 32253. 2016. Available also from: `https://www.dbu.de/projekt_32253/01_db_2848.html`.
16. DEUTSCHE VEREINIGUNG FÜR WASSERWIRTSCHAFT, ABWASSER UND ABFALL E.V. *Hydraulische Bemessung und Nachweis von Entwässerungssystemen: DWA-A 118*. März 2006. Hennef: DWA, 2006. DWA-Regelwerk. ISBN 9783939057154.
17. KALLESØE, C. S.; SKØDT, Jens; ERIKSEN, M. Optimal control in sewage applications. *World Pumps*. 2011, vol. 2011, no. 4, pp. 20–23. ISSN 02621762. Available from DOI: `10.1016/S0262-1762(11)70138-9`.
18. DEUTSCHE VEREINIGUNG FÜR WASSERWIRTSCHAFT, ABWASSER UND ABFALL E.V. *Planung und Bau von Abwasserpumpanlagen: ATV-DVWK-A 134:2000-06*. Hennef: DWA, 2000. Technische Regel. ISBN 3-933707-47-1.
19. DEUTSCHE VEREINIGUNG FÜR WASSERWIRTSCHAFT, ABWASSER UND ABFALL E.V. *Druckentwässerungssysteme außerhalb von Gebäuden: DWA-A 116-2*. Mai 2007. Hennef: DWA, 2007. DWA-Regelwerk. ISBN 9783940173003.
20. DEUTSCHE VEREINIGUNG FÜR WASSERWIRTSCHAFT, ABWASSER UND ABFALL E.V. *Besondere Entwässerungsverfahren - Teil 3: Druckluftgespülte Abwassertransportleitungen: DWA-A 116-3*. Mai 2013. Hennef: DWA, 2013. DWA-Regelwerk. ISBN 978-3-942964-84-5.
21. DEUTSCHES INSTITUT FÜR NORMUNG E.V. *Entwässerungssysteme außerhalb von Gebäuden, Pumpsysteme - Teil 2: Druckentwässerungssysteme; Deutsche Fassung EN 16932-2:2018, [Drain and sewer systems outside buildings - Pumping systems - Part 2: Positive pressure systems]*. Berlin: Beuth Verlag GmbH, 16932-2: 2018-07. No. 16932-2: 2018-07.
22. DEUTSCHE VEREINIGUNG FÜR WASSERWIRTSCHAFT, ABWASSER UND ABFALL E.V. *Hydraulische Dimensionierung und Leistungsnachweis von Abwasserdrucksystemen: DWA-A 113*. Januar 2020. Hennef: DWA, 2020. DWA-Regelwerk. ISBN 3887218663.

23. RINAS, M.; TRÄNCKNER, J.; KOEGST, T. Sedimentation of Raw Sewage: Investigations For a Pumping Station in Northern Germany under Energy-Efficient Pump Control. *Water*. 2019, vol. 11, no. 1, pp. 40. Available from DOI: 10.3390/w11010040.

24. RINAS, M.; TRÄNCKNER, J.; KOEGST, T. Erosion characteristics of raw sewage: investigations for a pumping station in northern Germany under energy efficient pump control. *Water Science and Technology*. 2018. ISSN 02731223. Available from DOI: 10.2166/wst.2018.474.

25. RINAS, M.; TRÄNCKNER, J.; KOEGST, T. Sediment Transport in Sewage Pressure Pipes, Part I: Continuous Determination of Settling and Erosion Characteristics by In-Situ TSS Monitoring Inside a Pressure Pipe in Northern Germany. *Water*. 2019, vol. 11, no. 10, pp. 2125. Available from DOI: 10.3390/w11102125.

26. RINAS, M.; FRICKE, A.; TRÄNCKNER, J.; FRISCHMUTH, K.; KOEGST, T. Sediment Transport in Sewage Pressure Pipes, Part II: 1 D Numerical Simulation. *Water*. 2020, vol. 12, no. 1, pp. 282. Available from DOI: 10.3390/w12010282.

27. KIRCHHEIM, N. *Kanalablagerungen in der Mischkanalisation*. Hennef: Deutsche Vereinigung für Wasserwirtschaft, Abwasser und Abfall e.V., 2005. ISBN 3-937758-78-X.

28. BENOIST, A. P.; LIJKLEMA, L. Distribution of sedimentation rates of suspended solids and heavy metals in combined sewer overflows. *Water Science and Technology*. 1990, vol. 22, no. 10-11, pp. 61–68. ISSN 02731223. Available from DOI: 10.2166/wst.1990.0289.

29. MICHELBACH, S.; WOEHRLE, C. Settleable solids in a combined sewer system - Measurement, quantity, characteristics. *Water Science and Technology*. 1992, vol. 25, no. 8, pp. 181–188. ISSN 02731223. Available from DOI: 10.2166/wst.1992.0192.

30. TYACK, J. N.; HEDGES, P. D.; SMISSON, R.P.M. The relationship between settling velocity grading and the characteristics of the contributing catchment. *Water Science and Technology*. 1996, vol. 33, no. 9, pp. 135–142. ISSN 02731223. Available from DOI: 10.1016/0273-1223(96)00379-4.

31. HEDGES, P. D.; BECKER, F. A.; SMISSON, R.P.M. The application of settling velocity as a parameter for characterising wastewater solids. *Water Science and Technology*. 1998, vol. 37, no. 1, pp. 45–52. ISSN 02731223. Available from DOI: 10.1016/S0273-1223(97)00754-3.

32. CHEBBO, G.; GROMAIRE, M.-C.; LUCAS, E. Protocole VICAS: Mesure de la vitesse de chute des MES dans les effluents urbains. *TSM. Techniques - Sciences - Methodes, génie urbain génie rural*. 2003, vol. A98, no. 12, pp. 39–49.

33. GROMAIRE, M. C.; KAFI-BENYAHIA, M.; GASPERI, J.; SAAD, M.; MOILLERON, R.; CHEBBO, G. Settling velocity of particulate pollutants from combined sewer wet weather discharges. *Water Science and Technology*. 2008, vol. 58, no. 12, pp. 2453–2465. ISSN 02731223. Available from DOI: 10.2166/wst.2008.835..

34. HASLER, M. *Field and laboratory experiments on settling process in stormwater storage tanks*. Lyon (France), Graz (Austria): Laboratoire URGC Hydrologie Urbaine, Institut für Siedlungswasserwirtschaft und Landschaftswasserbau, 2007. Diploma thesis. INSA de Lyon, Graz University of Technology.

35. LI, Y.; KANG, J.-H.; LAU, S.-L.; KAYHANIAN, M.; STENSTROM, M. K. Optimization of Settling Tank Design to Remove Particles and Metals. *Journal of Environmental Engineering*. 2008, vol. 134, no. 11, pp. 885–894. ISSN 0733-9372. Available from DOI: 10.1061/(ASCE)0733-9372(2008)134:11(885).

36. TE SLAA, S.; VAN MAREN, D. S.; HE, Q.; WINTERWERP, J. C. Hindered Settling of Silt. *Journal of Hydraulic Engineering*. 2015, vol. 141, no. 9, pp. 04015020. ISSN 0733-9429. Available from DOI: 10.1061/(ASCE)HY.1943-7900.0001038.

37. CHAKRABORTI, R. K.; KAUR, J. Noninvasive Measurement of Particle-Settling Velocity and Comparison with Stokes' Law. *Journal of Environmental Engineering*. 2014, vol. 140, no. 2, pp. 04013008. ISSN 0733-9372. Available from DOI: 10.1061/(ASCE)EE.1943-7870.0000790.

38. NIKORA, V.; ABERLE, J.; GREEN, M. Sediment Flocs: Settling Velocity, Flocculation Factor, and Optical Backscatter. *Journal of Hydraulic Engineering*. 2004, vol. 130, no. 10, pp. 1043–1047. ISSN 0733-9429. Available from DOI: 10.1061/(ASCE)0733-9429(2004)130:10(1043).

39. SHAO, Y.; YAN, Y.; MAA, J. P.-Y. In Situ Measurements of Settling Velocity near Baimao Shoal in Changjiang Estuary. *Journal of Hydraulic Engineering*. 2011, vol. 137, no. 3, pp. 372–380. ISSN 0733-9429. Available from DOI: 10.1061/(ASCE)HY.1943-7900.0000312.

40. YAM, K.; BURNS, A. D.; INGHAM, D. B.; MCCAFFREY, W. D. Influence of Lift Force on the Settling Velocities of Rotating Particles in Two-Dimensional Shear Flow. *Journal of Hydraulic Engineering*. 2013, vol. 139, no. 12, pp. 1277–1285. ISSN 0733-9429. Available from DOI: 10.1061/(ASCE)HY.1943-7900.0000792.

41. CHENG, N. Effect of Concentration on Settling Velocity of Sediment Particles. *Journal of Hydraulic Engineering*. 1997, vol. 123, no. 8, pp. 728–731. ISSN 0733-9429. Available from DOI: 10.1061/(ASCE)0733-9429(1997)123:8(728).

42. WU, W.; WANG, S. S. Y. Formulas for Sediment Porosity and Settling Velocity. *Journal of Hydraulic Engineering*. 2006, vol. 132, no. 8, pp. 858–862. ISSN 0733-9429. Available from DOI: 10.1061/(ASCE)0733-9429(2006)132:8(858).

43. CAMENEN, B. Simple and General Formula for the Settling Velocity of Particles. *Journal of Hydraulic Engineering*. 2007, vol. 133, no. 2, pp. 229–233. ISSN 0733-9429. Available from DOI: 10.1061/(ASCE)0733-9429(2007)133:2(229).

44. CHEBBO, G. *Solides des rejets pluviaux urbains : caractérisation et traitabilité*. Paris: Hydrology, 1992. P.h.D. thesis. Ecole Nationale des Ponts et Chaussées.

45. CHANCELIER, J. Ph.; CHEBBO, G.; LUCAS-AIGUIER, E. Estimation of settling velocities. *Water Research*. 1998, vol. 32, no. 11, pp. 3461–3471. ISSN 00431354. Available from DOI: 10.1016/S0043-1354(98)00114-6.

46. BERTRAND-KRAJEWSKI, J.-L. *Détermination des vitesses de chute des polluants en phase particulaire des rejets urbains par ajustement numérique de la courbe M(t) pour le protocole VICTOR*. Villeurbanne (France): Laboratoire URGC Hydrologie Urbaine, 2001. research report. INSA de Lyon.

47. DEUTSCHES INSTITUT FÜR NORMUNG E.V. *Deutsche Einheitsverfahren zur Wasser-, Abwasser- und Schlammuntersuchung; Summarische Wirkungs- und Stoffkenngrößen (Gruppe H); Bestimmung des Gesamttrockenrückstandes, des Filtrattrockenrückstandes und des Glührückstandes (H 1) [German standard methods for the examination of water, waste water and sludge; general measures of effects and substances (group H); determination of the total solids residue, the filtrate solids residue and the residue on ignition (H 1)]*. Berlin: Beuth Verlag GmbH, 38409-1: 1987. No. 38409-1.

48. CHEBBO, G.; GROMAIRE, M.-C. VICAS—An Operating Protocol to Measure the Distributions of Suspended Solid Settling Velocities within Urban Drainage Samples. *Journal of Environmental Engineering*. 2009, vol. 135, no. 9, pp. 768–775. ISSN 0733-9372. Available from DOI: 10.1061/(ASCE)0733-9372(2009)135:9(768).

49. KRISHNAPPAN, B. G.; EXALL, K.; MARSALEK, J.; ROCHFORT, Q.; KYDD, S.; BAKER, M.; STEPHENS, R. P. Variability of Settling Characteristics of Solids in Dry and Wet Weather Flows in Combined Sewers: Implications for CSO Treatment. *Water, Air, & Soil Pollution*. 2012, vol. 223, no. 6, pp. 3021–3032. ISSN 0049-6979. Available from DOI: 10.1007/s11270-012-1085-9.

50. REGUEIRO-PICALLO, M.; NAVES, J.; ANTA, J.; SUÁREZ, J.; PUERTAS, J. Monitoring accumulation sediment characteristics in full scale sewer physical model with urban wastewater. *Water Science and Technology*. 2017, vol. 76, no. 1-2, pp. 115–123. ISSN 02731223. Available from DOI: 10.2166/wst.2017.118.

51. LEPOT, M.; POUZOL, T.; ALDEA BORRUEL, X.; SUNER, D.; BERTRAND-KRAJEWSKI, J.-L. Measurement of sewer sediments with acoustic technology: from laboratory to field experiments. *Urban Water Journal*. 2017, vol. 14, no. 4, pp. 369–377. ISSN 1573-062X. Available from DOI: 10.1080/1573062X.2016.1148181.

52. HOEFT, S. *In-Situ-Untersuchungen zum Erosionsverhalten von Sedimenten in Mischwasserkanalisationen*. Dresden: Institut für Siedlungs- und Industriewasserwirtschaft, 2015. Dissertation. Technische Universität Dresden.

53. PATERSON, D. M. Short term changes in the erodibility of intertidal cohesive sediments related to themigratory behaviour of epipelic diatoms. *Limnology and Oceanography*. 1989, vol. 34, no. 1, pp. 223–234.

54. SCHÜNEMANN, M.; KÜHL, H. *A device for erosion-measurements on naturally formed, muddy sediments: the EROMES-system*. Als Ms. vervielfältigt. Geesthacht: GKSS, 1991. GKSS E.

55. SECO, I.; GÓMEZ VALENTÍN, M.; SCHELLART, A.; TAIT, S. Erosion resistance and behaviour of highly organic in-sewer sediment. *Water Science and Technology*. 2014, vol. 69, no. 3, pp. 672–679. ISSN 02731223.

56. LIEM, R.; SPORK, V.; KÖNGETER, J. Investigations on erosional processes using an in-situ measuring device. *International journal of sediment research*. 1997, vol. 12, no. 3, pp. 139–147.

57. TOLHURST, T. J.; BLACK, K. S.; PATERSON, D. M.; MITCHENER, H. J.; TERMAAT, G. R.; SHAYLER, S. A. A comparison and measurement standardisation of four in situ devices for determining the erosion shear stress of intertidal sediments. *Continental Shelf Research*. 2000, vol. 20, no. 10-11, pp. 1397–1418. ISSN 02784343. Available from DOI: 10.1016/S0278-4343(00)00029-7.

58. TOLHURST, T. J.; RIETHMÜLLER, R.; PATERSON, D.M. In situ versus laboratory analysis of sediment stability from intertidal mudflats. *Continental Shelf Research*. 2000, vol. 20, no. 10-11, pp. 1317–1334. ISSN 02784343. Available from DOI: 10.1016/S0278-4343(00)00025-X.

59. WIDDOWS, J.; FRIEND, P. L.; BALE, A. J.; BRINSLEY, M. D.; POPE, N. D.; THOMPSON, C. E. Inter-comparison between five devices for determining erodability of intertidal sediments. *Continental Shelf Research*. 2007, vol. 27, no. 8, pp. 1174–1189. ISSN 02784343. Available from DOI: 10.1016/j.csr.2005.10.006.

60. LANGE, R.-L. *Untersuchungen zum Ablagerungsverhalten in der Mischkanalisation als Grundlage der Optimierung von Reinigungsintervallen*. Bochum: Fakultät für Bau- und Umweltingenieurwissenschaften, 2013. Dissertation. Ruhr-Universität Bochum.

61. SHIELDS, A. *Anwendung der Ähnlichkeitsmechanik und der Turbulenzforschung auf die Geschiebebewegung: Berlin, Techn. Hochsch., Diss., 1936*. Berlin: Triltsch & Huther, 1936.

62. SCHRÖDER, R.; ZANKE, U. *Technische Hydraulik: Kompendium für den Wasserbau*. 2. Auflage. Berlin, Heidelberg: Springer Berlin Heidelberg, 2003. Available from DOI: 10.1007/978-3-662-13100-8.

63. AMOS, C. L.; GIBSON, A. J. *The stability of dredge material at dumpsite B, Miramichi Bay, New Brunswick, Canada*. Dartmouth & Wolfville: Bedford Institute of Oceanography & Acadia Centre for Estuarine Research, 1994. Geological Survey of Canada, Open File No 3020, 51 pp. Atlantic Geoscience Centre & Acadia University.

64. AMOS, C. L.; FEENEY, T.; SUTHERLAND, T. F.; LUTERNAUER, J. L. The stability of fine-grained sediments from the Fraser River delta. *Estuarine, Coastal and Shelf Science*. 1997, vol. 45, no. 4, pp. 507–524.

65. AMOS, C. L.; BERGAMASCO, A.; UMGIESSER, G.; CAPPUCCI, S.; CLOUTIER, D.; DENAT, L.; FLINDT, M.; BONARDI, M.; CRISTANTE, S. The stability of tidal flats in Venice Lagoon—the results of in-situ measurements using two benthic, annular flumes. *Journal of Marine Systems*. 2004, vol. 51, no. 1-4, pp. 211–241. ISSN 09247963. Available from DOI: 10.1016/j.jmarsys.2004.05.013.

66. BANASIAK, R.; VERHOEVEN, R.; DE SUTTER, R.; TAIT, S. The erosion behaviour of biologically active sewer sediment deposits: Observations from a laboratory study. *Water Research*. 2005, vol. 39, no. 20, pp. 5221–5231. ISSN 00431354. Available from DOI: 10.1016/j.watres.2005.10.011.

67. DE SUTTER, R.; RUSHFORTH, P.J.; TAIT, S. J.; HUYGENS, M; VERHOEVEN, R.; SAUL, A.J. The erosion of cohesive mixed deposits: implications for sewer flow quality modelling. *Urban Water*. 2000, vol. 2, no. 4, pp. 285–294. ISSN 14620758. Available from DOI: 10.1016/S1462-0758(01)00007-3.

68. RISTENPART, E. *Feststoffe in der Mischwasserkanalisation: Vorkommen, Bewegung und Verschmutzungspotential*. 1995. Dissertation. Universität Hannover.

69. DETTE, H.-H.; MACKE, E.; VRIES, J. de; SCHULZ, O. Mischwasserschmutzfrachten in flachen Kanalnetzen: Stoffaustrag aus Kanalisationen. Hydrologie bebauter Gebiete. Forschungsbericht Deutsche Forschungsgemeinschaft. 1996, pp. 162–183.

70. WILCOCK, P. R.; MCARDELL, B. W. Surface-based fractional transport rates: Mobilization thresholds and partial transport of a sand-gravel sediment. *Water Resources Research*. 1993, vol. 29, no. 4, pp. 1297–1312. ISSN 00431397. Available from DOI: 10.1029/92WR02748.

71. XU, Z.; WU, J.; LI, H.; LIU, Z.; CHEN, Keli; CHEN, Hao; XIONG, L. Different erosion characteristics of sediment deposits in combined and storm sewers. *Water Science and Technology*. 2017, vol. 75, no. 7-8, pp. 1922–1931. ISSN 02731223. Available from DOI: 10.2166/wst.2017.076.

72. BERSINGER, T.; LE HÉCHO, I.; BAREILLE, G.; PIGOT, T.; LECOMTE, A. Continuous Monitoring of Turbidity and Conductivity in Wastewater Networks. *Revue des sciences de l'eau*. 2015, vol. 28, no. 1, pp. 9. Available from DOI: 10.7202/1030002ar.

73. BERSINGER, T.; LE HÉCHO, I.; BAREILLE, G.; PIGOT, T. Assessment of erosion and sedimentation dynamic in a combined sewer network using online turbidity monitoring. *Water Science and Technology*. 2015, vol. 72, no. 8, pp. 1375–1382. ISSN 02731223. Available from DOI: 10.2166/wst.2015.350.

74. LACOUR, C.; JOANNIS, C.; CHEBBO, G. Assessment of annual pollutant loads in combined sewers from continuous turbidity measurements: sensitivity to calibration data. *Water Research*. 2009, vol. 43, no. 8, pp. 2179–2190. ISSN 00431354. Available from DOI: 10.1016/j.watres.2009.02.017.

75. MÉTADIER, M.; BERTRAND-KRAJEWSKI, J.-L. From mess to mass: a methodology for calculating storm event pollutant loads with their uncertainties, from continuous raw data time series. *Water Science and Technology*. 2011, vol. 63, no. 3, pp. 369–376. ISSN 02731223. Available from DOI: 10.2166/wst.2011.230.

76. MÉTADIER, M.; BERTRAND-KRAJEWSKI, J.-L. The use of long-term on-line turbidity measurements for the calculation of urban stormwater pollutant concentrations, loads, pollutographs and intra-event fluxes. *Water Research*. 2012, vol. 46, no. 20, pp. 6836–6856. ISSN 00431354. Available from DOI: 10.1016/j.watres.2011.12.030.

77. LACOUR, C.; JOANNIS, C.; GROMAIRE, M-C; CHEBBO, G. Potential of turbidity monitoring for real time control of pollutant discharge in sewers during rainfall events. *Water Science and Technology*. 2009, vol. 59, no. 8, pp. 1471–1478. ISSN 02731223. Available from DOI: 10.2166/wst.2009.169.

78. SUN, S.; BARRAUD, S.; CASTEBRUNET, H.; AUBIN, J.-B.; MARMONIER, P. Long-term stormwater quantity and quality analysis using continuous measurements in a French urban catchment. *Water Research*. 2015, vol. 85, pp. 432–442. ISSN 00431354. Available from DOI: 10.1016/j.watres.2015.08.054.

79. BERTRAND-KRAJEWSKI, J.-L. TSS concentration in sewers estimated from turbidity measurements by means of linear regression accounting for uncertainties in both variables. *Water Science and Technology*. 2004, vol. 50, no. 11, pp. 81–88. ISSN 02731223. Available from DOI: 10.2166/wst.2004.0674.

80. BERTRAND-KRAJEWSKI, J.-L.; BARDIN, J.-P. Evaluation of uncertainties in urban hydrology: application to volumes and pollutant loads in a storage and settling tank. *Water Science and Technology*. 2002, vol. 45, no. 4-5, pp. 437–444. ISSN 02731223. Available from DOI: 10.2166/wst.2002.0645.

81. JCGM 100:2008. *Evaluation of measurement data — Guide to the expression of uncertainty in measurement*. Joint Committee for Guides in Metrology, 2008.

82. BAGNOLD, R. A. *An approach to the sediment transport problem from general physics*. Washington, DC: U.S. Gov. Print. Off, 1966. Geological Survey professional paper.

83. ENGELUND, F.; HANSEN, E. *A monograph on sediment transport in alluvial streams*. Copenhagen: Teknisk Forlag, 1967.

84. ACKERS, P.; WHITE, R. Sediment Transport: New Approach and Analysis. *Journal of the Hydraulics Division*. 1973, vol. 99, no. 11, pp. 2041–2060.

85. ENGELUND, F.; FREDSØE, J. A Sediment Transport Model for Straight Alluvial Channels. *Hydrology Research*. 1976, vol. 7, no. 5, pp. 293–306. ISSN 0029-1277. Available from DOI: 10.2166/nh.1976.0019.

86. VAN RIJN, L. C. Sediment Transport, Part I: Bed Load Transport. *Journal of Hydraulic Engineering*. 1984, vol. 110, no. 10, pp. 1431–1456. ISSN 0733-9429. Available from DOI: 10.1061/(ASCE)0733-9429(1984)110:10(1431).

87. CAMPISANO, A.; CREACO, E.; MODICA, C. Numerical modelling of sediment bed aggradation in open rectangular drainage channels. *Urban Water Journal*. 2013, vol. 10, no. 6, pp. 365–376. ISSN 1573-062X. Available from DOI: 10.1080/1573062X.2012.739627.

88. SHIRAZI, R. H. S. M.; CAMPISANO, A.; MODICA, C.; WILLEMS, P. Modelling the erosive effects of sewer flushing using different sediment transport formulae. *Water Science and Technology*. 2014, vol. 69, no. 6, pp. 1198–1204. ISSN 02731223. Available from DOI: 10.2166/wst.2013.810.

89. CREACO, E.; BERTRAND-KRAJEWSKI, J.-L. Numerical simulation of flushing effect on sewer sediments and comparison of four sediment transport formulas. *Journal of Hydraulic Research*. 2009, vol. 47, no. 2, pp. 195–202. ISSN 0022-1686. Available from DOI: 10.3826/jhr.2009.3363.

90. CORREIA, L. P.; KRISHNAPPAN, B. G.; GRAF, W. H. Fully Coupled Unsteady Mobile Boundary Flow Model. *Journal of Hydraulic Engineering*. 1992, vol. 118, no. 3, pp. 476–494. ISSN 0733-9429. Available from DOI: 10.1061/(ASCE)0733-9429(1992)118:3(476).

91. BONAKDARI, H.; EBTEHAJ, I.; AZIMI, H. Numerical Analysis of Sediment Transport in Sewer Pipe. *International Journal of Engineering*. 2015, vol. 28, no. 11, pp. 1564–1570. Available from DOI: 10.5829/idosi.ije.2015.28.11b.03.

92. DANISH HYDRAULIC INSTITUTE. *MOUSE - Pollution Transport Reference Manual*. Hørsholm, Denmark, 2017. Available also from: http://manuals.mikepoweredbydhi.help/2017/MIKE_Urban.htm.

93. ROSSMAN, L. A. *EPANET 2 Users Manual*. Cincinnati: U.S. Environmental Protection Agency, 2000. Available also from: https://www.epa.gov/water-research/epanet.

94. EBTEHAJ, I.; BONAKDARI, H. Evaluation of Sediment Transport in Sewer using Artificial Neural Network. *Engineering Applications of Computational Fluid Mechanics*. 2013, vol. 7, no. 3, pp. 382–392. ISSN 1994-2060. Available from DOI: 10.1080/19942060.2013.11015479.

95. AZAMATHULLA, H. Md; AB GHANI, A.; FEI, Seow Yen. ANFIS-based approach for predicting sediment transport in clean sewer. *Applied soft computing*. 2012, vol. 12, no. 3, pp. 1227–1230. ISSN 1568-4946. Available from DOI: 10.1016/j.asoc.2011.12.003.

96. BIZIMANA, H.; ALTUNKAYNAK, A. A novel approach for the prediction of the incipient motion of sediments under smooth, transitional and rough flow conditions using Geno-Fuzzy Inference System model. *Journal of Hydrology*. 2019, vol. 577, pp. 123952. ISSN 00221694. Available from DOI: 10.1016/j.jhydrol.2019.123952.

97. SAFARI, M. J. S.; DANANDEH MEHR, A. Multigene genetic programming for sediment transport modeling in sewers for conditions of non-deposition with a bed deposit. *International journal of sediment research*. 2018, vol. 33, no. 3, pp. 262–270. Available from DOI: 10.1016/j.ijsrc.2018.04.007.

98. ROUSHANGAR, K.; GHASEMPOUR, R. Estimation of bedload discharge in sewer pipes with different boundary conditions using an evolutionary algorithm. *International journal of sediment research*. 2017, vol. 32, no. 4, pp. 564–574. Available from DOI: 10.1016/j.ijsrc.2017.05.007.

99. EBTEHAJ, I.; BONAKDARI, H.; KHOSHBIN, F. Evolutionary design of a generalized polynomial neural network for modelling sediment transport in clean pipes. *Engineering Optimization*. 2016, vol. 48, no. 10, pp. 1793–1807. ISSN 0305-215X. Available from DOI: 10.1080/0305215X.2015.1137567.

100. TRÄNCKNER, J.; BÖNISCH, G.; GEBHARD, V. R.; DIRCKX, G.; KREBS, P. Model-based assessment of sediment sources in sewers. *Urban Water Journal*. 2008, vol. 5, no. 4, pp. 277–286. ISSN 1573-062X. Available from DOI: 10.1080/15730620802201491.

101. ROSSMAN, L. A.; BOULOS, P. F.; ALTMAN, T. Discrete Volume–Element Method for Network Water–Quality Models. *Journal of Water Resources Planning and Management*. 1993, vol. 119, no. 5, pp. 505–517. ISSN 0733-9496. Available from DOI: 10.1061/(ASCE)0733-9496(1993)119:5(505).

102. ROSSMAN, L. A.; BOULOS, P. F. Numerical Methods for Modeling Water Quality in Distribution Systems: A Comparison. *Journal of Water Resources Planning and Management*. 1996, vol. 122, no. 2, pp. 137–146. ISSN 0733-9496. Available from DOI: 10.1061/(ASCE)0733-9496(1996)122:2(137).

103. KLEIJWEGT, R. A.; VELDKAMP, R. G.; NALLURI, C. Sediment in Sewers: Initiation of Transport. *Water Science and Technology*. 1990, vol. 22, no. 10-11, pp. 239–246. ISSN 02731223.

104. KAMPHUIS, J. W. Littoral Transport Rate. In: EDGE, B. L. (ed.). *Coastal engineering 1990 proceedings*. New York, N.Y.: American Society of Civil Engineers, 1991-, pp. 2402–2415. ISBN 9780872627765. Available from DOI: 10.1061/9780872627765.184.

105. ASHLEY, R. M.; WOTHERSPOON, D. J. J.; GOODISON, M. J.; MCGREGOR, I.; COGHLAN, B. P. The Deposition and Erosion of Sediments in Sewers. *Water Science and Technology*. 1992, vol. 26, no. 5-6, pp. 1283–1293. ISSN 02731223. Available from DOI: 10.2166/wst.1992.0571.

106. WOTHERSPOON, D. J. J.; ASHLEY, R. M. Rheological Measurement of the Yield Strength of Combined Sewer Sediment Deposits. *Water Science and Technology*. 1992, vol. 25, no. 8, pp. 165–169. ISSN 02731223. Available from DOI: 10.2166/wst.1992.0190.

107. GUNKEL, M.; PAWLOWSKY-REUSING, E. Field campaign on sediment transport behaviour in a pressure main from pumping station to wastewater treatment plant in Berlin. *Water Science and Technology*. 2017, vol. 75, no. 9-10, pp. 2025–2033. ISSN 02731223. Available from DOI: 10.2166/wst.2017.044.

108. GRAF, W. H. *Hydraulics of sediment transport*. New York, N.Y.: McGraw-Hill, 1971. McGraw-Hill series in water resources and environmental engineering. ISBN 00702-39002.

109. DEUTSCHES INSTITUT FÜR NORMUNG E.V. *DIN 4049-1:1992-12, Hydrologie; Grundbegriffe*. Berlin: Beuth Verlag GmbH, 1992. Available from DOI: 10.31030/2525591.

110. ENGELKE, P. *Untersuchungen zur Modellierung des Feststofftransports in Abwasserkanälen: Validierung in SIMBA*. Rostock: Univ., Agrar- und Umweltwiss. Fak., 2014. Schriftenreihe Umweltingenieurwesen. ISBN 978-3-86009-408-2.

111. ASHLEY, R. M.; WOTHERSPOON, D. J. J.; COGHLAN, B. P.; MCGREGOR, I. The Erosion and Movement of Sediments and Associated Pollutants in Combined Sewers. *Water Science and Technology*. 1992, vol. 25, no. 8, pp. 101–114. ISSN 02731223. Available from DOI: 10.2166/wst.1992.0184.

In dieser Reihe bisher erschienen

Band I
10. DIALOG Abfallwirtschaft MV
– Von der Abfallwirtschaft zur Energiewirtschaft.
Tagungsband, erschienen im Juni 2007, ISBN 987-3-86009-004-6

Band II
Ellen-Rose Trübger
Entwicklung eines Ansatzes zur Berücksichtigung der ungesättigten Zone bei der Grundwassersimulation von Feuchtgebieten.
Dissertation, erschienen im August 2007, ISBN 978-3-86009-006-0

Band III
René Dechow
Untersuchungen verschiedener Ansätze der Wasserhaushalts- und Stofftransportmodellierung hinsichtlich ihrer Anwendbarkeit in Stickstoffhaushaltsmodellen.
Dissertation, erschienen im September 2007, ISBN 978-3-86009-016-9

Band IV
Carolin Wloczyk
Entwicklung und Validierung einer Methodik zur Ermittlung der realen Evapotranspiration anhand von Fernerkundungsdaten in Mecklenburg-Vorpommern.
Dissertation, erschienen im September 2007, ISBN 978-3-86009-009-1

Band 5
1. Rostocker Bioenergieforum.
Bioenergieland Mecklenburg-Vorpommern.
Tagungsband, erschienen im Oktober 2007, ISBN 978-3-86009-013-8

Band 6
Kulturtechniktagung 2007.
Ostseeverschmutzung und Flächenentwässerung.
Tagungsband, erschienen im Januar 2008, ISBN 978-3-86009-018-3

Band 7
Enrico Frahm
Bestimmung der realen Evapotranspiration für Weide (Salix spp.) und Schilf (Phragmites australis) in einem nordostdeutschen Flusstalmoor.
Dissertation, erschienen im Mai 2008, ISBN 978-3-86009-023-7

Band 8
Jenny Haide
Methode zur Quantifizierung der Einflüsse auf Vorgangsdauern lohnintensiver Arbeiten am Beispiel von Pflasterarbeiten.
Dissertation, erschienen im Juni 2008, ISBN 978-3-86009-024-4

Band 9
11. DIALOG Abfallwirtschaft MV
Chancen und Risiken für die deutsche Abfallwirtschaft im Ausland.
Tagungsband, erschienen im Juni 2008, ISBN 978-3-86009-029-9

Band 10
Stefan Cantré
Ein Beitrag zur Bemessung geotextiler Schläuche für die Entwässerung von Baggergut.
Dissertation, erschienen im Juni 2008, ISBN 978-3-86009-032-9

Band 11
Birgit Wüstenberg
Praxis der Standortwahl von Sportboothäfen im Küstenbereich Mecklenburg-Vorpommerns und Entwicklung einer Bewertungsmethode als Planungshilfe.
Dissertation, erschienen im Juli 2008, ISBN 978-3-86009-033-6

Band 12
André Clauß
Erhöhung der Trinkwasserversorgungssicherheit in Havarie- und Krisensituationen durch neue Handlungsalgorithmen sowie Einbeziehung bisher ungenutzter Ressourcen am Beispiel von Bergbaugrubenwasser.
Dissertation, erschienen im September 2008, ISBN 978-3-86009-037-4

Band 13
Peter Degener
Sickerwasserkreislauf zur Behandlung von Sickerwässern der aerob-biologischen Restabfallbehandlung (Restabfallrotte).
Dissertation, erschienen im Oktober 2008, ISBN 978-3-86009-043-5

Band 14
2. Rostocker Bioenergieforum
Innovationen für Klimaschutz und wirtschaftliche Entwicklung.
Tagungsband, erschienen im Oktober 2008, ISBN 978-3-86009-044-2

Band 15
7. Rostocker Abwassertagung
Fortschritte auf dem Gebiet der Abwasserentsorgung.
Tagungsband, erschienen im November 2008, ISBN 978-3-86009-045-9

Band 16
Christian Noß
Strömungsstrukturen kleiner naturnaher Fließgewässer unter Berücksichtigung von Turbulenztheorie und Dispersionsmodellen.
Dissertation, erschienen im Januar 2009, ISBN 978-3-86009-054-1

Band 17
Ralf Schröder
Entwicklung von Möglichkeiten zur Messung der N2-Übersättigung sowie Methoden zur Reduzierung der Schwimmschlammbildung.
Dissertation, erschienen im Februar 2009, ISBN 978-3-86009-055-8

Band 18
Elmar Wisotzki
Bodenverfestigungen mit Kalk-Hüttensand-Gemischen.
Dissertation, erschienen im April 2009, ISBN 978-3-86009-059-6

Band 19
Ramez Mashkouk
Untersuchungen zur Adsorption und biologischen Aktivität an Aktivkohlefilter unter den Bedingungen der Wasseraufbereitung im Wasserwerk Rostock.
Dissertation, erschienen im April 2009, ISBN 978-3-86009-060-2

Band 20
Torsten Birkholz
Handlungserfordernisse und Optimierungsansätze für kommunale Ver- und Entsorgungsunternehmen im Zusammenhang mit demografischen Veränderungen im ländlichen Raum aufgezeigt an einem Beispiel in Mecklenburg-Vorpommern.
Dissertation, erschienen im Mai 2009, ISBN 978-3-86009-061-9

Band 21
12. DIALOG Abfallwirtschaft MV
Aktuelle Entwicklungen in der Abfallwirtschaft.
Tagungsband, erschienen im Juni 2009, ISBN 978-3-86009-062-6

Band 22
Thomas Fritz
Entwicklung, Implementierung und Validierung eines praxisnahen Verfahrens zur Bestimmung von Biogas- bzw. Methanerträgen.
Dissertation, erschienen im Oktober 2009, ISBN 978-3-86009-065-7

Band 23
3. Rostocker Bioenergieforum
Bioenergie – Chance und Herausforderung für die regionale und globale Wirtschaft.
Tagungsband, erschienen im Oktober 2009, ISBN 978-3-86009-065-8

Band 24
Muhammad Mariam
Analyse von Gefahrenpotenzialen für die Trinkwasserversorgung der Stadt Rostock unter besonderer Berücksichtigung von Schadstoffausbreitungsvorgängen in der Warnow.
Dissertation, erschienen im Februar 2010, ISBN 978-3-86009-078-7

Band 25
Manja Steinke
Untersuchungen zur Behandlung von Abwässern der Fischverarbeitungsindustrie.
Dissertation, erschienen im Juni 2010, ISBN 978-3-86009-085-5

Band 26
13. DIALOG Abfallwirtschaft MV
Die Kreislauf- und Abfallwirtschaft im Wandel. Wohin gehen die rechtlichen und technischen Entwicklungen?
Tagungsband, erschienen im Juni 2010, ISBN 978-3-86009-087-9

Band 27
4. Rostocker Bioenergieforum
Zukunftstechnologien für Bioenergie
Tagungsband, erschienen im Oktober 2010, ISBN 978-3-940364-12-8

Band 28
Dirk Banemann
Einfluss der Silierung und des Verfahrensablaufs der Biomassebereitstellung auf den Methanertrag unter Berücksichtigung eines Milchsäurebakteriensiliermittel
Dissertation, erschienen im Januar 2011, ISBN 978-3-86009-087-9

Band 29
14. DIALOG Abfallwirtschaft MV
Abfall als Wertstoff- und Energiereserve
Tagungsband, erschienen im Juni 2011, ISBN 978-3-940364-18-0

Band 30
5. Rostocker Bioenergieforum
Tagungsband, erschienen im November 2011, ISBN 978-3-940364-20-3

Band 31
8. Rostocker Abwassertagung
Erhöhung der Effektivität von Abwasserentsorgungsanlagen
Tagungsband, erschienen im November 2011, ISBN 978-3-86009-120-3

Band 32
6. Rostocker Bioenergieforum
Tagungsband, erschienen im Juni 2012, ISBN 978-3-940364-27-2

Band 33
Ishan Machlouf
Untersuchungen zur Nitratelimination bei der Trinkwasseraufbereitung unter Berücksichtigung syrischer Verhältnisse
Dissertation, erschienen im März 2013, ISBN 978-3-86009-204-0

Band 34
Ralph Sutter
Analyse und Bewertung der Einflussgrößen auf die Optimierung der Rohbiogasproduktion hinsichtlich der Konstanz von Biogasqualität und -menge
Dissertation, erschienen im März 2013, ISBN 978-3-86009-202-6

Band 35
Wolfgang Pfaff-Simoneit
Entwicklung eines sektoralen Ansatzes zum Aufbau von nachhaltigen Abfallwirtschaftssystemen in Entwicklungsländern vor dem Hintergrund von Klimawandel und Ressourcenverknappung
Dissertation, erschienen im Mai 2013, ISBN 978-3-86009-203-3

Band 36
7. Rostocker Bioenergieforum
Tagungsband, erschienen im Juni 2013, ISBN 978-3-86009-207-1

Band 37
Markus Helftewes
Modellierung und Simulation der Gewerbeabfallaufbereitung vor dem Hintergrund der Outputqualität, der Kosteneffizienz und der Klimabilanz
Dissertation, erschienen im Oktober 2013, ISBN 978-3-86009-402-0

Band 38
Jan Stefan Riha
Detektion und Quantifizierung von Cyanobakterien in der Ostsee mittels Satellitenfernerkundung
Dissertation, erschienen im Oktober 2013, ISBN 978-3-86009-403-7

Band 39
Peter Helmke
Optimierung der Verarbeitungs-, Gebrauchs- und Entsorgungseigenschaften eines naturfaserverstärkten Kunststoffes unter Berücksichtigung automobiler Anforderungen
Dissertation, erschienen im November 2013, ISBN 978-3-86009-404-4

Band 40
Andrea Siebert-Raths
Modifizierung von Polylactid (PLA)für technische Anwendungen
Verfahrenstechnische Optimierung der Verarbeitungs- und Gebrauchseigenschaften
Dissertation, erschienen im Januar 2014 ISBN 978-3-86009-405-1

Band 41
Fisiha Getachew Argaw
Agricultural Machinery Traffic Influence on Clay Soil Compaction as Measured by the Dry Bulk Density
Dissertation, erschienen im Januar 2014 ISBN 978-3-86009-406-8

Band 42
Tamene Adugna Demissie
Climate change impact on stream flow and simulated sediment yield to Gilgel Gibe 1 hydropower reservoir and the effectiveness of Best Management Practices
Dissertation, erschienen im Februar 2014 ISBN 978-3-86009-407-5

Band 43
Paul Engelke
Untersuchungen zur Modellierung des Feststofftransports in Abwasserkanälen: Validierung in SIMBA®
Dissertation, erschienen im Februar 2014 ISBN 978-3-86009-408-2

Band 44
16. DIALOG Abfallwirtschaft MV
Aktuelle Entwicklungen in der Abfall- und Ressourcenwirtschaft
Tagungsband, erschienen im April 2014, ISBN 978-3-86009-410-5

Band 45
8. Rostocker Bioenergieforum, 19.-20. Juni 2014 an der Universität Rostock
Tagungsband, erschienen im Juni 2014, ISBN 978-3-86009-412-9

Band 46
Abschlussbericht Projekt CEMUWA − Climate protection, natural resources management and soil improvement by combined Energetic and Material Utilization of lignocellulosic agricultural WAstes and residues
Projektbericht, erschienen im September 2014, ISBN 978-3-86009-413-6

Band 47
8. Rostocker Baggergutseminar, 24.-25. September 2014 in Rostock
Tagungsband, erschienen im September 2014, ISBN 978-3-86009-414-3

Band 48
Michael Kuhn
Mengen und Trockenrückstand von Rechengut kommunaler Kläranlagen
Dissertation, erschienen im Oktober 2014 ISBN 978-3-86009-415-0

Band 49
8. Rostocker Abwassertagung, 10.-11. November 2014 in Rostock
Tagungsband, erschienen im November 2014, ISBN 978-3-86009-416-7

Band 50
Mulugeta Azeze Belete
Modeling and Analysis of Lake Tana Sub Basin Water Resources Systems, Ethiopia
Dissertation, erschienen im Dezember 2014 ISBN 978-3-86009-422-8

Band 51
Daniela Dressler
Einfluss regionaler und standortspezifischer Faktoren auf die Allgemeingültigkeit ökologischer und primärenergetischer Bewertungen von Biogas
Dissertation, erschienen im Mai 2015 ISBN 978-3-86009-424-2

Band 52
9. Rostocker Bioenergieforum, 18.-19. Juni 2015 in Rostock
Tagungsband, erschienen im November 2014, ISBN 978-3-86009-425-9

Band 53
Nils Engler
Spurenelementkonzentrationen und biologische Aktivität in NaWaRo-Biogas-fermentern
Dissertation, erschienen im September 2015 ISBN 978-3-86009-427-3

Band 54
Thomas Schmidt
Möglichkeiten der Effizienzsteigerung bei der anaeroben Vergärung von Weizenschlempe
Dissertation, erschienen im Oktober 2015 ISBN 978-3-86009-428-0

Band 55
Thomas Dorn
Principles, Opportunities and Risks associated with the transfer of environmental technology between Germany and China using the example of thermal waste disposal
Dissertation, erschienen im Dezember 2015 ISBN 978-3-86009-429-7

Band 56
Uwe Holzhammer
Biogas in einer zukünftigen Energieversorgungsstruktur mit hohen Anteilen fluktuierender Erneuerbarer Energien
Dissertation, erschienen im Dezember 2015 ISBN 978-3-86009-430-3

Band 57
17. DIALOG Abfallwirtschaft MV
Aktuelle Entwicklungen in der Abfall- und Ressourcenwirtschaft,
15. Juni 2016 in Rostock,
Tagungsband, erschienen im Juni 2016, ISBN 978-3-86009-432-7

Band 58
10. Rostocker Bioenergieforum, 16.-17. Juni 2016 in Rostock
Tagungsband, erschienen im Juni 2016, ISBN 978-3-86009-433-4

Band 59
Michael Friedrich
Adaptation of growth kinetics and degradation potential of organic material in activated sludge
Dissertation, erschienen im Juli 2016 ISBN 978-3-86009-434-1

Band 60
Nico Schulte
Entwicklung von Qualitätsprüfungen für die haushaltsnahe Abfallsammlung im Holsystem
Dissertation, erschienen im Juli 2016 ISBN 978-3-86009-435-8

Band 61
Ullrich Dettmann
Improving the determination of soil hydraulic properties of peat soils at different scales
Dissertation, erschienen im September 2016 ISBN 978-3-86009-436-5

Band 62
Anja Schreiber
Membranbasiertes Verfahren zur weitergehenden Vergärung
von feststoffreichen Substraten in landwirtschaftlichen Biogasanlagen
Dissertation, erschienen im Oktober 2016 ISBN 978-3-86009-446-4

Band 63
André Körtel
Entwicklung eines selbstgängigen statischen Verfahrens zur biologischen Stabilisierung und Verwertung organikreicher Abfälle unter extrem ariden Bedingungen für Entwicklungs- und Schwellenländer, am Beispiel der Stadt Teheran
Dissertation, erschienen im Oktober 2016 ISBN 978-3-86009-447-1

Band 64
Ayman Elnaas
Actual situation and approach for municipal solid waste treatment in the Arab region
Dissertation, erschienen im Oktober 2016 ISBN 978-3-86009-448-8

Band 65
10. Rostocker Abwassertagung, Wege und Werkzeuge für eine zukunftsfähige Wasserwirtschaft im norddeutschen Tiefland, 8. November 2016 in Rostock
Tagungsband, erschienen im November 2016, ISBN 978-3-86009-449-5

Band 66
Gunter Weißbach
Mikrowellen-assistierte Vorbehandlung lignocellulosehaltiger Reststoffe
Dissertation, erschienen im November 2016 ISBN 978-3-86009-450-1

Band 67
Leandro Janke
Optimization of anaerobic digestion of sugarcane waste for biogas production in Brazil
Dissertation, erschienen im Mai 2017 ISBN 978-3-86009-454-9

Band 68
11. Rostocker Bioenergieforum, 22.-23. Juni 2017 in Rostock
Tagungsband, erschienen im Juni 2017, ISBN 978-3-86009-455-6

Band 69
Claudia Demmig
Einfluss des Erntezeitpunktes auf die anaerobe Abbaukinetik der Gerüstsubstanzen im Biogasprozess
Dissertation, erschienen im Juli 2017, ISBN 9978-3-86009-456-3

Band 70
Christian Koepke
Die Ermittlung charakteristischer Bodenkennwerte der Torfe und Mudden Mecklenburg-Vorpommerns als Eingangsparameter für erdstatische Berechnungen nach Eurocode 7 / DIN 1054
Dissertation, erschienen im Juni 2017, ISBN 978-3-86009-457-0

Band 71
Sven-Henning Schlömp
Geotechnische Untersuchung und Bewertung bautechnischer Eignung von Müllverbrennungsschlacken und deren Gemischen mit Böden
Dissertation, erschienen im Juni 2017, ISBN 978-3-86009-458-7

Band 72
Anne-Katrin Große
Baggergut im Deichbau – Ein Beitrag zur geotechnischen Charakterisierung und Erosionsbeschreibung feinkörniger, organischer Sedimente aus dem Ostseeraum zur Einschätzung der Anwendbarkeit
Dissertation, erschienen im Juni 2017, ISBN 978-3-86009-459-4

Band 73
Thomas Knauer
Steigerung der Gesamteffizienz von Biogasanlagen durch thermische Optimierung
Dissertation, erschienen im Juli 2017, ISBN 978-3-86009-460-0

Band 74
Mathhar Bdour
Electrical power generation from residual biomass by combustion in externally fired gas turbines (EFGT)
Dissertation, erschienen im August 2017, ISBN 978-3-86009-468-6

Band 75
Johannes Dahlin
Vermarktungsstrategien und Konsumentenpräferenzen für Dünger und Erden aus organischen Reststoffen der Biogasproduktion
Dissertation, erschienen im September 2017, ISBN 978-3-86009-469-3

Band 76
Sören Weinrich
Praxisnahe Modellierung von Biogasanlagen
Systematische Vereinfachung des Anaerobic Digestion Model No. 1 (ADM1)
Dissertation, erschienen im März 2018, ISBN 978-3-86009-471-6

Band 77
18. DIALOG Abfallwirtschaft MV
Aktuelle Entwicklungen in der Abfall- und Ressourcenwirtschaft
Tagungsband, erschienen im Juni 2018, ISBN 978-3-86009-472-3

Band 78
12. Rostocker Bioenergieforum
Tagungsband, erschienen im Juni 2018, ISBN 978-3-86009-473-0

Band 79
Tatyana Koegst
Screening approaches for decision support in drinking water supply
Dissertation, erschienen im Juni 2018, ISBN 978-3-86009-474-7

Band 80
Liane Müller
Optimierung des anaeroben Abbaus stickstoffhaltiger Verbindungen durch den Einsatz von Proteasen
Dissertation, erschienen im September 2018, ISBN 978-3-86009-475-4

Band 81
Projektbericht Wasserwirtschaft
KOGGE – **Ko**mmunale **G**ewässer **G**emeinschaftlich **E**ntwickeln
Ein Handlungskonzept für kleine urbane Gewässer am Beispiel der Hanse- und Universitätsstadt Rostock
Projektbericht, erschienen im September 2018, ISBN 978-3-86009-476-1

Band 82
Adam Feher
Untersuchungen zur Bioverfügbarkeit von Mikronährstoffen für den Biogasprozess
Dissertation, erschienen im Oktober 2018, ISBN 978-3-86009-477-8

Band 83
Constanze Uthoff
Pyrolyse von naturfaserverstärkten Kunststoffen zur Herstellung eines kohlenstoffhaltigen Füllstoffs für Thermoplasten
Dissertation, erschienen im November 2018, ISBN 978-3-86009-478-5

Band 84
Ingo Kaundinya
Prüfverfahren zur Abschätzung der Langzeitbeständigkeit von Kunststoff-dichtungsbahnen aus PVC-P für den Einsatz in Dichtungssystemen von Straßentunneln
Dissertation, erschienen im Dezember 2018, ISBN 978-3-86009-484-6

Band 85
Eric Mauky
A model-based control concept for a demand-driven biogas production
Dissertation, erschienen im Januar 2019, ISBN 978-3-86009-485-3

Band 86
Michael Kröger
Thermochemical Utilization of Algae with Focus on hydrothermal Processes
Dissertation, erschienen im Februar 2019, ISBN 978-3-86009-486-0

Band 87
13. Rostocker Bioenergieforum
Tagungsband, erschienen im Juni 2019, ISBN 978-3-86009-487-7

Band 88
12. Rostocker Abwassertagung
Tagungsband, erschienen im September 2019, ISBN 978-3-86009-488-4

Band 89
Philipp Stahn
Wasser- und Nährstoffhaushalt von Böden unter Mischkulturen und Trockenstress
Dissertation, erschienen im Juli 2019, ISBN 978-3-86009-489-1

Band 90
BioBind: Luftgestützte Beseitigung von Verunreinigungen durch Öl mit biogenen Bindern
Projektbericht, erschienen im September 2019, ISBN 978-3-86009-490-7

Band 91
Jürgen Müller
Die forsthydrologische Forschung im Nordostdeutschen Tiefland: Veranlassung, Methoden, Ergebnisse und Perspektiven
Habilitation, erschienen im Oktober 2019, ISBN 978-3-86009-491-4

Band 92
Marcus Siewert
Bewertung der Ölhavarievorsorge im deutschen Seegebiet auf Grundlage limitierender Randbedingungen – Ein Beitrag zur Verbesserung des Vorsorgestatus
Dissertation, erschienen im November 2019, ISBN 978-3-86009-492-1

Band 93
Camilo Andrés Wilches Tamayo
Technical optimization of biogas plants to deliver demand oriented power
Dissertation, erschienen im Februar 2020, ISBN 978-3-86009-493-8

Band 94
Robert Kopf
Technisches Benchmarking mit Standortqualifikationsstudie biochemischer Energieanlagenprojekte (Beispiel Biogas)
Dissertation, erschienen im Februar 2020, ISBN 978-3-86009-494-5

Band 95
14. Rostocker Bioenergieforum und 19. DIALOG Abfallwirtschaft MV
Tagungsband, erschienen im Juni 2020, ISBN 978-3-86009-507-2
DOI: https://doi.org/10.18453/rosdok_id00002650

Band 96
Safwat Hemidat
Feasibility Assessment of Waste Management and Treatment in Jordan
Dissertation, erschienen im Juli 2020, ISBN 978-3-86009-509-6

Band 97
Andreas Heiko Metzing
Verdichtung von ungebundenen Pflasterdecken und Plattenbelägen - Untersuchungen zur Lagerungsdichte des Fugenmaterials
Dissertation, erschienen im Juli 2020, ISBN 978-3-86009-510-2
DOI: https://doi.org/10.18453/rosdok_id00002742

Band 98
Ying Zhou
Research on Utilization of Hydrochars Obtained by the Organic Components of Municipal Solid Waste
Dissertation, erschienen im November 2020, ISBN 978-3-86009-515-7

Band 99
Mathias Gießler
Ein prozessbasiertes Modell zur wirtschaftlich-technischen Abbildung von Abwasserunternehmen **–** Beispielhafte Anwendung für eine ländliche Region mit Bevölkerungsrückgang
Dissertation, erschienen im November 2020, ISBN 978-3-86009-516-4
DOI: https://doi.org/10.18453/rosdok_id00002790

Band 100
Dodiek Ika Candra
Development of a Virtual Power Plant based on a flexible Biogas Plant and a Photovoltaic-System
Dissertation, erschienen im Dezember 2020, ISBN 978-3-86009-518-8
DOI: https://doi.org/10.18453/rosdok_id00002814

Band 101
Thomas Zeng
Prediction and reduction of bottom ash slagging during small-scale combustion of biogenic residues
Dissertation, erschienen im Dezember 2020, ISBN 978-3-86009-519-5

Band 102
Edward Antwi
Pathways to sustainable bioenergy production from cocoa and cashew residues from Ghana
Dissertation, erschienen im Dezember 2020, ISBN 978-3-86009-520-1
DOI: https://doi.org/10.18453/rosdok_id00002818

Band 103
Muhammad Waseem
Integrated Hydrological and Mass Balance Assessment in a German Lowland Catchment with a Coupled Hydrologic and Hydraulic Modelling
Dissertation, erschienen im Januar 2021, ISBN 978-3-86009-521-8
DOI: https://doi.org/10.18453/rosdok_id00002884